POLITECNICO DI TORINO

Department of Energy

Master of Science Degree in Automotive Engineering

Master's Thesis

CFD Analysis of Lubrication in Rotating Gears for Experimental Design and Software Validation

Graduation Session November 2024

Supervisor:
Assoc. Prof. Massimo Rundo
Co-supervisor:
Assoc. Prof. Daniela Anna Misul

Candidate:
Davide Milli

"Good news, everyone!"
(Prof. Farnsworth, 1999).

Acknowledgement

Before delving into the discussion of this thesis, I would like to express my deepest gratitude to all the people who, with their support, made it possible for me to reach this important milestone.

My first thought goes to my parents, Roberto and Susanna, who have always encouraged me to pursue my passions and continue my studies. Even in moments when I doubted myself, they never stopped believing in me. I am aware of the sacrifices they made to allow me to get this far, and to them, I extend my most heartfelt gratitude.

My father taught me the value of practical thinking and the art of improvising in any situation. Many of the skills I now consider essential stem from his lessons, delivered with a firm, sometimes impatient approach, but always extremely effective. My mother, on the other hand, has been my emotional rock. She has always put me first, ever since my childhood, dedicating me unconditional time and care. She is and will always remain my favorite "stress ball". Without them, I would never have achieved this milestone, nor would I be the person I am today.

A special thanks goes to my grandmother Piga, who has supported me over the years with love and determination. I was fortunate to have a second mother so intelligent and progressive, who taught me so much, from deep values to culinary recipes we shared during my childhood. These moments remain among my most cherished memories. If I carry a few extra pounds today, I undoubtedly owe them to her exceptional meals, which have accompanied my studies since elementary school. Over the past five years, every "When are you graduating?" from her was a constant motivator: I couldn't have wished for a better source of encouragement.

A warm thought also goes to my grandfather Battista, who is no longer with us. It saddens me that he could not see his "pistola" reach this milestone. During my childhood, he was a fundamental figure, teaching me that with skill and dedication, anything can be fixed.

A special acknowledgment goes to my sister Marta. Although our relationship often turned into my role as her "personal assistant", her support and presence have been invaluable. No one in the world has been able to motivate and sustain me as much as she has. I am deeply proud of the person she has become and everything

she has achieved on her own. Having her by my side is a precious gift and one of my greatest blessings.

Finally, a special thanks goes to my supervisor, Professor Massimo Rundo. He has undoubtedly been one of the best professors I have had the pleasure of meeting during my academic journey, standing out for the quality of his teaching and the passion he brings to his work. I will remember him as one of the highlights of my university experience. I am immensely grateful for the opportunities he has offered me, both for this thesis and for my future. His dedication, availability, and technical expertise were fundamental during my work and made this experience even more meaningful. I am extremely satisfied with how my university journey concluded, and I owe much of it to him. I know I have been very fortunate. His guidance and support will remain a precious reference for me, and to him, I extend my sincerest gratitude.

To all of them, and to everyone who contributed to this journey, I offer my deepest thanks.

Ringraziamenti

Prima di addentrarmi nella trattazione di questa tesi, desidero esprimere la mia profonda gratitudine a tutte le persone che, con il loro supporto, hanno reso possibile il raggiungimento di questo importante traguardo.

Il mio primo pensiero va ai miei genitori, Roberto e Susanna, che mi hanno sempre incoraggiato a inseguire le mie passioni e a proseguire gli studi. Anche nei momenti in cui io stesso vacillavo, loro non hanno mai smesso di credere in me. Sono consapevole dei sacrifici che hanno affrontato per permettermi di arrivare fin qui, e a loro va la mia più sincera gratitudine.

Mio padre mi ha insegnato il valore del senso pratico e l'arte di arrangiarsi in ogni situazione. Molte delle competenze che oggi considero essenziali derivano dai suoi insegnamenti, impartiti con un approccio deciso, a volte impaziente, ma sempre estremamente efficace. Mia madre, invece, è stata la mia roccia emotiva. Ha sempre messo me al primo posto sin dall'infanzia, dedicandomi tempo e attenzioni incondizionati. È e rimarrà per sempre la mia "pallina antistress" preferita. Senza di loro non avrei mai raggiunto questo traguardo e non sarei la persona che sono diventato oggi.

Un ringraziamento speciale va a mia nonna Piga, che negli anni mi ha sostenuto con amore e determinazione. Sono stato fortunato ad avere una seconda mamma così intelligente e progressista, che mi ha insegnato tanto, dai valori più profondi alle ricette culinarie condivise durante l'infanzia. Questi momenti rimangono tra i miei ricordi più preziosi. Se oggi porto qualche chilo in più, lo devo sicuramente ai suoi pranzi eccezionali, che hanno accompagnato i miei studi sin dalle elementari. Negli ultimi cinque anni, ogni suo "Quando ti laurei?" è stato uno stimolo costante: non avrei potuto desiderare una motivatrice migliore.

Un pensiero affettuoso va anche a mio nonno Battista, che purtroppo non è più con noi. Mi rattrista che non abbia potuto vedere il suo "pistola" raggiungere questo traguardo. Durante la mia infanzia è stato una figura fondamentale, insegnandomi che con abilità e dedizione ogni cosa può essere aggiustata.

Un ringraziamento particolare va poi a mia sorella Marta. Nonostante il nostro rapporto si sia spesso tradotto nel mio ruolo di suo "assistente personale", il suo supporto e la sua presenza sono stati inestimabili. Nessuno al mondo è stato capace

di motivarmi e sostenermi quanto lei. Sono profondamente orgoglioso della persona che è diventata e di tutto ciò che ha conquistato con le sue sole forze. Averla accanto è un dono prezioso e una delle mie più grandi fortune.

Infine, un ringraziamento speciale va al mio relatore, il Professor Massimo Rundo. È stato senza dubbio uno dei migliori docenti che ho avuto il piacere di incontrare durante il mio percorso accademico, distinguendosi per la qualità del suo insegnamento e per la passione con cui svolge il suo lavoro. Lo ricorderò come uno dei punti di forza della mia esperienza universitaria. Sono infinitamente grato per le opportunità che mi ha offerto, sia per questa tesi sia per il futuro. La sua dedizione, disponibilità e competenza tecnica sono state fondamentali durante il mio lavoro e hanno reso questa esperienza ancora più significativa. Sono estremamente soddisfatto di come si è concluso il mio percorso universitario e lo devo in gran parte a lui, so di essere stato molto fortunato. La sua guida e il suo supporto resteranno per me un riferimento prezioso, e a lui va la mia più sincera gratitudine.

A tutti loro, e a coloro che hanno contribuito a questo percorso, va il mio più sentito ringraziamento.

Abstract

Lubrication plays a crucial role in enhancing the efficiency and durability of automotive gear systems by minimizing friction, wear, and heat generation. This study investigates gear lubrication using Computational Fluid Dynamics (CFD) simulations with Simerics MP+ software, focusing on validating its accuracy for various lubrication methods. The primary objective was to evaluate the performance of forced lubrication systems by examining key parameters such as mesh resolution, time step, oil jet position, and volumetric flow rate through a series of sensitivity analyses.

To validate the simulation results, a comprehensive physical experiment was designed, including all the necessary components, to replicate the simulated conditions. The experiment will involve the use of high-speed cameras to capture the oil distribution and behavior around rotating gears, along with precision instrumentation to measure resistive torque, with the goal of validating the simulation results in upcoming experiments. A direct comparison between the simulated and experimental results will help confirm the accuracy of the CFD model in predicting real-world lubrication behavior. Additionally, a secondary study on splash lubrication was conducted to assess its effectiveness relative to forced lubrication systems.

The findings from this research highlight the importance of balancing cell size and time step to achieve accurate and efficient simulations. Furthermore, the study identified optimal jet positions and flow rates for the experimental setup to obtain measurable results. Although the final validation of Simerics MP+ is contingent upon completing the physical experiment, the initial findings indicate its potential as a reliable tool for analyzing gear lubrication systems.

This study provides a framework for validating CFD models and sets a foundation for future research on advanced lubrication techniques. If the experimental results align with the simulations, Simerics MP+ can be confidently used in further studies, leading to improved design and performance of automotive and industrial gear systems. The broader implications of this research extend to developing more efficient and durable lubrication solutions for high-performance automotive and industrial applications.

Contents

List of Figures

List of Tables

Chapter 1

Introduction

1.1 Background and Motivation

With the advent of the internal combustion engine (ICE) and its integration into early automotive designs, such as the first car created by Karl Benz, the need for a mechanism to manage power transmission between the engine and the wheels became apparent. This led to the development of the first automotive gearbox, a device that remains fundamental in modern vehicles. The gearbox is crucial for adjusting the transmission ratio, which allows drivers to control the speed and torque of the vehicle efficiently.

As engines generate power, it must be transmitted smoothly to the wheels to ensure optimal vehicle performance. The gearbox facilitates this by altering gear ratios, enabling the vehicle to operate effectively across various driving conditions. However, for a gearbox to function correctly and last for a prolonged period, it requires proper lubrication.

Lubrication is essential for preventing direct metal-to-metal contact between sliding and rolling surfaces of the gearbox. By minimizing friction and wear, lubrication helps to reduce the risk of component damage and overheating. This, in turn, extends the life of the gearbox and ensures reliable performance. Effective lubrication also contributes to the overall efficiency of the vehicle by reducing energy losses and improving fuel economy.

In automotive engineering, understanding and optimizing gearbox lubrication is critical for enhancing the durability and performance of vehicles. Computational Fluid Dynamics (CFD) has emerged as a valuable tool for analyzing and improving lubrication processes within gear systems. CFD allows engineers to simulate and visualize fluid flow and its interaction with gearbox components, providing insights into lubrication efficiency, friction reduction, and heat dissipation. Figure 1.1 shows a group of gearbox gears surrounded by a graphic simulation of oil, symbolizing the role of lubrication in optimizing gear performance.

Figure 1.1: Gearbox gears surrounded by a graphic simulation of oil

This thesis is dedicated to exploring the lubrication of gears using the simulation software Simerics MP+, with a focus on validating its accuracy and effectiveness. The research will involve a series of simulations to evaluate how various parameters influence lubrication performance and the resulting impact on gearbox efficiency. Key aspects of the study will include analyzing the resistive torque generated by the

interaction between gears and lubricating oil, which is crucial for understanding the efficiency and performance of different lubrication methods.

The thesis will investigate two lubrication scenarios, with a primary emphasis on forced lubrication systems. In these systems, an oil jet is directed precisely at the gear teeth to ensure adequate lubrication under dynamic conditions. This method is critical for high-performance applications where effective lubrication is essential for minimizing friction and wear. Additionally, the study will include analyses of oil bath lubrication systems, which are commonly used in various applications and offer a different approach to managing gear lubrication.

To validate the simulation results, the research will also involve designing and recreating physical experiments that correspond to the simulated conditions. By comparing simulated results with experimental data, the thesis aims to assess the accuracy of the Simerics MP+ software in predicting real-world lubrication behavior. Special attention will be given to the resistive torque experienced by the gear, which directly affects the overall performance of the gearbox.

Furthermore, the research will utilize high-speed cameras to analyze and compare the distribution and trajectory of oil around the gear, between simulated environments and real-world experiments. This detailed analysis will allow for a direct comparison of oil behavior between simulation results and actual physical conditions. By observing how oil disperses and interacts with the gear teeth in both scenarios, the study aims to validate the accuracy of the simulations and gain deeper insights into the effectiveness of different lubrication methods. Understanding these dynamics will be crucial for evaluating how oil distribution affects gear performance and longevity, ultimately contributing to the development of more efficient and reliable lubrication strategies.

Overall, this thesis aims to bridge the gap between theoretical simulations and practical applications, providing valuable insights into gear lubrication that can enhance the design and performance of automotive gearboxes. An important objective of this research is to validate the Simerics MP+ software, ensuring its accuracy and reliability for use in future studies. By confirming the ability of the software to accurately simulate lubrication processes and predict real-world behavior, the findings will not only offer practical recommendations for optimizing lubrication systems but also establish a foundation for confidently using this tool in future research. The ultimate goal is to improve the reliability and efficiency of modern vehicles through more effective lubrication strategies.

1.2 Objectives of the Thesis

1.2.1 Completed Objectives

1. **To Investigate Gear Lubrication Performance**: Investigate different lubrication methods, along with their advantages and disadvantages, and analyze how effective lubrication impacts friction, wear, and overall performance in automotive gearboxes. Identify the key parameters influencing lubrication quality and efficiency, with a specific focus on forced lubrication and a brief consideration of splash lubrication systems.

2. **To Create the Simulation Environment in the CFD Software**: Using Simerics MP+, model and simulate a system composed of a simple gear in which the forced lubrication method is used, taking into consideration the feasibility of this system in the real-world when modeling the system.

3. **To Evaluate the Impact of Parameters on Lubrication**: Study the effects of the parameters of the simulations on the lubrication effectiveness and efficiency by evaluating the oil distribution and the variation in resistive torque created by the oil-gear interaction. Determine which parameters are the most important ones and which are the feasible range of operation.

4. **To Design the Physical Test**: Develop a comprehensive experimental setup and all the necessary components to replicate the virtual study with a laboratory experiment in the real world, utilizing the already available equipment present in the test bench. This involves creating a test enclosure and selecting instrumentation to accurately reproduce and measure the conditions simulated in the CFD analysis.

1.2.2 Future Objective

5. **To Perform the experiments and Compare the Results**: Employ high-speed cameras to observe and capture the oil distribution and trajectory around the gear, allowing for a detailed comparison between experimental observations and the simulated behavior. Measure the resistive torque using the torque meter of the test bench, and compare the recorded values with those predicted by the simulations.

Chapter 2

Literature Review

2.1 Basic Principles of Gear Lubrication

2.1.1 Introduction of Gear Lubrication

Gears are a ubiquitous component in machines, playing a critical role in transmitting power and motion in a wide range of applications, from simple household devices to complex automotive systems. Their functionality may often be taken for granted; however, the design and operation of gears involve a sophisticated interplay of mechanical principles. Ensuring the efficient and reliable performance of gears necessitates careful consideration of various factors, among which lubrication stands out as a paramount concern.

Lubrication serves multiple essential functions within a gear system. Primarily, it plays a crucial role in reducing the friction and wear between meshing gear teeth, thus significantly enhancing the efficiency and lifespan of gears. This reduction in friction is not only vital for minimizing energy losses but also for maintaining the precision and smooth operation of the gear mechanism. Furthermore, lubrication aids in dissipating the heat generated by frictional forces, thereby mitigating the risk of thermal damage that could compromise the integrity of the gear materials.

In addition to these primary functions, gear lubricants act as a protective barrier against corrosion, which can be particularly detrimental in environments where mois-

ture and contaminants like dirt and debris are present. The presence of a lubricant film on gear surfaces prevents direct exposure to these potentially harmful elements, thereby extending the operational life of the gear system. Moreover, the viscosity and chemical composition of lubricants can be tailored to meet the specific demands of different gear applications, such as high-speed or high-load conditions, ensuring optimal performance under various operating environments.

In summary, effective gear lubrication is not merely an ancillary consideration but a fundamental aspect of gear design and maintenance that directly influences the reliability, efficiency, and longevity of gear systems in automotive engineering and beyond.

2.1.2 Mechanism of Gear Lubrication

In the complex world of gear systems, lubrication serves as a critical factor in determining the performance, efficiency, and longevity of gears. The effectiveness of gear lubrication is influenced not only by the chemical composition of the lubricant but also by the specific operational conditions under which the gears function. These conditions, including load, speed, temperature, and the nature of the contact surfaces, give rise to distinct lubricating regimes. Each regime is characterized by varying levels of lubricant film thickness, pressure, and temperature, which collectively define the interaction between the gear surfaces and the lubricant.

A thorough understanding of these lubricating regimes is essential for selecting the most suitable lubricant and optimizing gear performance. The proper application of lubrication ensures the reduction of friction, minimization of wear, and prevention of surface damage, all of which are crucial for maintaining the durability and efficiency of gear systems, especially in demanding automotive environments. By analyzing how gear surfaces interact with lubricants under different regimes, engineers can make informed decisions that not only enhance the operational life of gears but also improve overall system reliability.

Lubrication Regimes in Gear Systems

Gear lubrication is generally categorized into three primary regimes, each with distinct characteristics and implications for gear performance:

Boundary Lubrication: Boundary lubrication occurs when the lubricant film is extremely thin, often too thin to completely separate the gear surfaces. This regime typically arises under conditions of high load, low speed, or during start-stop operations where there is not enough relative motion to develop a full lubricant film. In boundary lubrication, the friction coefficient is higher due to the direct contact between the gear surfaces, which can lead to increased wear and potential damage. To mitigate these effects, lubricants used in this regime are often fortified with special additives, such as anti-wear (AW) and extreme pressure (EP) additives. These additives form a protective layer on the gear surfaces, reducing wear and preventing surface degradation even when the lubricant film is insufficient to prevent metal-to-metal contact.

Mixed Lubrication: Mixed lubrication represents a transitional regime between boundary lubrication and full film lubrication. In this regime, the lubricant film is of intermediate thickness, meaning that some parts of the gear surfaces are in direct contact, while other areas are separated by a lubricant film. This regime is often encountered during variations in load and speed, where conditions are neither severe enough to cause boundary lubrication nor favorable enough to maintain a full lubricant film. Mixed lubrication is particularly challenging to manage because the balance between film formation and surface contact can fluctuate. Effective lubrication in this regime requires precise control of lubricant properties, such as viscosity and additive composition, to minimize friction and wear while maximizing gear performance.

Full Film Lubrication: Full film lubrication occurs when a continuous lubricant film completely separates the gear surfaces, preventing direct metal-to-metal contact. This regime is further subdivided into two distinct sub-regimes:

Elastohydrodynamic Lubrication (EHL): characterized by the presence of very high pressures at the gear contact points, leading to elastic deformation of the gear surfaces. Despite the high pressures, the lubricant forms a thin yet continuous film that separates the gear teeth. The viscosity of the lubricant increases significantly under these pressures, aiding in the formation of the film. The thickness of this film is comparable to the extent of the gear surface deformation, ensuring that the gears are adequately lubricated even under extreme conditions. EHL is commonly observed in heavily loaded gear systems, such as those found in automotive transmissions, where the combination of high loads and moderate speeds requires robust lubrication to prevent surface damage and ensure smooth operation.

Hydrodynamic Lubrication (HL): this regime occurs under conditions where the relative motion between the gear surfaces is sufficient to maintain a full lubricant film, and the pressures involved are lower than in EHL. In this regime, the gear surfaces experience minimal or no deformation, and the lubricant film is thick enough to completely separate the gears, effectively "floating" the gear teeth on a cushion of lubricant. The film thickness in hydrodynamic lubrication is primarily determined by factors such as gear speed, load, and lubricant viscosity. This regime is typical in lightly loaded gears or in scenarios where gear speeds are high, such as in certain

automotive applications where minimizing frictional losses is crucial for achieving high efficiency.

As shown in Figure 2.1, the friction coefficient is highest in boundary lubrication, while it reaches its minimum in elastohydrodynamic lubrication. This behavior is expected, as the metal-to-metal contact present in boundary lubrication results in higher friction compared to when the surfaces are fully separated by the lubricant. In mixed lubrication, the friction coefficient lies between the values of boundary and elastohydrodynamic lubrication. On the other hand, in fully developed hydrodynamic lubrication, the friction coefficient is higher than in elastohydrodynamic lubrication. This is due to the increased lubricant film thickness, which causes viscous shear in the fluid. In elastohydrodynamic lubrication, the lubricant undergoes significant compression, resulting in a thinner film and smaller contact area. This leads to lower friction due to the combination of higher viscosity and elastic effects in the contact region.

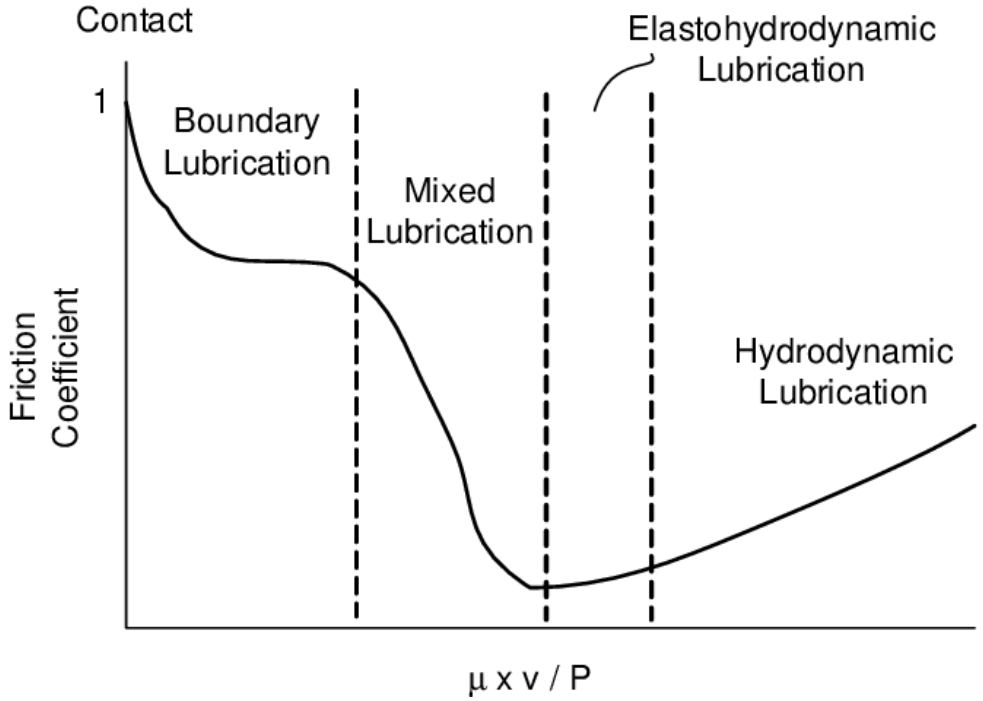

Figure 2.1: Lubrication regimes

2.1.3 Types of Gear Lubricants

In the realm of gear systems, the selection of an appropriate lubricant is a critical factor that directly influences the overall performance, durability, and efficiency of the machinery. Lubricants serve as the lifeblood of gear systems, reducing friction, minimizing wear, dissipating heat, and protecting against corrosion. The correct choice of lubricant is not merely a matter of preference but a necessity for ensuring the smooth operation and long-term reliability of gears. Engineers and maintenance professionals must possess a deep understanding of the various types of lubricants available, as each type is designed to meet specific operational conditions and performance requirements. Lubricants can be broadly categorized into three primary types: mineral oils, synthetic oils, and additives. Each category offers unique properties that make it suitable for different applications. Understanding the characteristics, advantages, and limitations of these lubricants allows for informed decision-making that can significantly enhance the longevity and efficiency of gear systems. By tailoring the lubricant selection to the specific operating environment and mechanical demands, it is possible to optimize gear performance, reduce maintenance costs, and extend the service life of the equipment. The primary categories of oil lubricants include mineral oils and synthetic oils.

Mineral Oils

Mineral oils are the traditional choice for gear lubrication and are derived from the refining of crude oil. These lubricants are composed of hydrocarbon molecules that provide a stable and reliable base for a wide range of applications. Mineral oils are often blended with various additives to enhance their performance characteristics, such as improving oxidation stability, boosting anti-wear properties, and providing corrosion resistance. The versatility of mineral oils makes them suitable for a broad spectrum of gear systems, including those found in automotive applications.

The primary advantage of mineral oils lies in their cost-effectiveness and widespread availability. They offer satisfactory performance in standard operating conditions and are compatible with many types of gear systems. However, mineral oils may not perform as well under extreme temperatures or high-load conditions, as their thermal stability and oxidation resistance are generally lower than that of synthetic alternatives. Despite these limitations, the right formulation of mineral oil, enhanced with appropriate additives, can still provide reliable lubrication for many applications.

Synthetic Oils

Synthetic oils represent a more advanced and engineered class of lubricants, offering superior performance compared to mineral oils. These lubricants are created through chemical synthesis, resulting in a more uniform molecular structure that delivers enhanced properties. Common types of synthetic base oils include polyalphaolefins (PAOs), esters, and polyalkylene glycols (PAGs). Synthetic oils are particularly valued for their excellent thermal stability, oxidation resistance, and performance in extreme temperatures, both high and low.

One of the key benefits of synthetic oils is their ability to maintain consistent viscosity across a wide temperature range, ensuring that the lubricant film remains intact under various operating conditions. This makes synthetic oils the preferred choice for high-performance gear systems, such as those found in racing vehicles, heavy machinery, and other applications where extreme operating conditions are the norm. Additionally, synthetic oils tend to have longer service intervals, reducing the frequency of oil changes and contributing to lower maintenance costs over time. However, the superior performance of synthetic oils comes at a higher cost, which may be a consideration for some applications.

Additives in Gear Lubricant

Additives are specialized chemicals that are blended into both mineral and synthetic oils to enhance their performance and protect gear systems from specific challenges. These additives play a crucial role in ensuring that the lubricant meets the demands of the application, especially under harsh operating conditions. Some of the most common and important additives used in gear lubricants include:

Anti-Wear Additives: Anti-wear additives, such as zinc dialkyldithiophosphate (ZDDP), form a protective layer on the gear surfaces. This layer helps to reduce wear, especially in boundary lubrication conditions where metal-to-metal contact might otherwise occur. These additives are essential for extending the life of gears operating under high loads and preventing surface damage.

Extreme Pressure (EP) Additives: Extreme pressure additives, including sulfur-phosphorus and sulfur-chlorine compounds, react with the metal surfaces to form a protective film. This film prevents welding and galling under extreme

load conditions, where the pressure between gear teeth could lead to significant damage. EP additives are particularly important in heavy-duty gear systems where high loads are frequently encountered.

Viscosity Index Improvers: Viscosity index improvers are polymers added to lubricants to stabilize their viscosity across a wide temperature range. This ensures that the lubricant maintains adequate film thickness, providing consistent protection for gears regardless of temperature fluctuations. Viscosity index improvers are especially valuable in applications where gear systems are exposed to varying ambient and operating temperatures.

Antioxidants: Antioxidants are added to gear lubricants to prevent oxidation, which can lead to the formation of sludge and varnish within the lubricant. These oxidation by-products can impair the performance of the lubricant and cause damage to gear surfaces. By preventing oxidation, antioxidants help maintain the effectiveness of the lubricant over time, ensuring long-term protection for the gear system.

Anti-Foaming Agents: Anti-foaming agents are designed to reduce the formation of foam within the lubricant. Foam can lead to lubricant starvation in gears, as air bubbles can impede the proper distribution of the oil. By minimizing foam, these additives ensure that the lubricant maintains consistent coverage and protection across all gear surfaces, even in high-speed applications where aeration might otherwise be a concern.

2.1.4 Factors Influencing Gear Lubrication

The effectiveness of gear lubrication is determined by a complex interplay of various factors that must be carefully considered to ensure optimal performance, durability, and reliability of gear systems. Each factor influences the selection and application of lubricants, making it essential for engineers and maintenance professionals to understand these dynamics thoroughly. By addressing the specific needs of the gear system and its operating environment, the right lubricant can be chosen to minimize wear, reduce friction, and prevent premature gear failure. The primary factors that influence gear lubrication include load and speed, temperature, gear type, and environmental conditions.

Load and Speed

Load Considerations: The load applied to the gears plays a critical role in determining the type of lubricant required. Higher loads exert greater pressure on gear surfaces, leading to increased friction and potential wear. To counteract these effects, lubricants with higher viscosity or those fortified with superior load-carrying additives, such as extreme pressure (EP) additives, are often necessary. These additives help form a protective film that can withstand the intense pressures without breaking down, thereby preventing direct metal-to-metal contact and reducing wear.

Speed Considerations: The speed at which gears operate also significantly impacts the choice of lubricant. Higher speeds generally generate more frictional heat, which can lead to overheating and reduced efficiency. To mitigate these issues, lower viscosity lubricants are typically favored for high-speed applications. Lower viscosity oils reduce internal drag within the lubricant film, allowing for smoother operation and better heat dissipation. However, it is important to balance viscosity with load requirements, as too low a viscosity could result in inadequate film strength under heavy loads.

Temperature

Operating Temperature: Temperature is a critical factor influencing the viscosity of a lubricant, and it must be carefully managed to maintain the proper lubrication regime. As temperatures rise, lubricants tend to thin out, reducing

their viscosity and potentially compromising their ability to provide adequate film thickness. Conversely, at lower temperatures, lubricants may become too thick, increasing drag and making it difficult for the gears to move freely. Selecting a lubricant with a viscosity that remains stable across the expected temperature range is essential for ensuring consistent performance.

Temperature Extremes: In environments where gears are exposed to extreme temperature variations, such as in automotive applications or industrial machinery, synthetic lubricants are often preferred. Synthetic oils typically exhibit superior thermal stability, maintaining their viscosity and protective qualities even under severe temperature fluctuations. This stability reduces the risk of thermal degradation, oxidation, and lubricant breakdown, ensuring that the gears remain properly lubricated regardless of external conditions.

Gear Type

Spur and Helical Gears: Spur gears, characterized by their straightforward design and rolling contact, typically require lubricants that can handle moderate loads and speeds with good anti-wear properties. Helical gears, on the other hand, involve both rolling and sliding actions due to their angled teeth. This sliding action can generate additional heat, necessitating the use of lubricants with better thermal stability and anti-wear additives to protect the gear surfaces.

Bevel Gears: Bevel gears, which transmit motion between intersecting shafts, often experience varied load distributions depending on their configuration. These gears may require lubricants with enhanced load-carrying capacity and good film strength to ensure reliable operation under fluctuating loads.

Worm Gears: Worm gears, known for their high sliding action and potential for significant frictional heat generation, often require specialized lubricants with extreme pressure (EP) additives. The EP additives help to reduce wear and prevent surface damage by forming a resilient protective layer that can withstand the intense contact pressures and sliding motion inherent in worm gear operation.

Environmental Conditions

Impact of Contaminants: The operating environment can introduce various contaminants, such as water, dust, and chemicals, that can degrade lubricants and increase the risk of gear failure. Contaminants can lead to the formation of sludge, corrosion, and abrasive wear, all of which can compromise the effectiveness of the lubricant and shorten the lifespan of the gear system.

Protective Measures: In harsh or contaminated environments, it is crucial to select lubricants that offer enhanced protective properties. This may include the use of lubricants with robust anti-corrosion additives, water resistance, and the ability to resist chemical degradation. Sealed gear systems, which are designed to protect internal components from external contaminants, may also benefit from specially formulated lubricants that provide additional protection against the ingress of harmful substances.

Sealed Systems: For gear systems operating in particularly challenging environments, such as those exposed to high levels of moisture or abrasive particles, sealed systems are often employed. These systems help to prevent contamination and maintain the integrity of the lubricant over extended periods. The choice of lubricant for sealed systems should consider the need for long-term stability, low volatility, and the ability to maintain performance despite potential exposure to harsh environmental factors.

2.1.5 Lubrication Methods

In the study of gear lubrication within the automotive industry, particularly in gearbox lubrication, several methods have been developed to ensure the longevity, efficiency, and performance of transmission systems. Understanding these methods is crucial for automotive engineers aiming to optimize vehicle performance under varying conditions. Three primary lubrication systems are commonly employed in automotive gearboxes, each with its distinct advantages and drawbacks.

Splash Lubrication System

The splash lubrication system is the simplest and most cost-effective method, frequently employed in manual transmissions. This system operates by allowing gears and other moving parts to dip into a reservoir of lubricating oil. As the components rotate, they splash the oil throughout the transmission casing, thereby lubricating themselves and adjacent parts.

Advantages:

- The simplicity of the splash lubrication system is one of its most significant benefits. With fewer moving parts and no need for an oil pump, this system is both economical to produce and requires minimal maintenance.
- Due to its straightforward design, the risk of mechanical failure is relatively low, making it a reliable option for many manual transmissions.

Disadvantages:

- The system has limitations, particularly at high speeds or under heavy loads. The distribution of oil can be uneven, leading to inadequate lubrication of certain components, which may result in increased wear and tear over time.
- Additionally, because the oil distribution depends on the movement of the gears, there may be instances where some parts are not adequately lubricated, particularly during initial startup or in low-speed operation.

Circulation Oil Lubrication System

The circulation oil lubrication system represents a more advanced and sophisticated approach, commonly found in automatic transmissions. This system employs an oil pump to continuously circulate lubricant to various parts of the transmission. The oil is drawn from a sump, filtered, and often cooled before being distributed to the transmission components. This ensures that all parts receive consistent lubrication, regardless of the speed or load of the vehicle.

Advantages:

- The primary advantage of this system is its ability to provide consistent lubrication across all components, significantly reducing the risk of wear and enhancing the overall longevity of the transmission.
- The inclusion of an oil cooler within the circulation system helps maintain optimal operating temperatures, further contributing to the durability of the transmission.
- This system is particularly effective in heavy-duty and high-performance vehicles, where maintaining stable lubrication under extreme conditions is essential.

Disadvantages:

- The circulation oil system is more complex and costly than splash lubrication systems, requiring more sophisticated engineering and regular maintenance to ensure optimal performance.
- The need for additional components, such as the oil pump, filter, and cooler, increases the potential for mechanical failure and adds to the overall cost of the vehicle.

Subcategories of Circulation Oil Systems

The circulation oil lubrication system can be further divided into two main types, each designed to meet specific performance requirements: dry sump and wet sump lubrication systems.

Dry Sump Lubrication System

This advanced system uses an external oil reservoir instead of an oil sump within the transmission casing. The oil is pumped into the transmission, lubricates the components, and is then returned to the external reservoir. This method is particularly common in racing cars and high-performance vehicles where maintaining oil pressure and avoiding oil starvation are critical.

Advantages:

- The dry sump system prevents oil starvation during high-speed cornering or braking, and it allows for a lower engine placement, improving the center of gravity of the vehicle.

Disadvantages:

- Despite its advantages, the dry sump system is expensive and complex to design, requiring frequent maintenance and checks.

Wet Sump Lubrication System

More common in conventional automatic transmissions, the wet sump system integrates the oil sump within the transmission housing. The oil is collected in the sump and recirculated by an oil pump.

Advantages:

- The wet sump system offers a simpler design and operation, making it reliable and easy to maintain.

Disadvantages:

- It can be prone to oil starvation during extreme maneuvers, and its cooling efficiency might be less effective compared to more advanced systems

Additional Subsystems

Within these systems, there are additional specialized subsystems that address specific lubrication needs:

Pressure Lubrication System

Here, an oil pump is used to circulate the lubricant under pressure to various parts of the transmission. This system is commonly found in modern automatic transmissions, ensuring that even the most demanding components receive adequate lubrication.

Mist Lubrication System

In mist lubrication, oil is atomized into a fine mist and distributed throughout the transmission system. This method ensures that all parts, even those that are difficult to reach, are adequately lubricated. It is often used in high-performance or specialized transmission systems where precise lubrication is critical.

Hybrid Lubrication System

The hybrid lubrication system combines elements of both splash and circulation oil lubrication methods to achieve optimal lubrication under varying conditions. This system is typically found in high-performance and luxury vehicles, where both efficiency and reliability are paramount. In a hybrid system, critical components may receive lubrication via a pressure system, ensuring they are protected under extreme conditions, while other parts might be lubricated using splash lubrication. This combination allows the system to take advantage of the benefits of both methods, offering superior protection and performance.

Advantages:

- The hybrid lubrication system offers the benefits of multiple lubrication methods, making it highly customizable to the specific needs of a vehicle's transmission. It ensures that all components are adequately lubricated under all operating conditions, enhancing both efficiency and durability.

Disadvantages:

- The complexity of the hybrid system makes it more challenging to design and maintain. The sophisticated control systems required to manage the different lubrication methods add to the overall cost of the vehicle.

2.1.6 Traditional Method of analysis

The study of lubrication in gear systems is critical for optimizing performance, reducing wear, and improving the efficiency of mechanical transmissions. This research primarily focuses on the resistive torque generated by oil-gear interactions and the distribution of lubricating oil within the gear mechanism. While this study employs a Computational Fluid Dynamics (CFD) approach to gain detailed insights into these phenomena, it is essential to recognize the traditional methods historically used for such analyses.

Traditional methods for analyzing gear lubrication encompass a variety of empirical and experimental techniques that provide critical insights into the behavior of lubricants in gear systems. These methods have evolved over time and remain relevant for practical applications, providing a foundation for understanding gear lubrication performance and assisting in the selection of suitable lubricants for specific gear applications.

Traditional methods of analyzing gear lubrication and resistive torque rely heavily on empirical and experimental approaches. These methods often involve direct inspection or physical testing to assess the quality and distribution of lubrication. One common approach is to visually inspect gears after operation or use dye tracers to observe oil distribution patterns, helping to identify areas of inadequate lubrication or oil starvation.

For measuring resistive torque, traditional methods include direct measurement techniques using torque sensors or dynamometers. These devices allow researchers to assess the torque losses due to lubrication and other factors in a controlled environment. The data obtained from such tests can then be used to evaluate the efficiency of the lubrication system and identify areas for improvement.

Additionally, analytical models and empirical formulas have been developed to estimate the resistive torque and lubrication characteristics. These models often rely on simplified assumptions and idealized conditions to predict the behavior of oil within gear systems. For instance, the classic Reynolds equation and its derivatives have been widely used to model the flow of lubricants in hydrodynamic and elastohydrodynamic lubrication regimes, albeit with limitations in capturing complex flow dynamics, such as churning losses or splash lubrication, encountered in real-world gear applications.

Traditional methods provide valuable insights but often suffer from limitations such as lower accuracy, inability to capture transient and three-dimensional effects, and the need for extensive experimentation, which can be time-consuming and costly. Furthermore, they may struggle with capturing the influence of high-speed operations, temperature variations, and complex gear geometries on lubrication performance.

Despite these limitations, traditional methods have laid the groundwork for understanding gear lubrication and continue to serve as a benchmark against which more advanced simulation techniques, such as CFD, can be validated. The ongoing evolution of these methods, combined with modern advancements in digital sensors and data analysis, still plays a significant role in industrial applications where quick and practical assessments are required.

This section will further detail the specific traditional methods used, their application contexts, and their comparative effectiveness relative to modern CFD approaches.

Visual Inspection and Microscopy

Visual inspection is one of the most straightforward yet essential methods for evaluating the condition of gears and the effectiveness of lubrication. By inspecting gears either directly or through microscopy, engineers can observe wear patterns, pitting, scuffing, or other forms of surface damage that occur due to inadequate lubrication or excessive friction. Visual inspection can reveal immediate signs of failure modes, such as surface discoloration or metal debris, which are indicative of lubricant breakdown or gear distress.

Microscopy provides a more detailed examination of gear surfaces, using tools such as optical microscopes or scanning electron microscopes (SEM). SEM, in particular, allows for high-resolution imaging of the gear surfaces, enabling the identification of microscopic wear mechanisms, surface cracks, or material transfer that are not visible to the naked eye. These microscopic observations help in understanding the micro-scale interactions between the gear surfaces and the lubricant, thus offering valuable data on the performance and failure of lubrication under operational conditions.

Tribological Testing

Tribological testing is a critical component of traditional gear lubrication analysis, focusing on the study of friction, wear, and lubrication performance under controlled conditions. Various tribological tests are designed to simulate the contact conditions in gears using simpler geometries, making them valuable for evaluating the fundamental properties of lubricants.

One common tribological test is the pin-on-disk test, which uses a pin sliding against a rotating disk to replicate the contact between gear teeth. This test is effective in studying the frictional behavior, wear rates, and lubrication film formation under different loads, speeds, and temperatures. Another widely used test is the four-ball wear test, which evaluates the wear prevention properties of lubricants by using steel balls to mimic the high-pressure and sliding motions found in gear applications. This test measures wear scar diameters on the balls to determine the effectiveness of the lubricant in reducing wear.

For more gear-specific testing, the FZG gear test rig is employed, which is a standardized testing apparatus designed specifically for evaluating gear lubrication. The FZG test assesses the scuffing load capacity, wear resistance, and efficiency of lubricants under conditions that closely mimic real-world gear operations. By systematically varying the load, speed, and temperature, the FZG test provides a comprehensive evaluation of the performance of a lubricant in gear systems.

Oil Analysis

Oil analysis is a critical component of traditional gear lubrication studies, offering a way to monitor the condition of the lubricant over time. Regular sampling and analysis of the lubricant oil can reveal important information about contamination, degradation, and the presence of wear particles. Techniques such as spectroscopy are used to detect trace elements in the oil, which can indicate wear of specific materials within the gear system.

Ferrography, another oil analysis technique, involves the separation of wear particles from the oil and their examination under a microscope. This allows for the identification of the types and sizes of wear particles, which can be correlated with specific wear mechanisms or gear failures. Viscosity measurement is also commonly

performed, as changes in the viscosity of the oil can indicate degradation of the lubricant, which can lead to inadequate lubrication and increased wear.

By continuously monitoring the condition of the oil, engineers can predict potential gear failures and determine the optimal time for oil changes or maintenance, ensuring the longevity and reliability of the gear system.

Analytical Modeling

Traditional methods also include the use of analytical modeling to predict lubrication performance in gear systems. Mathematical models and equations are developed to describe key parameters such as lubrication film thickness, pressure distribution, and temperature within the gear contacts. These models are often based on the principles of fluid dynamics and tribology, allowing for the prediction of lubricant behavior under various operating conditions.

One of the most widely used models in gear lubrication studies is the Elastohydrodynamic Lubrication (EHL) theory. EHL theory describes the formation of a lubrication film under high pressure, which is typical in gear contacts. The theory takes into account the elastic deformation of the gear surfaces and the viscous behavior of the lubricant, providing a comprehensive understanding of how lubrication films form and maintain separation between the gear teeth under load.

These analytical models are invaluable for predicting gear lubrication performance without the need for extensive physical testing. They allow for the simulation of different scenarios, such as changes in load, speed, or lubricant properties, providing insights that can guide the design and selection of lubricants for specific gear applications.

Direct Measurement of Resistive Torque

Direct measurement of resistive torque is a critical method used in traditional gear lubrication analysis to assess the energy losses due to friction and lubrication inefficiencies in gear systems. This approach typically involves the use of torque meters, torque sensors, or dynamometers, which are designed to precisely measure the torque required to drive the gear under various operating conditions.

Torque meters are installed directly onto the gear shafts to capture real-time data on the resistive forces acting against the rotation of the gear. These measurements provide an immediate and quantitative assessment of the resistive torque, allowing for a detailed evaluation of how different lubricants and operating conditions affect gear performance. By comparing the measured resistive torque with theoretical values or baseline measurements from well-lubricated systems, engineers can determine the effectiveness of the lubrication and identify areas where friction losses are excessive.

In a typical setup, the torque meter is connected to a data acquisition system, which records the torque values continuously or at specified intervals during the operation of the gear system. This setup enables engineers to monitor the resistive torque dynamically, capturing the effects of changes in load, speed, temperature, and lubricant properties over time. For instance, an increase in resistive torque could indicate lubricant breakdown, contamination, or insufficient lubrication film thickness, all of which can lead to increased friction and wear.

Dynamometers, which can be used in test rigs simulating real-world gear operation, are another powerful tool for direct torque measurement. These devices can measure the input and output torque of gear systems under controlled conditions, allowing for the calculation of efficiency losses due to lubrication. By systematically varying the test conditions, such as changing the type of lubricant, load, or speed, engineers can study the impact of each variable on the resistive torque and identify the optimal lubrication strategies for minimizing energy losses.

The use of torque meters and dynamometers also allows for the validation of analytical models and simulation results. By comparing direct measurements with predictions from models such as those based on elastohydrodynamic lubrication theory or computational fluid dynamics simulations, researchers can refine their models to better reflect real-world conditions. This iterative process of measurement and validation is crucial for developing accurate and reliable predictive tools for gear lubrication.

Overall, the direct measurement of resistive torque provides invaluable data that not only helps in evaluating the current performance of gear lubricants but also guides the development of new lubrication formulations and technologies aimed at reducing friction and improving the overall efficiency of gear systems.

Temperature Measurement

Monitoring the temperature of gears during operation is another traditional method used to assess lubrication performance. Temperature sensors are strategically placed on or near the gears to record the temperature rise, which can indicate the effectiveness of the lubricant in reducing friction and preventing overheating. High temperatures can lead to lubricant breakdown, increased wear, and ultimately, gear failure.

Infrared thermography is a more advanced technique used to visualize the temperature distribution across the gear surfaces. By capturing thermal images of the gears in operation, engineers can identify hotspots where lubrication may be inadequate or where excessive friction is occurring. This information is crucial for optimizing the lubrication system and ensuring that the gears operate within safe temperature limits.

Friction Measurement

Direct measurement of friction is another important method for evaluating lubricant performance in gear systems. Torque sensors or strain gauges are commonly used to measure the friction torque generated during gear operation. This data provides a direct indication of the ability of the lubricant to reduce friction between the gear teeth, which is critical for minimizing wear and improving efficiency.

By analyzing the friction torque data, engineers can compare the performance of different lubricants and make informed decisions about which lubricant is best suited for a particular gear system. This method also allows for the detection of changes in lubrication performance over time, which can signal the need for maintenance or lubricant replacement.

Acoustic Emission and Vibration Analysis

Acoustic emission and vibration analysis are non-invasive techniques used to monitor the condition of gear systems and detect changes in lubrication. Acoustic emission involves listening to the sounds generated by the gears during operation, with specific attention to changes in the frequency or amplitude of the emitted sounds. These

changes can indicate issues such as lubricant film breakdown, increased wear, or the onset of gear damage.

Similarly, vibration analysis involves monitoring the vibrations of the gear system to detect abnormalities. Changes in vibration patterns can signal issues with lubrication, such as increased friction or gear misalignment, which can lead to premature wear or failure. By continuously monitoring acoustic emissions and vibrations, engineers can detect problems early and take corrective action before serious damage occurs.

Surface Roughness and Hardness Testing

Finally, surface roughness and hardness testing are traditional methods used to assess the impact of lubrication on gear wear. Surface roughness is measured before and after testing to determine how the lubrication has affected the gear teeth. A smoother surface typically indicates better lubrication, as the lubricant has effectively reduced friction and wear.

Hardness testing, on the other hand, evaluates the material properties of the gear teeth under operating conditions. Changes in hardness can occur due to the effects of lubrication, temperature, and wear. By understanding how these factors influence the hardness of the gear material, engineers can make better decisions about lubricant selection and gear design to ensure long-term durability.

2.1.7 Applications of Computational Fluid Dynamics Analysis

Computational Fluid Dynamics (CFD) is an advanced and versatile tool increasingly used in the study of gear lubrication systems. CFD software enables the simulation of fluid flow and its interaction with solid objects, such as the gears and the lubricant in a gearbox. By solving complex mathematical equations that govern fluid dynamics, CFD provides a detailed insight into the behavior of lubricants under various operating conditions, making it possible to predict performance in the real world without extensive physical testing.

A critical aspect of using CFD in gear lubrication analysis is the validation of the simulation models. Validation ensures that the numerical models accurately represent real-world phenomena, which is typically achieved by comparing CFD results with experimental data from physical tests. Once validated, CFD models can be trusted to provide reliable predictions, which significantly reduces the need for time-consuming and costly experimental trials.

The benefits of using CFD for gear lubrication analysis are numerous. One of the key advantages is the ability to conduct virtual experiments, which allows for rapid iteration and optimization of the design. Engineers can quickly modify the model based on simulation results, exploring different parameters such as oil viscosity, gear geometry, and operating speeds. This iterative approach enhances the development process by reducing the number of real-world experiments needed, thus saving both time and resources.

CFD also offers the ability to visualize complex fluid behaviors that are difficult or impossible to observe experimentally. For example, it can illustrate the formation of lubrication films, the distribution of oil throughout the gear mesh, and the impact of centrifugal forces at high speeds. This level of detail aids in understanding how lubrication failures might occur and what design modifications could mitigate such risks.

Furthermore, CFD allows for the exploration of advanced lubrication techniques, such as spray lubrication or jet lubrication, and their effectiveness in various gear configurations. By simulating different lubrication strategies, engineers can optimize the design to achieve better efficiency, reduce wear, and enhance the overall durability of the gear system.

One of the new challenges in simulating gear lubrication with CFD arises from the dynamic nature of the gear system. Gears are used to transmit motion and to do so they rotate, this creates a new difficulty. Unlike typical CFD simulations where the object under study is stationary and the mesh remains fixed, gears are in constant motion, particularly rotation. This rotational movement complicates the simulation because the position of the gear changes over time, necessitating modifications to the mesh to accurately represent the new location and orientation of the gear.

In traditional CFD simulations, the mesh within the studied domain is static, with only the fluid moving through it. However, in the case of rotating gears, the mesh must adapt to the movement of the gear. This requirement introduces additional complexity and can significantly increase computational time, as the mesh needs to be updated to reflect the changing position of the gear.

There are primarily two methods for handling this dynamic mesh scenario:

Dynamic Mesh (Re-meshing): In this approach, the mesh is regenerated at each time step to account for the new position of the gear. This method, while accurate, can be computationally expensive and time-consuming due to the frequent need to recreate the mesh.

Rigid Mesh Movement: Alternatively, the mesh can be rigidly moved into the space. For example, a cylindrical mesh can be created around the rotating gear, which moves rigidly with the gear. This mesh will then be surrounded by a fixed mesh where only the interfaces between the two are moving. This method avoids the need for re-meshing by keeping the mesh fixed with the gear. Although this approach still requires updating the interface connections between the rotating mesh and the fixed mesh, it generally results in lower computational costs compared to dynamic re-meshing.

The software Simerics MP+, used in this study, employs the latter method of variable mesh handling, which allows for efficient simulation of rotating gears by using a mesh that moves with the gear, reducing the need for continuous re-meshing.

Computational Fluid Dynamics in Gear Lubrication Analysis

The application of Computational Fluid Dynamics (CFD) in gear lubrication analysis represents a significant advancement for engineering design and optimization. As drivetrain and transmission systems become more complex and demanding, understanding lubrication behavior at a granular level is crucial to achieving high performance and longevity. CFD analysis provides engineers with a robust framework for investigating fluid dynamics within gears, helping to address key challenges related to efficiency, wear, and durability. This approach not only accelerates the design process but also enhances reliability by simulating real-world conditions with great precision. Below are some of the main benefits and limitations of using CFD in gear lubrication analysis.

Advantages:

- **Detailed Insights**: CFD provides a comprehensive visualization of fluid flow and lubrication distribution within the gear system, which is difficult to achieve through experimental methods alone.
- **Cost and Time Efficiency**: By reducing the need for extensive physical prototyping and testing, CFD saves both time and costs associated with the development process.
- **Flexibility and Optimization**: CFD allows for rapid adjustments to the model, enabling quick evaluation of various design scenarios and optimization of lubrication strategies.
- **Enhanced Predictive Capabilities**: Once validated, CFD models offer reliable predictions that can improve the understanding of gear performance under different operating conditions.
- **Risk Reduction**: CFD helps in identifying potential lubrication issues, such as inadequate film formation or excessive friction, early in the design process, thus reducing the risk of failure in actual applications.
- **Complex Problem Solving**: CFD is capable of handling complex geometries and interactions within the gear system, such as transient effects, turbulence, and multiphase flows.

Disadvantages:

- **High Computational Resources**: CFD simulations can be computationally intensive, requiring significant processing power, memory, and time, especially for high-fidelity models.
- **Model Validation and Accuracy**: Ensuring the accuracy of CFD simulations requires rigorous validation against experimental data, which can be time-consuming and costly.
- **Complex Setup and Expertise**: Setting up CFD simulations requires a high level of expertise in fluid dynamics, meshing, and numerical methods, which can be a barrier for some users.
- **Sensitivity to Input Parameters**: CFD results can be highly sensitive to the choice of input parameters, such as boundary conditions, turbulence models, and fluid properties, which may impact the reliability of the outcomes.
- **Potential for Over-Simplification**: To manage computational costs, some aspects of the gear and lubrication system may need to be simplified, which could lead to less accurate or incomplete results.
- **Dependence on Software Capabilities**: The accuracy and reliability of CFD analysis are dependent on the capabilities of the chosen software and its algorithms, which may have limitations in certain scenarios.

Difference Between Eulerian and Lagrangian Approach in CFD Analysis

In modern computational fluid dynamics (CFD), two main numerical methods are widely used to solve fluid dynamics problems: Eulerian and Lagrangian. These approaches differ fundamentally in how they track the movement and interaction of fluid particles, and each has its advantages and limitations depending on the application. The two approaches will be explained in the next paragraphs, but the basic idea is illustrated in Figure 2.2.

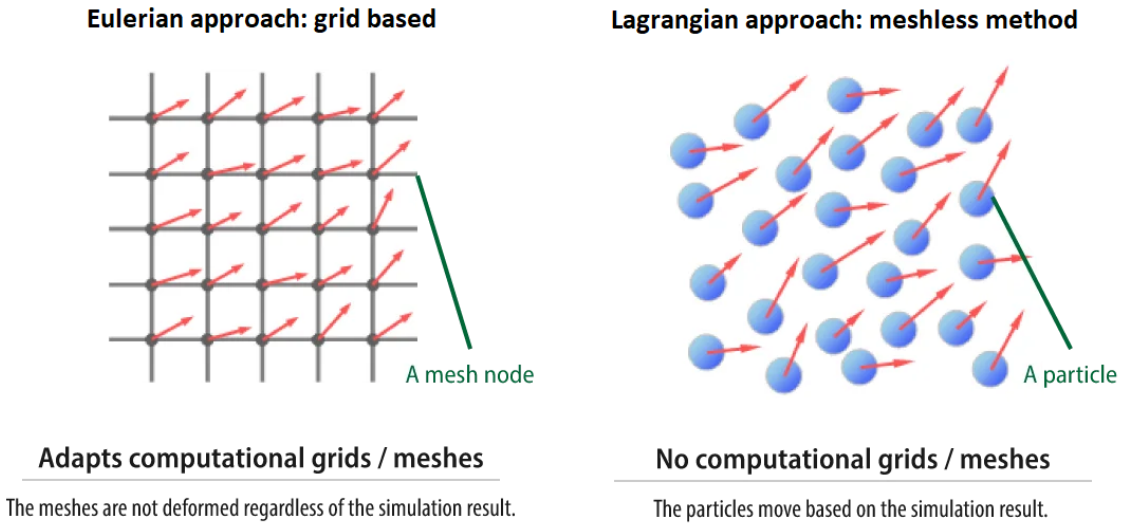

Figure 2.2: Eulerian vs Lagrangian method in CFD analysis

Eulerian Approach: Grid-Based Methods

The Eulerian approach is the more traditional and widely used method in CFD simulations. In this approach, the focus is on specific locations in the spatial domain, and the fluid flow is analyzed as it passes through these fixed points over time. The spatial domain is discretized into a grid or mesh, and the unknown variables, such as pressure, velocity, and temperature, are computed at the nodal points of this mesh. Eulerian approaches, often referred to as grid-based methods, include the finite element method (FEM), finite volume method (FVM), and finite difference

method (FDM). These methods have been extensively applied to a variety of engineering fields, including structural mechanics, heat transfer, electromagnetics, and fluid dynamics.

Finite Element Method (FEM) The Finite Element Method (FEM) is a numerical technique originally developed for structural analysis but has since found widespread application in other fields such as fluid dynamics and electromagnetics. In FEM, the CAD model is divided into small, finite-sized elements of simple geometric shapes, forming what is known as the finite-element mesh.

For fluid dynamic analysis, partial differential equations (PDEs) governing the flow behavior, such as the Navier-Stokes equations, are solved over each element. The solution is approximated using basis functions, typically linear or quadratic polynomials, which describe how the field variables (velocity, pressure, etc.) behave within each element. These local solutions are then assembled into a global system of equations, resulting in a large, sparse matrix that can be solved using specialized numerical solvers.

The flexibility of FEM allows it to handle complex geometries and boundary conditions, but it may be computationally expensive, particularly when applied to fluid-structure interaction (FSI) or multiphase flow problems.

Finite Volume Method (FVM) The Finite Volume Method (FVM) is another grid-based method that is especially popular for solving fluid flow problems. Like FEM, the domain is discretized into small regions, but in FVM these regions are called control volumes or cells. The governing equations are derived from the principle of conservation (mass, momentum, and energy), ensuring that fluxes entering and exiting a control volume are balanced.

FVM is particularly suited for fluid dynamics because it ensures the conservation of physical quantities across the domain, making it highly accurate for solving the Navier-Stokes equations. This method is the basis for many commercial CFD codes, including Simerics MP+ software used in this study, and is commonly applied in applications ranging from automotive aerodynamics to turbomachinery and gear lubrication.

Finite Difference Method (FDM) The Finite Difference Method (FDM) is a simpler, more direct approach to discretizing partial differential equations. In FDM, the derivatives in the governing equations are approximated using finite differences at discrete points on a grid. This method is most effective on structured grids (regular, rectangular grids) and is known for its computational efficiency in problems with simple geometries.

FDM is widely used in meteorology, oceanography, and astrophysical simulations, where regular grids can be applied. However, its application in engineering problems involving complex geometries, such as automotive components, is limited due to the difficulty in fitting a regular grid to irregular shapes.

Limitations of the Eulerian Approach While Eulerian methods are highly successful in a wide range of fluid dynamics applications, they can face significant challenges in problems involving discontinuities or topological changes in the domain, such as those seen in rotating machinery or free surface flows. In cases where the domain itself changes during the simulation, re-meshing or mesh deformation is required, which can be computationally expensive and time-consuming. This re-meshing process is one of the key limitations of grid-based methods when dealing with moving or deforming boundaries, making them less efficient for certain types of simulations.

Lagrangian Approach: Meshless Methods

In contrast to the Eulerian approach, the Lagrangian approach focuses on the motion of individual fluid particles as they move through space and time. Instead of solving the equations at fixed points in the domain, Lagrangian methods track the trajectory and properties of discrete fluid particles or nodes, which move with the flow. This approach is particularly effective in cases where the domain undergoes large deformations or where free surfaces are present. Unlike the Eulerian framework, where the properties of the fluid are distributed over a fixed grid, in the Lagrangian approach the fluid properties are tied to the particles themselves, and their evolution is tracked based on the history of the particles.

Some of the widely used Lagrangian-based methods include the Smoothed Particle Hydrodynamics (SPH), MPS (Moving Particle Simulation), and Discrete Element Method (DEM).

Smoothed Particle Hydrodynamics (SPH) Smoothed Particle Hydrodynamics (SPH) is a popular meshless method, particularly for simulating free surface flows, fluid-structure interactions, and multiphase flows. In SPH, the fluid is represented by a collection of particles, and the fluid properties are computed by averaging or "smoothing" over a certain neighborhood of particles. Each particle carries its own set of properties, such as velocity and pressure, and these values are updated based on interactions with neighboring particles.

SPH is particularly useful in scenarios with complex boundary conditions, large deformations, or discontinuities, such as wave breaking, splashing, and gear lubrication in dynamic environments. Its Lagrangian nature allows for more natural handling of problems where the fluid interfaces or boundaries are in motion, without the need for re-meshing as in grid-based methods.

Moving Particle Simulation (MPS) The Moving Particle Simulation (MPS) method, also known as the Moving Particle Semi-Implicit (MPS) method, is a meshless numerical approach primarily used for simulating fluid flows, particularly incompressible and multiphase flows, as well as applications in fluid dynamics involving complex or dynamic geometries. The MPS method is particularly well-suited for scenarios involving large deformations or fluid motion, such as waves, free-surface flows, fluid-structure interactions (FSI), and impact simulations.

In the MPS method, the fluid is represented by particles, and the motion of each particle is determined based on interactions with neighboring particles, using a kernel function. The MPS method is conceptually similar to the Smoothed Particle Hydrodynamics (SPH) method, with both methods approximating the strong form of the partial differential equations (PDEs) through integral interpolants. However, there are key differences between the two methods:

- The MPS method applies simplified differential operators based solely on a local weighted averaging process, without requiring the gradient of the kernel function.
- In contrast to SPH, the MPS method employs a semi-implicit prediction-correction process to solve the governing equations, while the original SPH method uses a fully explicit solution approach.

These differences allow the MPS method to offer advantages in certain types of fluid simulations, particularly in cases involving free-surface flows or large-scale deformations, where the stability and accuracy of the semi-implicit approach can be beneficial.

Discrete Element Method (DEM) The Discrete Element Method (DEM) is another Lagrangian approach that focuses on simulating the motion of individual particles, often applied in granular flows or where solid particles are suspended in a fluid. Similar to SPH, DEM tracks the motion of particles, but it is more often applied to simulate solid bodies than fluid dynamics. When combined with CFD (often referred to as CFD-DEM), it can be used to study fluid-particle interactions, such as those in slurry flows or sediment transport.

Advantages of the Lagrangian Approach Lagrangian methods have several advantages over Eulerian methods in specific cases. For instance, they are better suited for problems involving free surfaces, fluid-structure interaction, and large deformations, such as those encountered in gear lubrication simulations with rotating components. In these scenarios, the fluid interacts with moving surfaces, and tracking the motion of individual particles allows for a more accurate and computationally efficient solution. Moreover, the absence of a fixed mesh eliminates the need for complex re-meshing algorithms, reducing computational overhead and improving accuracy in cases of large domain deformation.

The choice between Eulerian and Lagrangian approaches in CFD analysis largely depends on the nature of the problem being studied. While Eulerian grid-based methods such as FEM, FVM, and FDM are highly effective for a wide range of engineering problems, they may struggle with cases involving complex boundary movements, discontinuities, or large deformations. In contrast, Lagrangian methods such as SPH and DEM excel in such scenarios, providing a more flexible and computationally efficient solution. In the context of gear lubrication simulations, where rotating components and dynamic fluid-structure interactions are prominent, Lagrangian methods offer distinct advantages, making them a promising alternative to traditional grid-based approaches.

Hybrid Methods: Combining Eulerian and Lagrangian Approaches

In addition to the classical Eulerian and Lagrangian approaches, hybrid methods have been developed to take advantage of the strengths of both frameworks. These methods are particularly useful in situations where complex interactions between fluids and solid particles occur, or where moving boundaries and multiphase flows need to be accurately simulated. Hybrid methods allow for a more flexible representation of the fluid domain by combining the fixed-grid nature of Eulerian methods with the particle-tracking characteristics of Lagrangian approaches.

One of the most prominent examples of hybrid approaches is the Immersed Particle Method (IPM), but other methods such as the Particle-in-Cell (PIC), Arbitrary Lagrangian-Eulerian (ALE), and Finite Volume Particle Method (FVPM). methods are also used in specialized CFD applications.

Immersed Particle Method (IPM) The Immersed Particle Method (IPM) is a hybrid approach where fluid flow is modeled using an Eulerian framework (on a fixed grid), while individual solid particles are treated using a Lagrangian description. IPM is particularly useful in scenarios involving fluid-particle interactions, where solid objects or particles are immersed in the fluid and interact dynamically with the surrounding flow.

In IPM, the fluid is modeled using the Navier-Stokes equations on a traditional fixed mesh, while particles are tracked in a Lagrangian manner. The interaction between the particles and the fluid is handled using immersed boundary techniques, which apply source terms to the governing equations to represent the forces exerted by the particles on the fluid and vice versa.

The key benefit of IPM is that it allows the particles to move freely within the fluid without requiring the grid to deform or re-mesh. This is especially useful in cases like gear lubrication, where the rotating components inside the fluid would otherwise necessitate constant re-meshing in purely Eulerian approaches.

IPM is commonly applied in:

- **Particle-laden flows**: Simulating solid particles suspended in a fluid, such as sediment transport or particulate matter in lubrication systems.
- **Fluid-structure interactions**: Modeling the movement of solid particles or bodies through fluids, such as the interaction between rotating gears and lubrication oil.
- **Multiphase flows**: Capturing complex behaviors in flows involving multiple fluid phases or fluid-solid interactions.

Particle-in-Cell (PIC) The Particle-in-Cell (PIC) method is another hybrid approach that combines an Eulerian grid with Lagrangian particles to track fluid properties such as velocity and pressure. The particles move according to the velocity field computed on the Eulerian grid, making PIC suitable for simulations involving complex advection-dominated flows. This method reduces numerical diffusion, which can occur in Eulerian-only approaches.

Arbitrary Lagrangian-Eulerian (ALE) The Arbitrary Lagrangian-Eulerian (ALE) method is a hybrid approach that allows the mesh to deform and move with the flow in a manner that blends both Eulerian and Lagrangian characteristics. This allows ALE to efficiently handle large domain deformations, such as those in fluid-structure interactions or rotating machinery, while maintaining the computational advantages of a fixed grid in regions where the fluid flow is stable.

Finite Volume Particle Method (FVPM) The Finite Volume Particle Method (FVPM) is a numerical approach that combines the traditional Finite Volume Method (FVM) with the concept of Lagrangian particles. Essentially, this method merges the benefits of a discrete grid (common in FVM) with the flexibility of Lagrangian particles (as in meshless methods like SPH). It is particularly well-suited for simulating complex fluid dynamics and fluid-structure interactions (FSI), such as turbulent flows, multiphase flows, and scenarios involving moving solid bodies in a fluid. However, it can be computationally intensive and may face challenges in particle management and numerical stability.

Advantages and Challenges of Hybrid Methods Hybrid methods like IPM, PIC, ALE, and FVPM offer several benefits over purely Eulerian or Lagrangian methods:

- **Improved handling of moving boundaries**: By tracking particle motion and fluid flow simultaneously, hybrid methods handle situations with complex moving boundaries or interfaces without the need for frequent re-meshing.
- **Increased accuracy in fluid-particle interactions**: These methods offer better accuracy when modeling interactions between solid objects and fluid flow, such as in gear lubrication or sediment transport.
- **Reduced computational cost**: Compared to fully Lagrangian approaches, hybrid methods can be more computationally efficient since they rely on a fixed grid for much of the fluid domain.

However, hybrid methods also come with some challenges, such as the need for more complex coupling between the Eulerian and Lagrangian components and potentially higher computational costs when simulating large numbers of particles or complex interactions.

Simerics MP+ Approach

Simerics MP+, the software utilized for this study, operates using a finite volume method (FVM) based on the Eulerian framework. This numerical approach is widely used in CFD applications due to its ability to conserve fluxes across control volumes, making it particularly well-suited for fluid flow simulations. However, one of the standout features that distinguishes Simerics MP+ from similar CFD software is its efficient handling of dynamic or evolving geometries during simulations, specifically in cases where traditional re-meshing would be computationally expensive.

In conventional CFD software, when the geometry of the domain changes over time, such as in simulations involving rotating machinery or moving boundaries, a common approach is to re-mesh the computational domain at each time step. This process, known as re-meshing, involves generating a new mesh that adapts to the updated geometry. While this method can accurately capture the changes in the domain, it is computationally demanding, especially for complex geometries or when the domain changes rapidly. Re-meshing often leads to significant increases in computational cost due to the need to frequently reconstruct the mesh and reinitialize the solution at each new time step.

Simerics MP+, on the other hand, uses a more innovative approach by implementing a rigid mesh movement technique that avoids the need for frequent re-meshing. Instead of completely regenerating the mesh at every time step, Simerics MP+ moves the mesh rigidly to accommodate changes in the domain geometry. This technique is particularly effective for problems involving rotating or translating objects where the motion can be described without altering the overall topology of the mesh.

However, Simerics MP+ is also capable of deforming the mesh, for example in the case of two meshing gears. Specifically, the mesh is deformed in the meshing region while maintaining a constant number of cells, thus preserving the integrity and functionality of the mesh thanks to its advanced algorithms. This mesh deformation process enables the study of phenomena where the mesh cannot move rigidly while allowing for significantly faster mesh updates. In contrast, traditional re-meshing techniques can alter the number of cells, which may result in the appearance or disappearance of cells, causing issues with mesh reconstruction and solution reinitialization, problems that are entirely avoided with Simerics MP+.

For example, in the case of simulating the flow around a rotating gear, a cylindrical mesh can be constructed around the gear to handle its rotational movement. The

rest of the computational domain, which may not experience any dynamic changes, can be meshed using a stationary or fixed mesh. At each time step, instead of re-meshing the entire domain, Simerics MP+ simply rotates the cylindrical mesh with the rotating gear in a rigid manner, ensuring that the computational mesh conforms to the movement of the gear while the fixed portion of the mesh remains unchanged. This strategy not only maintains the mesh quality but also significantly reduces the computational time required for the simulation, as the only operation needed is updating the mesh interface connections between the rotating and stationary regions.

The benefit of this rigid mesh movement approach becomes particularly evident in rotating machinery or automotive gear lubrication simulations, where the rotating components, such as gears, continuously move through the lubricant. By applying rigid mesh movement, Simerics MP+ avoids the high computational cost of re-meshing, which would otherwise be necessary at every time step to track the motion of the gears. The software only needs to update the connections between the rotating and fixed mesh regions, which is computationally less demanding than a full re-mesh.

Moreover, this approach provides greater stability and accuracy in simulations where the geometry does not undergo drastic topological changes, making it ideal for cases like gear lubrication, where the rotational motion of gears is repetitive and predictable. The ability to apply this method efficiently translates into shorter simulation times without sacrificing the precision of the results. Consequently, for scenarios where rigid mesh movement is applicable, this method proves to be far more efficient than a complete re-meshing strategy, particularly when large-scale simulations or time-sensitive analyses are required.

This approach highlights the adaptability of Simerics MP+ to industrial applications where rotating components are a key focus, such as in pumps, turbines, compressors, and automotive systems. By reducing computational overhead and allowing for faster simulations, Simerics MP+ enables conducting more detailed analyses in shorter times, facilitating design optimization and performance evaluation.

The use of the rigid mesh movement approach, combined with its foundation in the finite volume method, offers a significant advantage in terms of computational efficiency, making it a highly effective tool for dynamic fluid simulations, especially those involving rotating machinery or moving boundaries. The ability to simulate complex fluid-structure interactions with reduced computational demands makes it a valuable asset in both academic research and industrial applications.

Analytical Analysis of the Resistive Torque

Before starting with the experiment an analytical study of the expected resistive torque value due to the oil jet impacting into the rotating teeth of the gear has been conducted. Figure 2.3 shows the general geometry configuration, in which the oil is aimed at the center of the gear, while the clockwise rotation of the gear causes the air around it to acquire a velocity in the same direction.

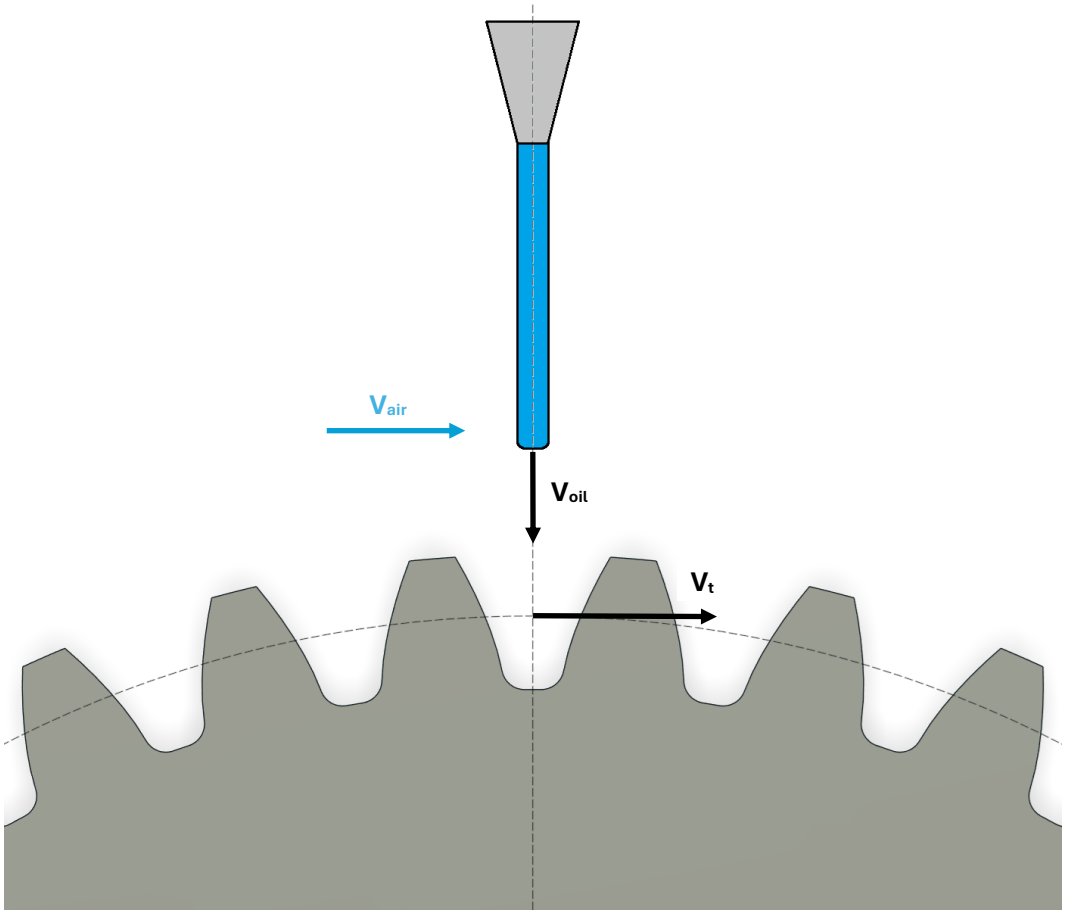

Figure 2.3: Oil jet configuration

The resistive torque created by the oil jet impacting the teeth of the gear can be estimated by calculating the variation in oil momentum during the impact of the oil. In the case reported in Figure 2.3, this value can be calculated using Equations 2.1 and 2.2.

$$F_{res} = \dot{m}_{oil} \cdot \Delta V_p = \dot{m}_{oil} \cdot V_t \tag{2.1}$$

$$T_{res} = \frac{P_{res}}{\omega} = \frac{F_{res} \cdot V_t}{\omega} = \frac{\dot{m}_{oil} \cdot V_t^2}{\omega} = \dot{m}_{oil} \cdot \omega \cdot R_{pitch}^2 \tag{2.2}$$

Where:

F_{res}: is the resistive force acting on the gear $[N]$,

$\dot{m}_{oil}$: is the oil mass flow rate $[kg/s]$,

ΔV_p: is the variation of tangential velocity of the oil at the pith circle $[m/s]$,

V_t: is the tangential velocity of the gear at the pith circle height $[m/s]$,

T_{res}: is the resistive torque acting on the gear $[Nm]$,

P_{res}: is the resistive power acting on the gear $[W]$,

ω: is the rotating speed of the gear $[rad/s]$,

R_{pitch}: is the pitch radius of the gear $[m]$.

As shown in Equation 2.2 the resistive torque is expected to be directly proportional to the mass flow rate of the oil and to the rotating speed of the gear, while it is quadratic proportional to the gear dimensions. This means that by varying these parameters it will be possible to change the output torque during the experiment, and, as will be shown in the next chapter, it will be necessary to modify some of them in order to obtain a measurable result.

Nevertheless, these results are only valid when the oil jet is pointed at the center of the gear. If the oil jet is inclined, as shown in Figure 2.4, the resistive torque changes as a function of the α angle, according to Equations 2.3 and 2.4.

$$F_{res} = \dot{m}_{oil} \cdot \Delta V_p = \dot{m}_{oil} \cdot (V_t - V_{oil} \cdot sin(\alpha)) \tag{2.3}$$

$$T_{res} = \dot{m}_{oil} \cdot \left(\omega \cdot R_{pitch}^2 - \frac{V_{oil} \cdot \sin(\alpha)}{\omega} \right) \tag{2.4}$$

From Equation 2.4 the resistive torque is expected to increase when the angle α is negative, and so when the oil jet is directed opposite to the gear rotation. In the following chapter, these results will be exploited during the experimental laboratory setup.

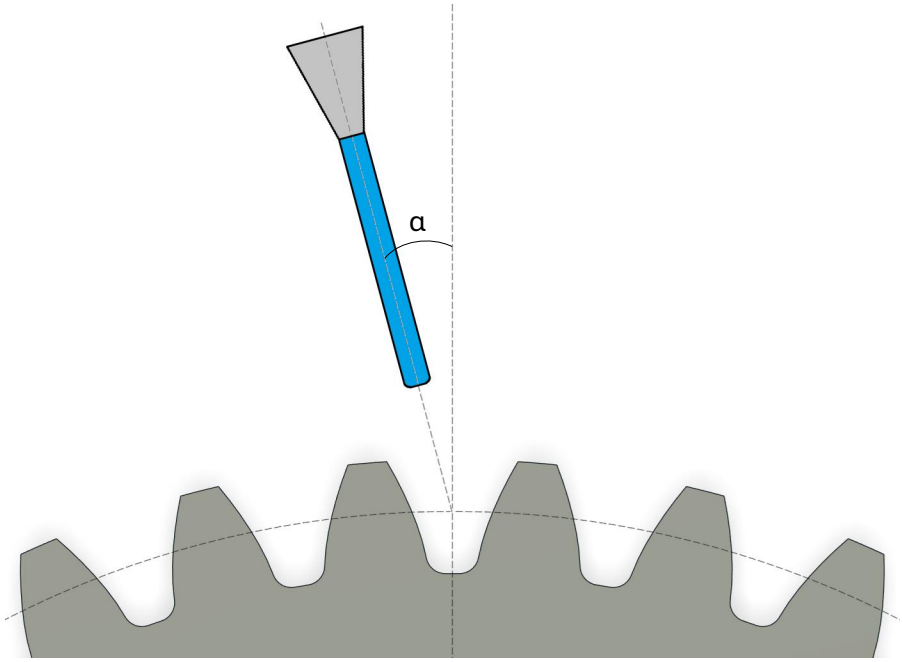

Figure 2.4: Angled oil jet configuration

In the experimental conditions set within the laboratory environment, it is anticipated that the velocity of the surrounding air could have a significant influence on the behavior of the oil jet. This is primarily due to the interplay between the pressure and temperature of the air, which results in a value of air density that is substantial under these controlled conditions. As the air moves around the gear, it interacts with the oil jet, exerting forces that alter its trajectory and dynamics.

The velocity of the air, in particular, plays a crucial role in modifying the behavior of the jet, as it is not only moving around the gear but also directly colliding with the oil stream. This interaction can cause the jet to deform, bend, or even potentially break up, especially when the volumetric flow rate of the oil is low and the speed of the gear is high. In such cases, the shear forces generated by the air movement can destabilize the jet, leading to a disruption in the uniformity of the flow. The magnitude of this effect is expected to be more pronounced at lower flow rates, where the jet is more susceptible to external disturbances, due to the lower velocity of the jet.

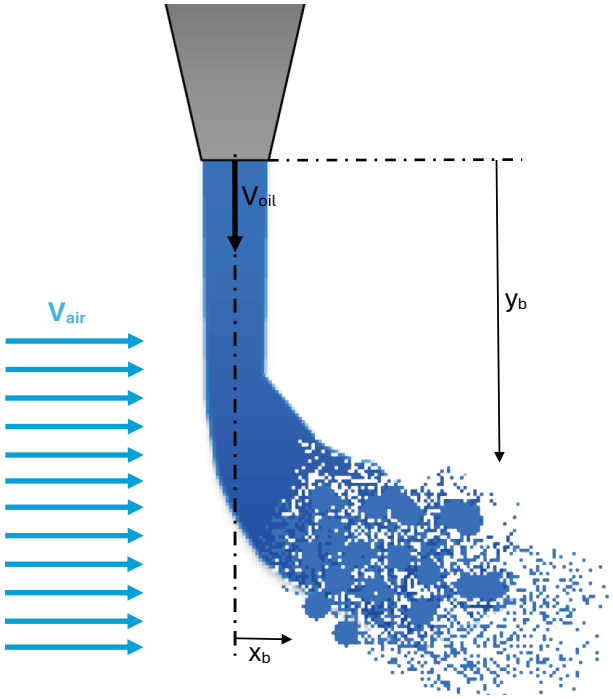

Figure 2.5: Oil jet breakup

This phenomenon, often referred to as jet break-up or jet instability, is influenced by a variety of factors, including the relative velocity between the air and the oil, the viscosity of the fluid, and the ambient pressure and temperature within the laboratory setting. The extent to which the air velocity influences the behavior of the jet can be observed and quantified in the laboratory experiments, as depicted in Figure 2.5. This figure illustrates the observable effect of air movement on the oil jet, showing how the jet deforms or breaks apart.

To further evaluate this behavior and predict the conditions under which the jet will break or remain stable, a set of governing equations can be applied, and have been reported in Equations 2.5, 2.6, and 2.7.

$$q = \frac{\rho_{oil} \cdot V_{oil}^2}{\rho_{air} \cdot V_{air}^2} \tag{2.5}$$

$$We_{cf} = \frac{\rho_{air} \cdot d_{oil} \cdot V_{air}^2}{\sigma} \tag{2.6}$$

$$\frac{y_b}{d_{oil}} = k \cdot q^n \tag{2.7}$$

Where:

q: is the liquid to gas momentum ratio $[-]$,

ρ_{oil}: is the oil density $[kg/m^3]$,

V_{oil}: is the oil velocity $[m/s]$,

ρ_{air}: is the air density $[kg/m^3]$,

V_{air}: is the air velocity $[m/s]$,

We_{cf}: is the crossflow Weber number $[-]$,

d_{oil}: is the oil jet diameter $[m]$,

σ: is the oil surface tension $[N/m]$,

y_b: is the breakup height of the oil jet $[m]$,

k e n: are constants that depend on experimental conditions and properties of the fluid $[-]$.

From Equation 2.7, it can be noted that the breakup height y_b of the oil jet exhibits a power-law dependence on the liquid-to-gas momentum ratio, q, with an exponent n. This relationship implies that the breakup height y_b of the oil jet increases proportionally to q^n. In practical terms, any increase in q results in a proportional increase to the n-th power in the jet penetration or breakup height. The liquid-to-gas momentum ratio q, as defined in Equation 2.5, depends on the densities and velocities of both the oil and the air. This equation indicates that:

- An increase in oil density ρ_{oil} raises q, thereby enhancing the penetration depth of the oil jet.
- Conversely, higher air density ρ_{air} reduces q, leading to decreased jet penetration. This suggests that denser air conditions counteract oil jet penetration.
- Increasing the oil velocity V_{oil} results in a higher q, thus promoting greater jet penetration.
- Increasing the air velocity V_{air}, however, reduces q, limiting jet penetration due to the stronger resistance from the crossflow.

Equation 2.7 also highlights the proportional dependence of the breakup height y_b on the oil jet diameter d_{oil}, meaning that an increase in the oil jet diameter leads to a corresponding increase in jet penetration. The constants k and n in Equation 2.7 are empirically derived and reflect the specific dependencies of the breakup height on q and other parameters, based on experimental conditions and fluid properties. Their values are critical for accurate CFD simulations, enabling precise predictions of oil jet behavior under varying operating conditions.

This analysis is essential for the CFD simulation of gear lubrication, as it provides insights into how adjusting parameters such as oil jet velocity, density, and diameter, along with understanding crossflow effects, can optimize jet penetration and improve lubrication performance under different airflow conditions.

Chapter 3

Methodology

In this chapter, a comprehensive explanation of the methodology, the tools utilized in the virtual study, and the experimental equipment for the laboratory testing will be presented. The aim of this section is to provide a thorough understanding of the process used to investigate the dynamics of gear lubrication, as well as to outline the software and equipment selected to support this investigation. A key objective of this research is to assess the performance and accuracy of Simerics MP+, a computational fluid dynamics (CFD) software, in modeling complex fluid behavior under real-world conditions.

The central focus of this thesis is to validate the use of Simerics MP+ as a reliable simulation tool for future engineering studies, particularly those involving gear lubrication and other fluid-mechanical systems. To achieve this, a real-world case study will first be modeled and simulated in the virtual environment using Simerics MP+. This case study will then be replicated in a laboratory experiment using a test bench, where the main parameters will be measured. The simulated results will subsequently be carefully analyzed and compared to the empirical data obtained from the physical testing. This comparison will serve as the foundation for evaluating the accuracy and predictive capability of the software.

The ultimate goal is not only to validate the simulation tool but also to assess its efficiency, accuracy, and practicality for future use in design and optimization processes. In particular, the study will focus on determining whether Simerics MP+ can provide a cost-effective, time-efficient, and reliable method for simulating gear

lubrication, potentially reducing the need for extensive physical testing in future research and development. Through a systematic comparison between simulation and experimental results, this study will also highlight any limitations of the software and propose potential improvements or considerations for future studies. Additionally, this chapter will outline the specific equipment and methodologies used in both the simulation and experimental phases, ensuring a clear understanding of the processes involved in the validation study.

The general interface of the Simerics MP+ software has been reported in Figure 3.1.

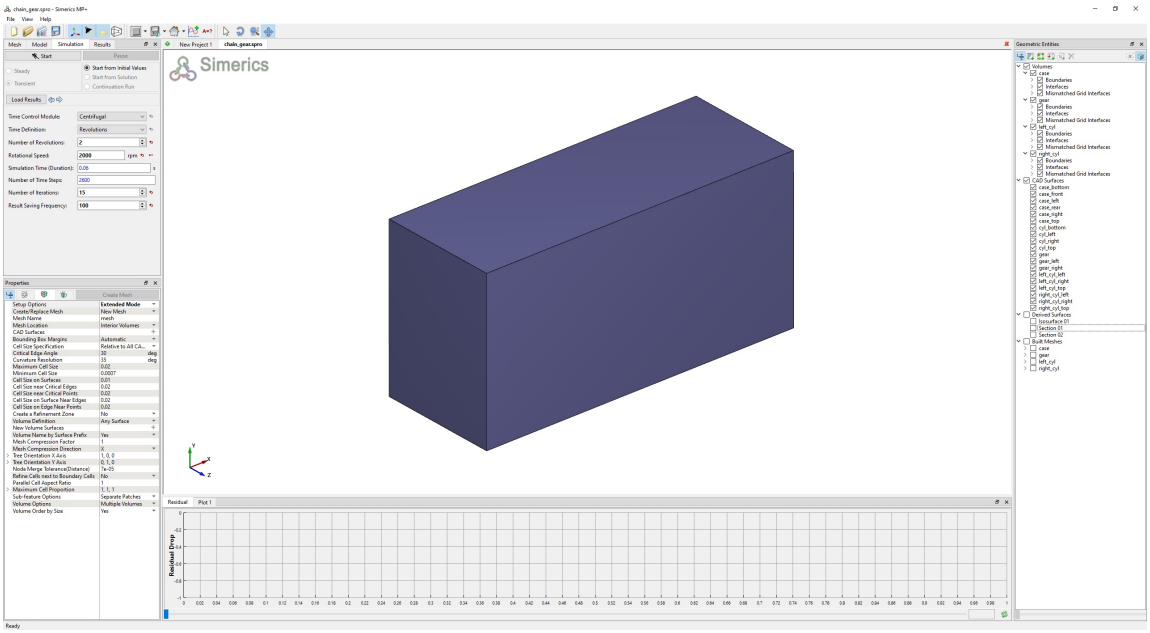

Figure 3.1: Simerics MP+ interface

3.1 Overview and Application of Simerics MP+ in Gear Lubrication CFD Modeling

In this study, the computational fluid dynamics (CFD) software Simerics MP+ has been employed to model gear lubrication, a critical aspect of the overall performance of the system. Simerics MP+ is an advanced, multi-physics CFD software, specifically designed to simulate complex fluid dynamics, thermal behavior, cavitation, and turbulence. Widely used across various industries such as automotive, aerospace, and industrial manufacturing, Simerics MP+ offers cutting-edge simulation capabilities that make it ideal for gear lubrication modeling, where high levels of accuracy and computational efficiency are paramount.

One of the key strengths of Simerics MP+ is its ability to handle a variety of simulation challenges with high computational efficiency. It integrates robust solvers that are well-suited for simulating the interaction between fluids and moving mechanical components. This feature is especially relevant for modeling systems like pumps, valves, compressors, and heat exchangers, which involve complex fluid behavior. For gear lubrication, the ability of the software to simulate detailed fluid flow patterns around moving gears is invaluable for optimizing lubrication performance, predicting wear, and improving the reliability of mechanical components.

A major reason for selecting Simerics MP+ for this research is its innovative handling of domain variations over time. Unlike traditional CFD software that relies on a complete re-meshing of the domain at each time step, Simerics MP+ utilizes a unique approach where the rigid motion of the mesh is recalculated at every time step. This technique maintains computational integrity while significantly reducing the simulation time. In traditional CFD approaches, re-meshing is a time-consuming process, as the entire domain must be recalculated every time the position of objects within the fluid environment changes. The mesh motion approach in Simerics MP+ preserves accuracy while streamlining the computational process, making it particularly suited for applications involving rapidly moving components, such as gears in lubrication modeling.

Although the reduction in simulation time is a significant advantage, the primary goal of this study remains the accuracy and validation of the simulation results. A critical aspect of using any CFD software is ensuring that the simulated results reflect real-world behavior, especially in complex fluid dynamics cases like gear lu-

brication. To achieve this, the study will involve a comprehensive validation process. A controlled test case will be modeled in Simerics MP+ and then replicated in a laboratory environment. In this experimental setup, key physical parameters such as oil pressure, temperature, and volumetric flow rate will be measured.

Most importantly, the primary measurement will focus on the average resistive torque generated by the oil as it interacts with the rotating gear. This resistive torque, caused by the oil colliding and flowing around the teeth of the gear, is a critical factor in determining the efficiency and performance of the gear lubrication system. By capturing this resistive torque data, it is possible to directly evaluate the ability of the software to accurately predict the mechanical losses due to fluid resistance. Additionally, high-speed cameras will be used to visually inspect the fluid motion around the gears, further validating the accuracy of the simulation in terms of fluid dynamics.

This dual approach, quantitative measurements and visual analysis, will enable a detailed comparison between the simulated and actual fluid behavior, providing a robust evaluation of Simerics MP+ predictive accuracy in modeling gear lubrication dynamics.

The choice of Simerics MP+ as the CFD software for this gear lubrication modeling study is driven by its advanced capabilities, innovative simulation techniques, and efficiency in handling moving components. Its application in this research not only aims to reduce simulation time but also to ensure the high fidelity of the results, which will be rigorously validated through experimental testing. By leveraging the strengths of Simerics MP+, this study contributes to a deeper understanding of lubrication dynamics in gear systems, facilitating more accurate predictions and improved design optimization for automotive applications.

3.2 Laboratory Test Setup

Before initiating the simulations, a thorough evaluation of the available equipment in the laboratory was conducted. This evaluation was crucial to ensure that the experimental setup would be feasible with the resources at hand. The capabilities and limitations of the equipment had to be carefully considered in order to design an experiment that could accurately replicate the conditions modeled in the simulations. The equipment available in the lab was found to be suitable for conducting the necessary tests, providing both the precision and control required to validate the computational results. The core of the laboratory setup is the test bench, a photo of which has been reported in Figure 3.2.

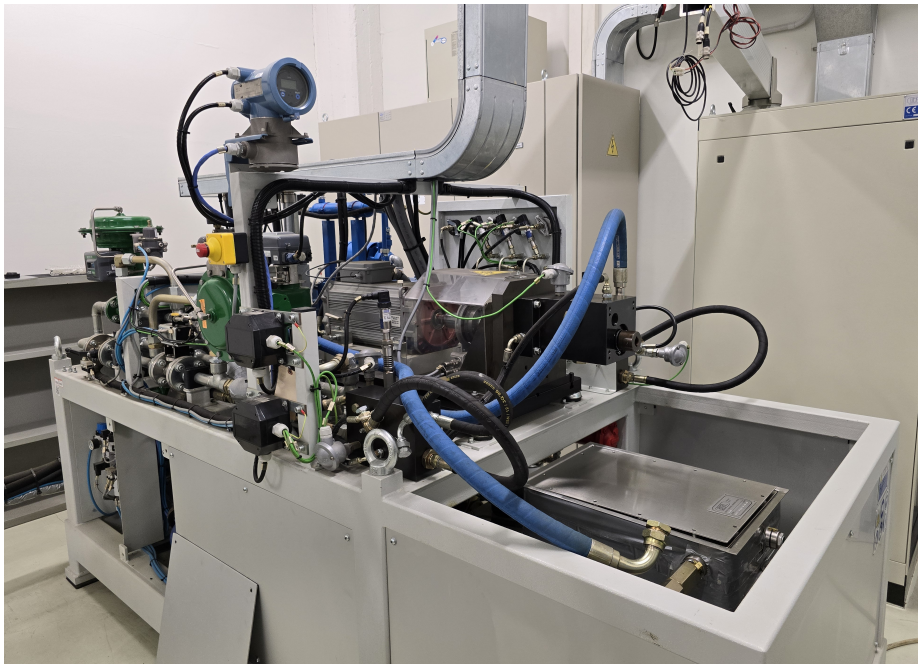

Figure 3.2: Laboratory test bench

The test bench features an electric motor capable of reaching rotational speeds of up to 9000 revolutions per minute (rpm), Figure 3.3 shows a picture of the electric motor. This high-speed motor is ideal for replicating the operational conditions of rotating mechanical components such as gears, which are central to the lubrication study. The motor is connected to a mounting shaft through a torque meter, a critical

piece of equipment for this experiment. The torque meter has a measurement range from 0.1 Nm to 50 Nm, allowing for precise detection of the torque generated during the rotation of the gears. This wide measurement range ensures that even small variations in resistive torque, such as those caused by the oil film interacting with the gear teeth, can be accurately captured. In Figure 3.4 it is possible to see the torque meter of the test bench.

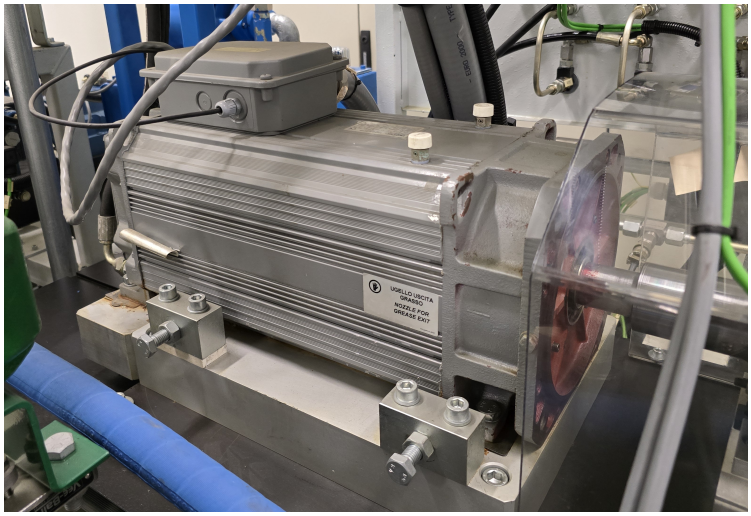

Figure 3.3: Test bench electric motor

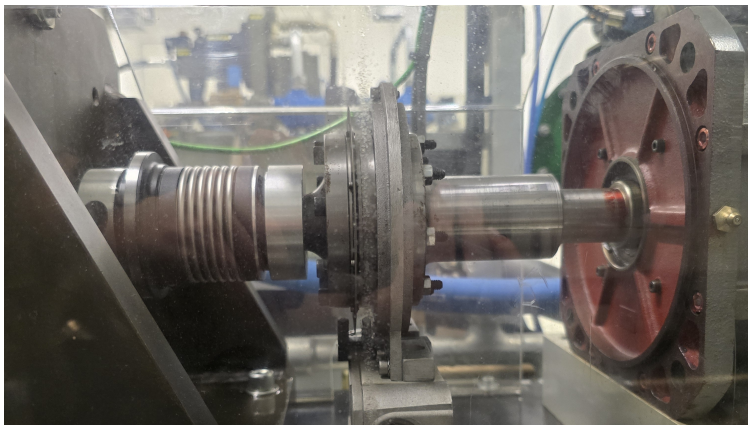

Figure 3.4: Test bench torque meter

In addition to the motor and torque meter, the laboratory is equipped with an oil supply line, a photo of which has been reported in Figure 3.5. This circuit is capable of delivering pressurized hydraulic oil to the test setup and can reach pressures of up to 75 bar, with a maximum volumetric flow rate of 25 liters per minute (L/min).

Figure 3.5: Hydraulic oil delivery system

The limit of 25 L/min is due to the spool type chosen for the proportional control valve present in the circuit. The valve model is Danfoss PGV 32 and the progressive oil flow characteristics depending on spool type have been reported in Figure 3.6. Looking at the plots the proportional valve can regulate different maximum volumetric flow rates depending on the inserted spool, from 10 to 130 L/min.

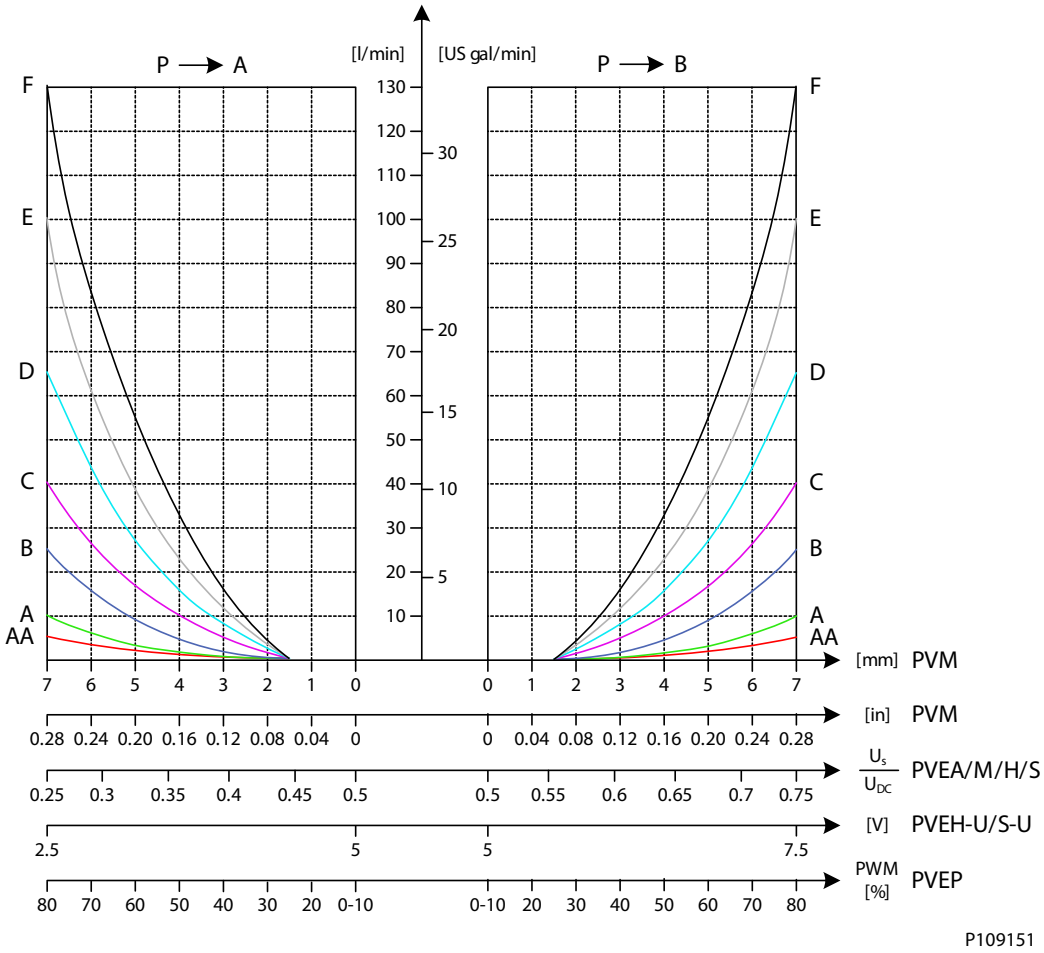

Figure 3.6: PVG 32 - Progressive oil flow characteristics for different spool type

As will be explained in the Results section, for the experimental setup a maximum requested volumetric flow rate of 10 L/min will be used during the experiments. For this reason, spool B has been chosen in the laboratory setup. Having a maximum volumetric flow rate comparable to the requested one allows for more precise control of the delivered volumetric flow rate. This value is set on the valve with a proportional control command and not by a close loop control. For this reason, a gear flow meter will be present at the delivery port of the circuit, this allows the operator to check the actual volumetric flow rate and to act on the proportional control to fine-tune the delivered volumetric flow rate.

These specifications are more than enough to simulate the high-pressure lubrication systems typically found in automotive and industrial applications. The oil used in this experiment is hydraulic oil, which closely resembles the properties of lubricants commonly used in gear systems, ensuring that the test conditions closely mimic real-world scenarios.

To better understand the circuit of the oil delivery system a hydraulic scheme has been reported in Figure 3.7. As highlighted the system has several components. First, the system has a reservoir in which the oil is stored. From this reservoir is connected the inlet of a fixed positive displacement pump driven by an electric motor. In the outlet of the pump is visible a pressure gauge to monitor the delivery pressure of the pump. Other than the pressure monitoring instrument on the pump delivery side there is a pressure relief valve, connected with the return line to the reservoir. the pressure setting of this valve is 75 bar and it is the limiting factor of the system, however, this will be more than enough for the study.

After this part, the delivery side of the pump is fed to the proportional flow control valve. This four-port three-position valve is spring-centered with float center, it can be activated manually or with a proportional solenoid. When the valve is activated the volumetric flow rate is proportional to the valve position and so to the solenoid command, following the trend previously presented in Figure 3.6.

On the delivery side of the valve is mounted a gear flow meter, this instrument is used to verify the delivered volumetric flow rate and to accordingly change the solenoid command. After that, it is visible the final component of the delivery line, a pressure transducer, used to measure the pressure upstream of the nozzle.

On the other side of the valve is possible to see the return line, after exiting the valve the oil passes through a cooler and a filter with optical access and magnetic element before returning into the reservoir. A final measuring instrument is available in the reservoir and is a temperature sensor used to record the oil temperature value to accordingly evaluate the density and viscosity of the hydraulic oil.

The pump in the oil delivery circuit has a maximum volumetric flow rate of 55 L/min. The flow meter mounted on the circuit is a VSE 1 GPO12V with a measure range from 0.05 to 80 L/min.

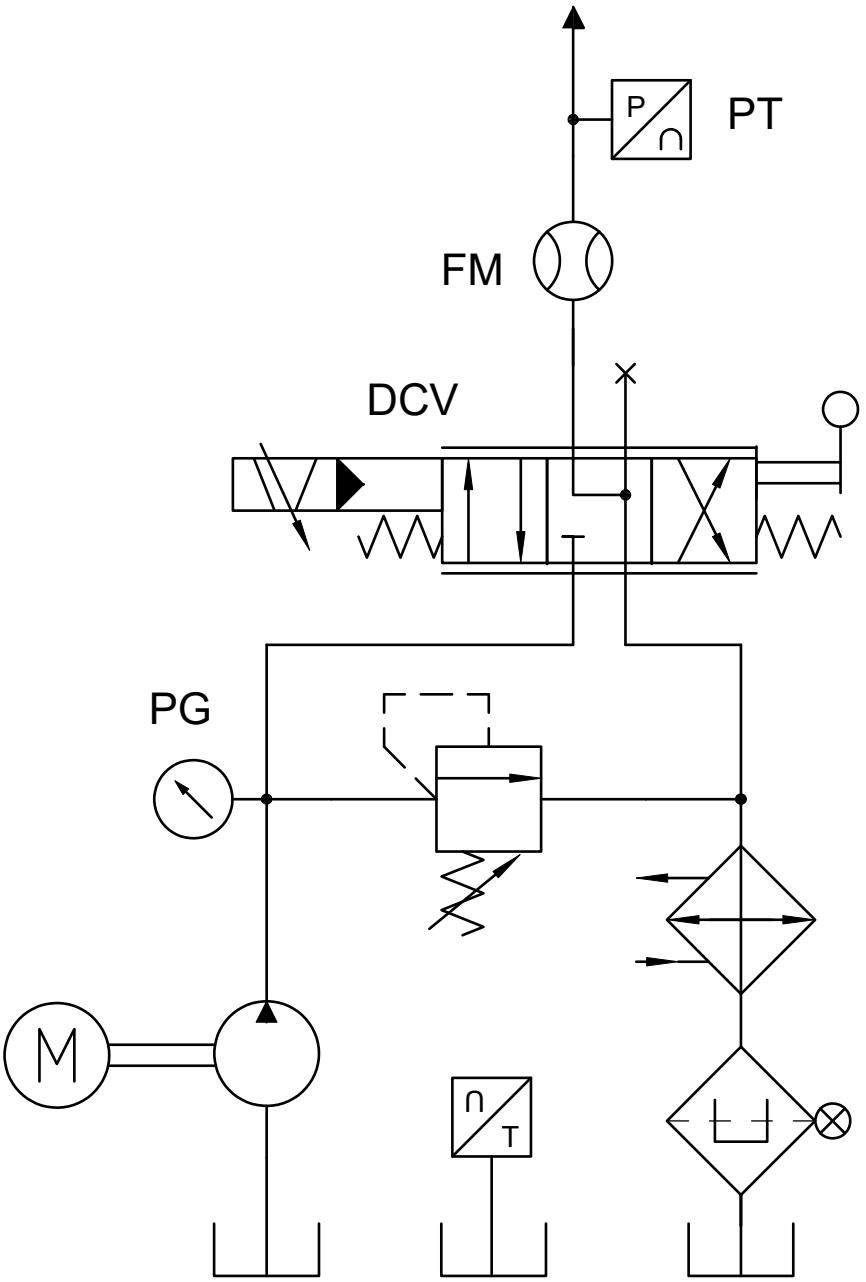

Figure 3.7: Hydraulic circuit of the oil delivery system

The pressure transducer used on the threaded rod is a GS XPM5 with a maximum measurement value of 100 bar, a picture of this sensor is reported in Figure 3.8. As visible the sensor resembles a bolt with the sensing part on the tip. It uses an M5 threading and will be directly mounted onto the threaded rod, a few centimeters upstream of the nozzle.

Figure 3.8: Oil pressure sensor

The high-speed camera that will be used for the recording is a Photron FASTCAM MINI AX200 type 900k. This camera is equipped with a monochromatic 12-bit sensor with dimensions of 1024x1024px (20um x 20um) and it is capable of reaching a maximum frame rate acquisition of 9000,000 frames per second (fps). Despite the high technical characteristics, the camera body has a compact dimension, being 120 mm high, 120 mm wide, and 94 mm deep. A picture of the camera has been reported in Figure 3.9.

Figure 3.9: High speed camera

The test bench and oil supply system are housed in a controlled laboratory environment, with the test bench located in a dedicated room for safety and operational efficiency. This room is equipped with remote monitoring and control capabilities, allowing the experiment to be managed from an adjacent control room. The control room is separated from the test area by a safety glass window, providing a clear view of the test bench while ensuring that operators can monitor the test in real time without being exposed to any potential hazards. This setup not only enhances safety but also facilitates precise control of the test conditions, as adjustments to motor speed, torque measurements, and oil flow can be made remotely with high accuracy.

The laboratory setup, with its combination of high-speed rotational capabilities, precise torque measurement, and controlled oil flow, provides an ideal platform for validating the simulation results generated in Simerics MP+. By replicating the gear lubrication process in a controlled, real-world environment, this setup allows for a de-

tailed comparison between simulated predictions and actual physical measurements. The use of high-speed cameras to capture fluid motion during the tests will further enhance the validation process, offering visual insights into the fluid dynamics at play, and complementing the quantitative data collected from the torque meter and oil supply system.

Figure 3.10 shows a close-up view of the test bench spindle and mounting system. The threads in the four corners will be used for the fastening of the case, while the gear drive shaft will be secured to the spindle using its securing system.

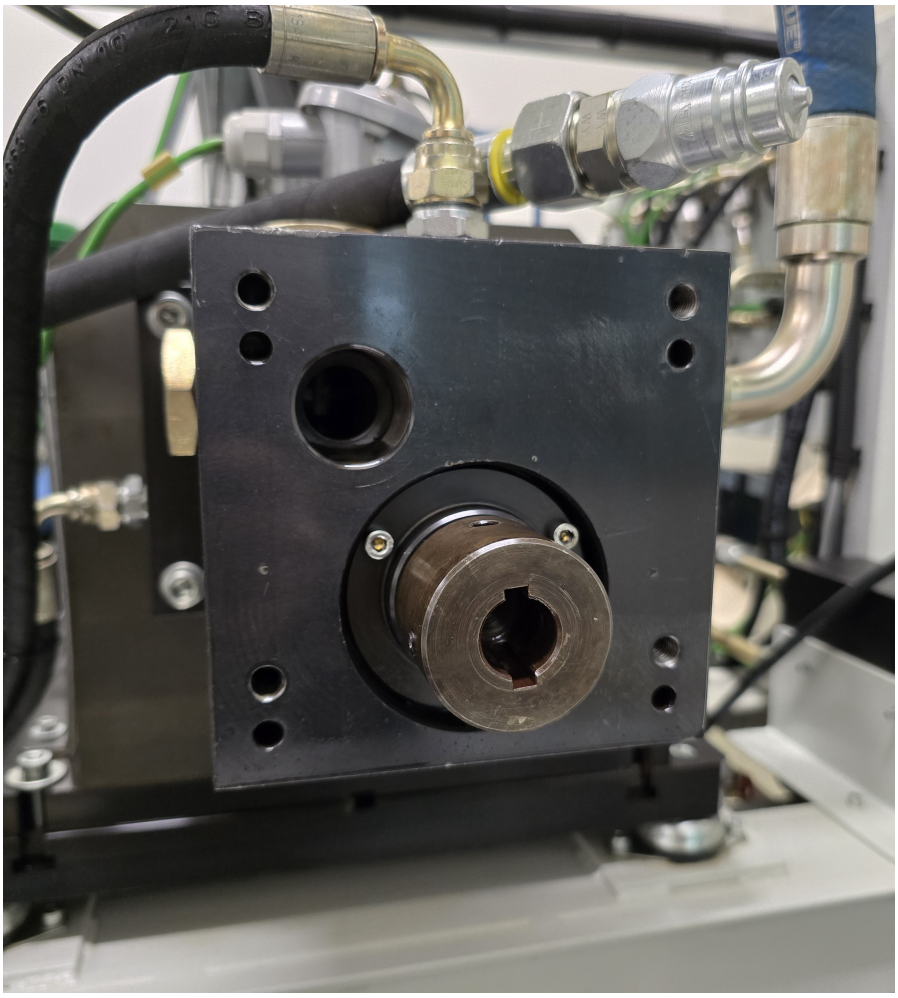

Figure 3.10: Test bench spindle

3.3 Design of the Experimental Case Study

Taking into account the capabilities and limitations of the available test bench equipment, the initial concept for the experimental case study was developed. The main idea revolves around a rotating gear housed inside a controlled environment, such as an enclosed metal box, where an oil jet is directed at the gear. The primary objective of this setup is to analyze the interaction between the oil and the gear teeth, which is expected to induce a resistive torque on the gear shaft. Depending on the orientation of the oil jet and the rotational direction of the gear, this torque could either oppose or assist the rotation of the gear, allowing for a detailed examination of how the fluid dynamics influence gear performance in real-world applications.

While the test bench provides an excellent platform for this study, certain constraints had to be accounted for when designing the experiment. The oil supply system, with its high-pressure capacity of up to 75 bar and a volumetric flow rate of up to 25 L/min, does not present any limitations for the type of gear lubrication study proposed. However, the resolution of the torque meter does impose a restriction on the experiment. The torque meter can measure torques in the range of 0.1 to 50 Nm, but to ensure meaningful and reliable data, the test case was configured to generate a resistive torque of at least 1 Nm. This threshold ensures that the torque generated by the interaction between the oil and the gear is sufficiently large to be accurately measured by the torque meter, minimizing the effect of noise and measurement inaccuracies. Moreover, the torque meter also measures the resistance of the supporting slide bearings, this value must be measured and subtracted from the output value of the torque meter. Having a resistive torque value that is too low could make it difficult to distinguish between the two torques, resulting in a measuring error larger than acceptable. However, with a minimum torque of 1 Nm, this issue is significantly mitigated.

Another crucial aspect of the experimental design was the selection of the gear dimensions. Several considerations were made to optimize the experiment while ensuring safety and ease of operation. The gear thickness was limited to 12 mm, and the maximum radius was restricted to 80 mm. These dimensions strike a balance between providing a large enough surface area for the oil jet to impact while still maintaining manageable operating conditions within the test bench. Additionally, the relatively small gear size allows for practical adjustments to the setup, such as changing the jet offset from the center of the gear. By increasing this offset, the experiment is expected to generate a greater resistive torque due to the increased

moment arm, offering more flexibility in controlling the variables of the experiment.

The final gear geometry has been reported in Figure 3.11 and was chosen after reviewing similar studies and considering feasible gear dimensions. A spur gear geometry was chosen to simplify high-speed recording, designed with 38 teeth, a pitch circle diameter of 152 mm, an outer circle diameter of 160 mm, and a pressure angle of 20 degrees. The module of the gear was set at 4 mm, which is consistent with standard industrial gears. For mounting purposes, the gear will be equipped with a central centering hole with a diameter of 10 mm, and three screws will be used to securely fasten the gear to the drive shaft. This mounting configuration ensures stability during high-speed rotation and precise alignment, critical for the accuracy of both the experimental and simulated results. The parameters of the gear have been reported also in Table 3.1.

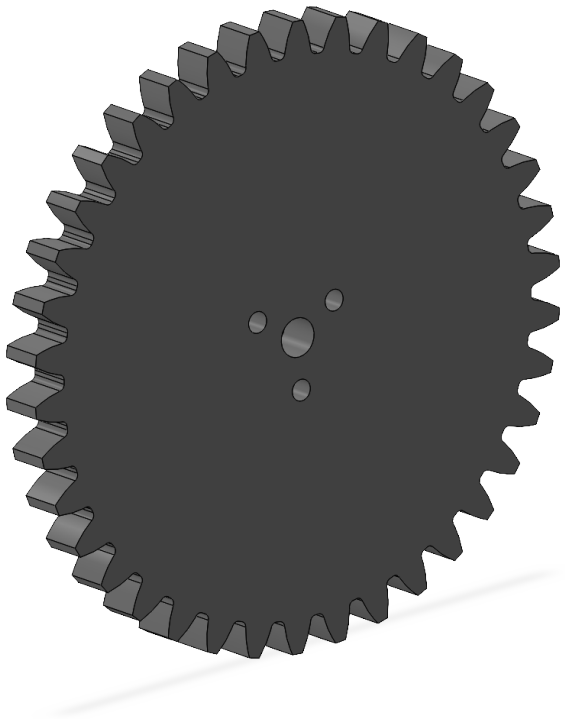

Figure 3.11: CAD model of the gear

Gear parameters	
tooth number [−]	38
module [mm]	4
pressure angle [°]	20
pitch circle diameter [mm]	152.00
outer circle diameter [mm]	160.00
centering hole diameter [mm]	10.00
thickness [mm]	12.00

Table 3.1: Gear parameters

Once the basic configuration and experimental limitations were defined, the next step was to initiate the virtual simulation study. A simplified model of the gear geometry was used to conduct preliminary simulations, focusing on identifying the most significant parameters that influence the resistive torque generated by the oil interacting with the gear. This initial approach allowed for faster simulation times, which was critical for exploring different configurations and narrowing down the test conditions that would later be validated through physical experiments. By simplifying the model, secondary effects, such as the gear interaction with the air inside the case, were intentionally neglected to streamline the computational process. However, the results obtained from these simplified simulations were still valuable, as they allowed for a direct comparison between different scenarios, guiding the selection of the optimal configuration for the final, more detailed simulations.

The final stage of the virtual study will involve the creation of a fully detailed simulation model that incorporates all relevant physical factors, such as fluid dynamics, gear motion, and oil-gear interaction. This comprehensive model will then be used to simulate the exact conditions that will be recreated in the laboratory. Although the initial simplified simulations will not provide results directly comparable to the physical experiments due to the omission of certain secondary effects, they will serve as an essential tool in refining the final experimental setup. By focusing on the most influential parameters during the initial phase, the study will be able to significantly reduce the time required for each simulation, ensuring that the laboratory experiments are conducted efficiently and with a high degree of accuracy.

3.3.1 Jet Velocity Evaluation

During the laboratory experiment, could be interesting to evaluate the effect of different ratios between the oil jet speed and the tangential speed of the gear. In order to easily know the oil jet velocity based on nozzle size and volumetric flow rate a quick analytical study on this aspect has been conducted. The limiting factor in the laboratory is the maximum pressure that the oil supply circuit can deliver, and this value is 75 bar. For this reason, the maximum Δp available at the nozzle is of 75 bar. Using this information and assuming a C_d value of 0.85, it is possible to evaluate the maximum volumetric flow rate for each nozzle diameter and the corresponding jet speed using Equations 3.1 and 3.2.

$$Q = C_d \cdot A \cdot \sqrt{\frac{2 \cdot \Delta p}{\rho}} \tag{3.1}$$

$$V_{oil} = \frac{Q}{A} \tag{3.2}$$

Where:

Q: is the volumetric flow rate $[m^3/s]$,

C_d: is the discharge coefficient $[-]$,

A: is the area of the nozzle $[m^2]$,

Δp: is the pressure drop across the nozzle $[Pa]$,

ρ: is the oil density $[kg/m^3]$.

V_{oil}: is the oil velocity $[m/s]$.

Once the maximum volumetric flow rate and maximum oil jet velocity have been calculated for each nozzle size, with Equations 3.1 and 3.2, it is possible to create a line passing from the maximum of each nozzle size and the axis origin. Doing so, every intermediate value can be deducted from the graph reported in Figure 3.12. All the nozzle sizes can reach a maximum velocity of 112.26 m/s with a limit pressure of 75 bar, but for every nozzle a different value of volumetric flow rate is necessary, with higher flow rates necessary for the bigger nozzle. With this plot, starting from the desired oil jet velocity, it is possible to choose which combination of volumetric flow rate and nozzle diameter matches the requested jet velocity.

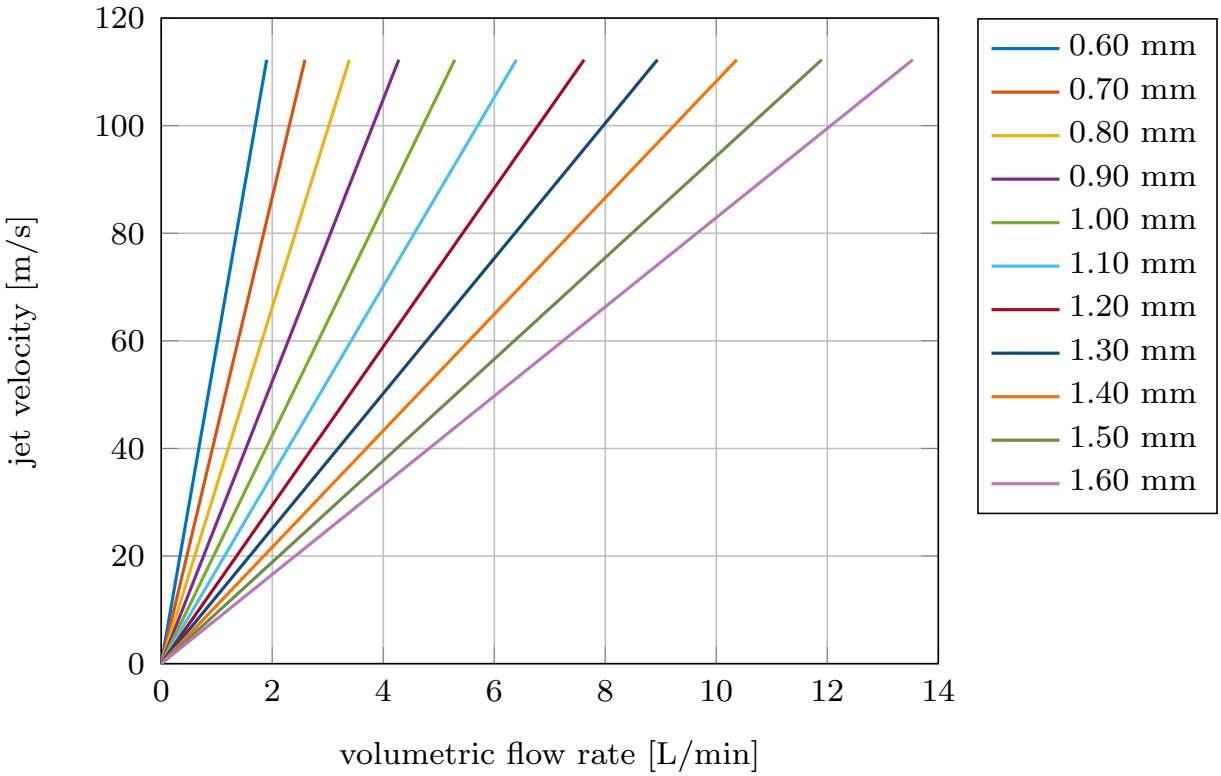

Figure 3.12: Jet velocity as a function of volumetric flow rate for different jet diameters

3.4 Simulation Setup of the Experimental Case Study

After thoroughly defining the experimental setup, it became possible to initiate the simulation phase to establish the operating conditions that would later be applied in the real-world laboratory experiment. This phase of the research is critical, as it allows for the exploration and refinement of key parameters within a virtual environment, reducing the risk of unforeseen issues when transitioning to physical testing. The simulations not only serve to predict the behavior of the system under various conditions but also help in optimizing the experimental parameters for the most accurate comparison between simulated and real-world results.

As previously mentioned, the simulation process is divided into two stages: a preliminary set of partial simulations and a final complete simulation of the full gear system. The initial simulations are intentionally simplified, focusing on modeling only a portion of the gear system, typically a few teeth, to gain insights into the general behavior of specific parameters, such as resistive torque and oil flow interaction. These partial simulations provide a fast and efficient means of evaluating the sensitivity of the system to changes in variables, such as the angle of the oil jet or the rotational speed of the gear. Based on the findings from these simplified models, more refined settings can be identified and used to inform the full-scale simulations.

For both the partial and complete simulation stages, several key parameters remain constant to ensure consistency between the virtual and real-world experiments. The type of oil used in the simulation mirrors the hydraulic oil that will be supplied in the laboratory, and its temperature is controlled to reflect the conditions of the lab testing. Additionally, ambient air conditions, such as temperature and pressure, are set according to the predefined environment of the test bench room. These baseline parameters are crucial for ensuring that the simulations accurately replicate the experimental setup, thereby providing meaningful and comparable results between the virtual and physical studies.

Table 3.2 has outlined the fixed parameters for both the simplified and complete simulation stages, detailing the properties of the oil, the environmental conditions, and any other relevant constants. For what concern the rotating speed of the gear it was immediately fixed to 8000 rpm, as will be seen in the simulation results this value is necessary to obtain the requested minimum torque. The speed was not set

to the test bench limit to guarantee continuous operation and to maintain a margin between the operational and max speed.

Constant simulation parameters	
oil density $[km/m^3]$	860
air density $[km/m^3]$	1.1766
ambient pressure $[Pa]$	101325
oil viscosity $[Pa \cdot s]$	0.06
oil surface tension $[N/m]$	0.04
gravity acceleration $[m/s^2]$	9.81
gear rotational speed $[rpm]$	8000

Table 3.2: Constant simulation parameters

By keeping these parameters constant across all simulations, any observed variations in results can be directly attributed to the specific changes made to the operating conditions, such as gear speed, oil jet position, or the volumetric flow rate of the oil. This consistency is essential for isolating the effects of individual variables and ensuring that the insights gained from the virtual simulations can be effectively applied in the real-world experimental setup.

The final step in this phase will be the execution of the full simulation for each operating condition identified in the partial studies. These full simulations will incorporate the entire gear system, allowing for a comprehensive analysis of fluid-structure interactions and the overall behavior of the gear under conditions that closely resemble those of the forthcoming laboratory tests. In the next sections, the two types of simulations, partial and complete, will be discussed in detail, along with the methods used to interpret the results and prepare for the final experimental validation.

The simulations were performed on a Dell Precision 7820 workstation, configured for high-performance computational tasks. The system is powered by an Intel Xeon Platinum 8268 processor, featuring 24 cores and 48 threads, with a base clock speed of 2.90 GHz and a maximum turbo frequency of 3.90 GHz. It is equipped with 192 GB of DDR4 RAM, provided by six 32 GB modules running at 2666 MT/s, ensuring

ample memory capacity for complex simulations.

The workstation also includes a Radeon Pro WX 5100 dedicated GPU. However, as the simulation software relies solely on CPU resources, the GPU was not utilized in this context.

3.4.1 Partial Simulations

In the early stages of the simulation process, a simplified geometry, referred to as partial simulation, was employed. The purpose of this initial study is to reduce the computational demands by focusing on a smaller section of the gear system, specifically a few teeth, while still capturing the essential interactions between the oil jet and gear teeth. This method allows for rapid exploration of key variables such as resistive torque and oil flow behavior, without the need for full-scale simulations of the entire gear. The insights gained from these partial simulations will serve as the basis for refining the final complete simulation.

The geometry for the partial simulations is a fraction of the total domain. The axial length of the domain is constrained to the thickness of the gear, which is 12 mm, thus representing only the active cross-section of the gear interacting with the oil jet. However, all lateral boundaries of the domain are left open, allowing oil to exit from both sides of the gear. This is essential for maintaining the realism of the simulation since, in real-world conditions, the oil would not be trapped within the thickness of the gear, and unwanted boundary effects would distort the flow pattern, leading to unrealistic results. Allowing the oil to freely exit prevents artificial accumulation and ensures that the flow dynamics mimic those found in actual operating conditions.

Additionally, the domain surrounding the gear in the radial direction is minimized to around a distance of 20 mm from the tip of the gear tooth, providing just enough space to capture the flow characteristics without unnecessarily increasing the domain size. In this reduced model, the top walls of the domain are also open, allowing the oil to exit freely radially from the gear. These open boundaries at the top and sides are a key feature of the simulation, as they prevent the oil from being recirculated back into the gear, which could otherwise create unrealistic fluid pressure and resistive forces.

The most significant simplification in this partial simulation lies in limiting the

circumferential span to only a few teeth, rather than modeling the entire circumference of the gear. Typically, only three to five teeth are modeled in this phase, enough to capture the essential fluid-gear interaction without incurring in the computational expense of simulating the full gear. By isolating a section of the gear, the simulation can focus more closely on understanding how the oil jet impacts the gear tooth surfaces and how resistive forces are generated. This setup allows for an efficient analysis of fluid behavior and torque effects with faster computation times and manageable meshing requirements.

The domain in the vicinity of the oil jet injection point is similarly simplified. Instead of modeling the entire surrounding case or nozzle system, the jet is represented by a small annular section with a thin cylindrical guide that controls the oil trajectory of the jet. This simplified setup is sufficient to verify whether the oil jet can traverse between the different mesh zones and still maintain realistic flow patterns. Furthermore, limiting the jet region significantly reduces the complexity and dimension of the mesh, allowing for a higher mesh density in critical areas around the gear teeth without extending the overall computational cost. A finer mesh is especially crucial in capturing the precise interactions between the oil and the surface of the gear, which in turn impacts the accuracy of the resistive torque measurements.

This partial simulation configuration strikes a balance between model simplicity and detail, focusing computational power on the most critical aspects of the gear-lubrication system. By minimizing the domain, using open boundaries, and concentrating on a small number of teeth, the simulation achieves a high level of resolution while maintaining reasonable processing times. The ability to conduct fast simulations enables iterative testing, where different gear speeds, oil jet angles, and volumetric flow rates can be explored and optimized before proceeding to the complete simulation phase.

Figure 3.13 illustrates the CAD model used for the partial simulations, clearly showing the reduced domain and the position of the oil jet relative to the gear teeth. This geometry provides an ideal starting point for understanding the most significant variables affecting gear lubrication dynamics, paving the way for more detailed and comprehensive simulations later in the process. The figure depicts the base gear geometry with two additional bodies added to facilitate the meshing process in Simerics MP+. An annular section, added to the gear teeth under study to define the meshing area in the CFD software and an annular case, inserted at the top of the gear, to created the fixed case mesh. To the case is connected the jet injection point, which consists of a small cylinder with a diameter matching the one of the

threaded nozzle hole. The general idea of this configuration is to rotate the gear and the annular section clockwise while maintaining the case with the oil injection point fixed. However, the two bodies are not in contact. This is because an annulus template mesh will be added in the software, which will be inserted between the two bodies to maintain a constant cell orientation between the rotating and fixed mesh. Once the geometry is complete it needs to be saved as a .stl file, allowing it to be uploaded into the Simerics MP+ environment.

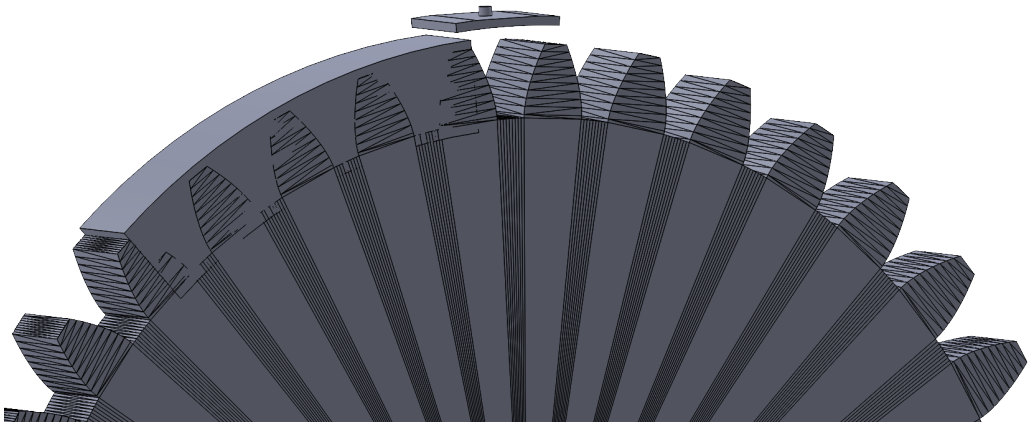

Figure 3.13: CAD model of the partial simulations

The result of importing the geometry and defining the mesh is reported in Figure 3.14 and with more detail in 3.15. The final mesh consists mainly of three components:

1. **Rotating gear mesh**: This mesh follows the rotational movement of the gear. As illustrated in the figure, it is created using the gear teeth profile and the annular circular section added in the CAD model. During the simulation, this mesh rotates rigidly around the center of the gear while its top part maintains constant contact with the bottom of the annulus mesh. The mesh was created using the general mesh template.

2. **Rotating annulus mesh**: This mesh follows the rotational motion of the gear mesh and is created using the annulus mesh template available in Simerics MP+. The main purpose of this mesh is to maintain a consistent cell orientation along the MGI between the rotating and fixed meshes. This is achieved by exploiting the annulus mesh template, which defines the mesh

with fixed elements in the radial, axial, and tangential directions, rather than in the Cartesian coordinate system employed by the general mesh template.

3. **Fixed case mesh**: This mesh remains stationary throughout the entire simulation duration and its primary function is to create the oil jet injection point. Its bottom surface always maintains contact with the rotating annulus mesh and was created using the general mesh template with dimensions matching those of the gear.

The three meshes are always in contact with one another, for this reason, it is important to define these surfaces as a mismatched grid interface (MGI) in the software. Defining an MGI enables information exchange between the meshes and it is fundamental for the success of the simulation. The MGI must be defined for both, stationary and moving meshes.

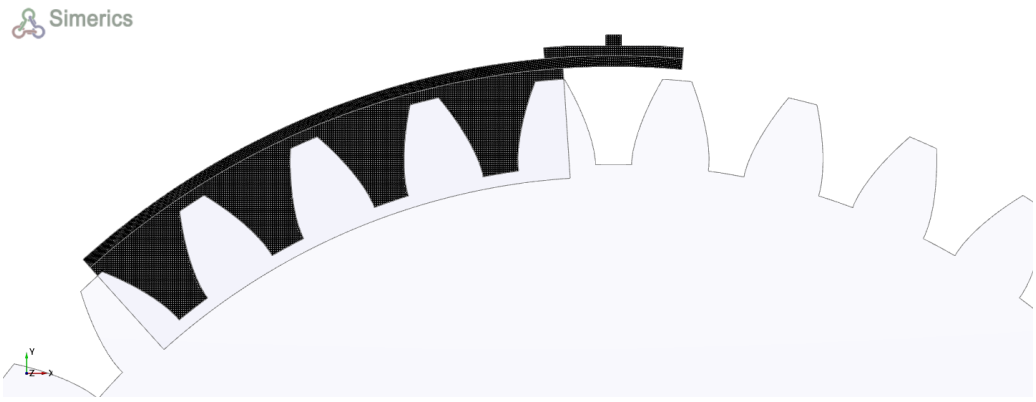

Figure 3.14: Mesh of the partial simulations

In Figure 3.16, a screenshot from Simerics MP+ shows the configuration parameters of the three meshes. On the left, the gear mesh settings are displayed, which are the same as those used in the case mesh shown in the middle. At the right, the annulus template setup is highlighted.

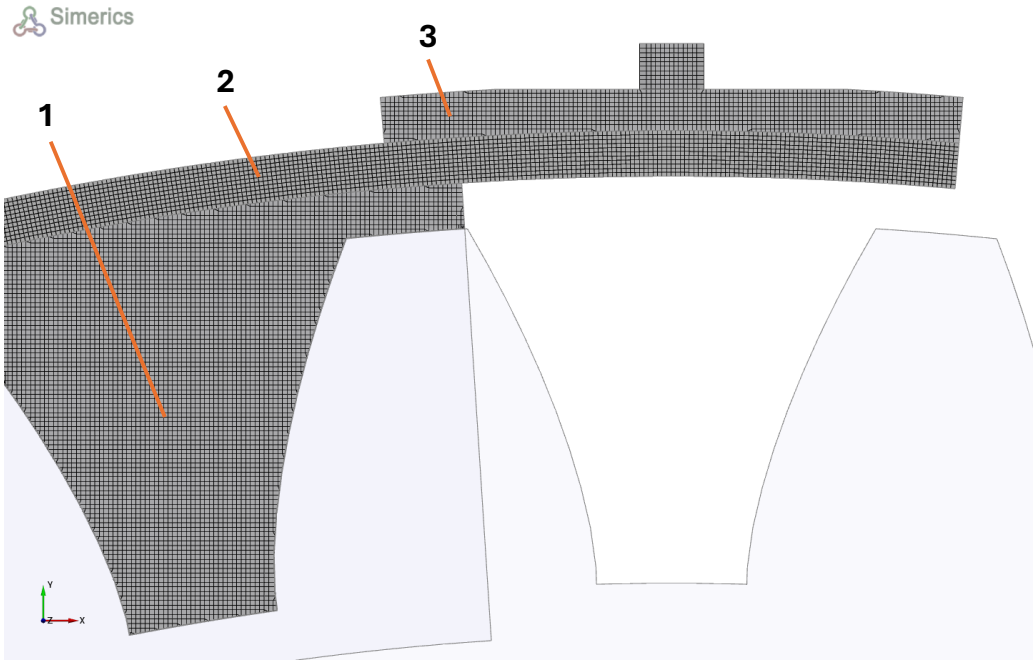

Figure 3.15: Mesh details of the partial simulations

Properties

Create Mesh

Setup Options	**Extended Mode**	
Create/Replace Mesh	Replace: gear	
Mesh Location	Interior Volumes	
CAD Surfaces	cyl_front, cyl_left, cyl_rear, cyl_righ...	
Bounding Box Margins	Automatic	
Cell Size Specification	Absolute	
Critical Edge Angle	30	deg
Curvature Resolution	35	deg
Maximum Cell Size	0.0001	m
Minimum Cell Size	2e-05	m
Cell Size on Surfaces	0.0001	m
Cell Size near Critical Edges	0.0001	m
Cell Size near Critical Points	0.0001	m
Cell Size on Surface Near Edges	0.0001	m
Cell Size on Edge Near Points	0.0001	m
Create a Refinement Zone	No	
Volume Definition	Any Surface	
New Volume Surfaces		
Volume Name by Surface Prefix	Yes	
Mesh Compression Factor	1	
Mesh Compression Direction	X	
Tree Orientation X Axis	1, 0, 0	
Tree Orientation Y Axis	0, 1, 0	
Node Merge Tolerance(Distance)	2e-06	m
Refine Cells next to Boundary Cells	No	
Parallel Cell Aspect Ratio	1	
Maximum Cell Proportion	1, 1, 1	
Sub-feature Options	Separate Patches	
Volume Options	Multiple Volumes	
Volume Order by Size	Yes	

Properties

Create Mesh

Setup Options	**Extended Mode**	
Create/Replace Mesh	Replace: case	
Mesh Location	Interior Volumes	
CAD Surfaces	case_bottom, case_front, case_in, c...	
Bounding Box Margins	Automatic	
Cell Size Specification	Absolute	
Critical Edge Angle	30	deg
Curvature Resolution	35	deg
Maximum Cell Size	0.0001	m
Minimum Cell Size	2e-05	m
Cell Size on Surfaces	0.0001	m
Cell Size near Critical Edges	0.0001	m
Cell Size near Critical Points	0.0001	m
Cell Size on Surface Near Edges	0.0001	m
Cell Size on Edge Near Points	0.0001	m
Create a Refinement Zone	No	
Volume Definition	Any Surface	
New Volume Surfaces		
Volume Name by Surface Prefix	Yes	
Mesh Compression Factor	1	
Mesh Compression Direction	X	
Tree Orientation X Axis	1, 0, 0	
Tree Orientation Y Axis	0, 1, 0	
Node Merge Tolerance(Distance)	2e-06	m
Refine Cells next to Boundary Cells	No	
Parallel Cell Aspect Ratio	1	
Maximum Cell Proportion	1, 1, 1	
Sub-feature Options	Separate Patches	
Volume Options	Multiple Volumes	
Volume Order by Size	Yes	

Properties

Build Annulus Mesh

Create/Replace Mesh	Replace: annulus	
Shape	Annulus	
Volume or Surface	Volume	
Type	Concentric Cylinders	
Reference Point	0, 0, 0	m
1st Point	0, 0, 0.01	m
Pie Angle (0-360)	47	deg
Inner Radius	0.071	m
Outer Radius	0.072	m
No. of Grid in 1st Dir.	100	
No. of Grid in 2nd Dir.	11	
No. of Grid in 3rd Dir.	591	
Grid Distribution	Uniform	

Figure 3.16: Mesh settings of the partial simulations

3.4.2 Complete simulations

Following the insights gained from the partial simulations, full simulations were conducted to model the behavior of the gear-oil interaction in a more comprehensive manner. These simulations are essential for replicating the actual laboratory conditions as closely as possible, ensuring that the virtual tests are aligned with real-world experiments. The full simulations focus on the most critical cases identified in the partial simulations, namely those expected to yield meaningful data when tested in the physical setup. The primary objective of these complete simulations is to model the entire gear system and oil flow interactions under realistic conditions, ultimately providing data that will be directly comparable to experimental results.

Unfortunately, as will be discussed in detail in the results chapter, a simulation of the entire gear enclosure was not possible with the available hardware resources. Two primary challenges emerged during the initial attempts to simulate the full domain: mesh resolution and computational capacity.

The first challenge involved balancing the number of mesh cells with hardware constraints. In the initial full-domain simulation, the number of cells was kept at a level known to be manageable with the available hardware, but this led to mesh cells being too large, particularly in the region far from the gear. The high disparity in mesh cell sizes between the area close to the gear and the regions farther away created issues with convergence. Specifically, while the simulation started without problems, the residuals, which are key indicators of solution stability and accuracy, would stop converging after a certain number of iterations, causing the simulation to fail.

The second challenge occurred when an attempt was made to improve mesh resolution by increasing the total number of cells. A finer mesh, particularly in the regions where oil-gear interactions were most critical, was necessary to ensure accurate results. However, increasing the number of cells dramatically increased the computational load, exceeding the capabilities of the available hardware. In this case, the simulations either crashed due to memory overload or slowed to such an extent that completing even a single simulation was impractical.

To overcome these issues, it became necessary to reduce the complexity of the complete simulation by limiting the domain. Instead of simulating the entire enclosure, the domain was restricted to a section in the axial length of the gear, focusing

specifically on the region where the oil-gear interaction occurs. This modification involved reducing the simulated domain to 52 mm in the axial direction, 20 mm on either side of the gear, leaving the other dimensions of the surrounding case unchanged to maintain consistency with the actual enclosure used in the physical experiment. By focusing on the most relevant section of the gear, the simulation could still capture the essential interactions without overwhelming the computational resources.

The CAD model has been reported in Figure 3.17 and is made of three main bodies. The gear under study, the cylinder used to define the region for the gear mesh and the external case.

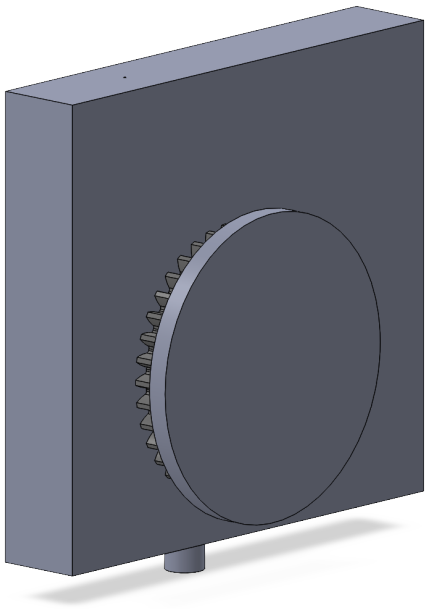

Figure 3.17: CAD model of the complete simulations

The bodies are not in their final position because is better to have them disconnected from each other and then move them to their final position for meshing inside the Simerics MP+ environment. The cylinder has a radius of 90 mm, adding a distance of 10 mm from the top surface of the teeth. The width and height of the case are exactly the ones of the experimental one, instead, the thickness has been reduced to 52 mm as previously explained. On its bottom, it is possible to see the outlet port in which the return line to the reservoir will be connected. On the top part, it is possible to see a small hole used to cut inside the case model in order to properly

position the jet injection point, this detail will be better highlighted in Figure 3.18 of the mesh. The dimension of the cylinder is always chosen equal to the one of the threaded nozzle hole to set the correct oil jet dimension. For this final case, a travel distance of the jet of 40 mm has been chosen. This picture represents the case study with a jet offset of 50 mm where in the picture of the partial simulation the center jet position has been reported. However, for both cases the simulations have been run in various oil jet offset positions.

With the revised domain, a carefully refined mesh was generated for the complete simulation. The mesh for the gear was designed to rotate rigidly around the gear center at a speed of 8000 rpm, replicating the operating conditions of the experimental setup. The mesh within the gear region remained detailed to capture the precise oil interactions, while larger cells were used in the surrounding case to reduce computational overhead. A critical refinement zone was added along the path of the oil jet to improve the accuracy of mesh crossings between the gear and the surrounding domain. This refinement ensured that the trajectory and impact on the gear of the oil jet were simulated with high precision, avoiding mesh-induced distortions in fluid flow. Another two refinement zones were added around the gear mesh, this has been done to gradually guide the variation in cell size from the small gear cells to the larger case cells size. This helps prevent simulation issues like residual non-convergence as the one that happened for the full domain simulation. Even the total variation between the smallest and the biggest cells has been limited.

For both, the case and the gear mesh, the general mesh template was used. The decision to use a general mesh template also for the gear mesh is due to the limitation of the general gear template. First of all this template creates the mesh considering a constant number of elements in axial, radial, and tangential directions. The problem with this approach is that in the radial direction, there is a large variation in height between the top and bottom of the teeth profile, leading to heavily distorted cells. This distortion causes strange behaviors in the oil jet, like problems in the mesh crossing or wobbly and unrealistic jet patterns, which will be discussed in more detail in the results chapter. However, even if the program has an algorithm to correct for the extreme skewness of the cells in the general gear mesh, this is not sufficient for the scenarios involving a jet crossing through the meshes.

In total, the mesh for the complete simulation comprised approximately 10 million cells, with 3800 time steps per rotation. The selection of the time step was particularly important to ensure that the oil jet crossing between the stationary and rotating meshes through the MGI, as well as the interaction between the oil jet

and each tooth, were accurately captured, without causing excessive time dilation that could unnecessarily slow down the simulation. These parameters balanced the need for accuracy with the practical limitations of the available hardware, ensuring that the simulations could run within a reasonable time frame while still delivering detailed results.

Figure 3.18 shows the mesh generated for the complete simulation, highlighting the refinement zones around the oil jet and the gear. This setup allows for precise tracking of the interaction of the oil with the surface of the gear as it rotates while maintaining a feasible computational load. The open boundaries, similar to those used in the partial simulation, were also applied in this simulation for the walls facing the front and rear of the gear to allow for realistic fluid behavior, preventing the artificial recirculation of oil that could lead to distorted results. The open boundaries are the ones present in the axial direction of the gear since these walls are not present in the real-world experiment configuration.

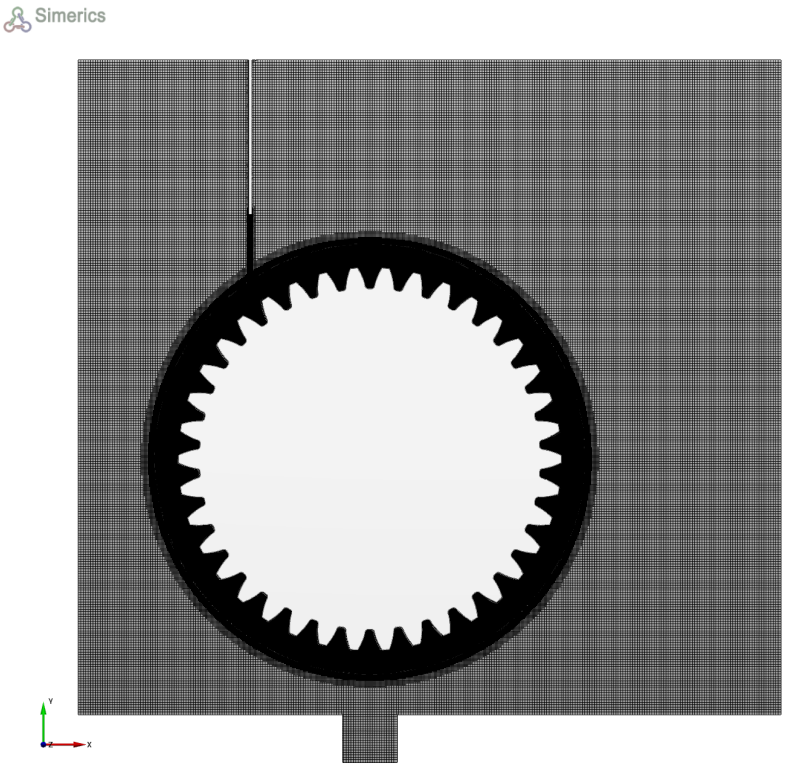

Figure 3.18: Mesh of the complete simulations

Figure 3.19 shows the detailed view of the mesh enlarged around the nozzle area. The are mainly two meshes, the gear and the case one, but many refinement zones are present in the case one. In the final mesh can be highlighted five main areas:

1. **Rotating gear mesh**: This mesh follows the rotational movement of the gear. As illustrated in the figure, it is created using the gear teeth profile and the cylinder added in the CAD model. During the simulation, this mesh rotates rigidly around the center of the gear while its external part maintains in constant contact with the internal part of the case mesh. The mesh was created using the general mesh template and, with a maximum cell size of 0.00025 m, it is the finest mesh.

2. **Fixed case mesh**: This mesh remains stationary throughout the entire simulation and its primary function is to replicate the real-world environment around the gear. Its internal surface always maintains contact with the rotating gear mesh and was created using the general mesh template with dimensions larger than those of the gear mesh, specifically 0.001 m.

3. **First refinement zone around the gear**: This part of the case mesh is refined to a size comparable to that of the gear mesh, 0.0004 m. It surrounds the gear mesh and is designed to prevent issues when the oil passes between the two different meshes, with a smooth transition in cell size.

4. **Second refinement zone around the gear**: This part of the case mesh is a second refined zone, with cells size of 0.0005 m, that wraps around the first refinement area, facilitating the smooth transition of information from the smallest to the largest cells of the case mesh.

5. **Refinement zone along the oil jet**: This part of the case mesh is refined to match the dimensions of the gear mesh and guarantee an adequate level of resolution at the oil jet injection point, allowing smooth passage of the MGI between the rotating and stationary meshes.

The three meshes are always in contact with each other. For this reason, it is important to define these common surfaces as a mismatched grid interface (MGI) in the software. Defining an MGI enables the exchange of information between the different meshes and is essential for the success of the simulation. The MGI must be defined for both the stationary and moving meshes.

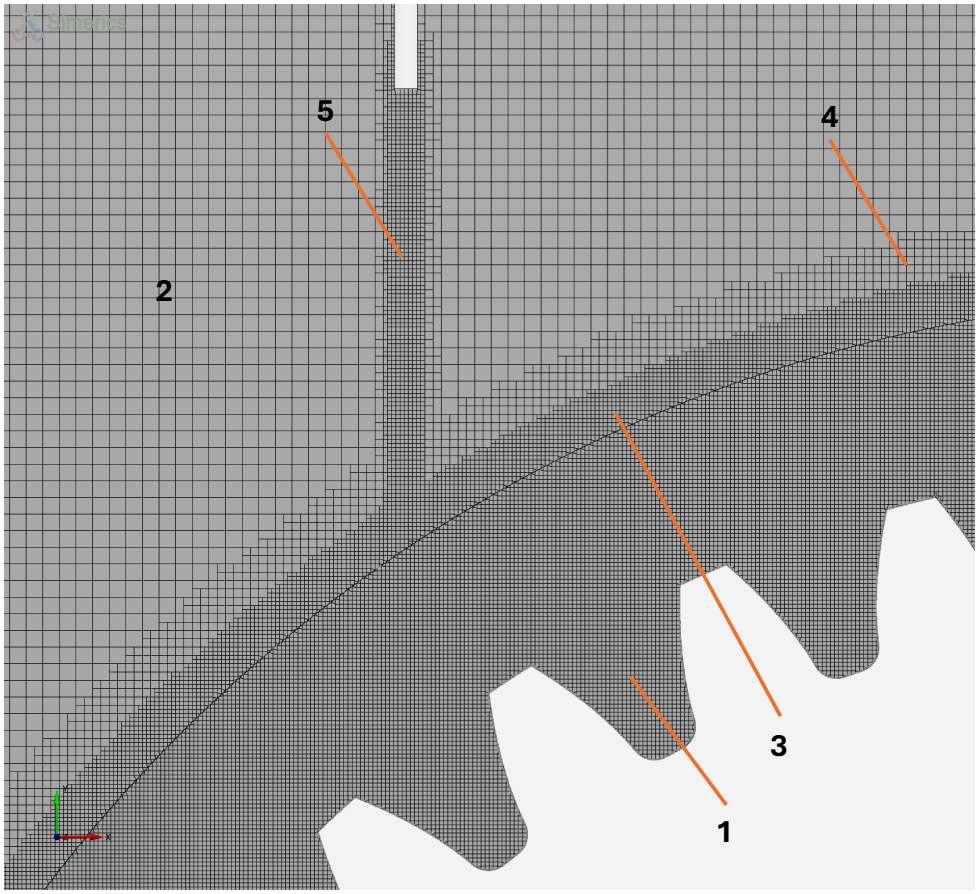

Figure 3.19: Mesh details of the complete simulations

Figure 3.20 contains screenshots from Simerics MP+ showing the settings used in the meshing process for the complete simulation. On the left, the case mesh is shown with the three refinement zones, while on the right, the settings for the gear mesh are presented.

The complete simulation provides a far more comprehensive analysis of the system compared to the partial simulations. By modeling the full gear and a larger portion of the domain, the complete simulations capture more complex interactions, including the effects of fluid pressure on adjacent teeth and how the rotation of the gear impacts the oil flow. These additional factors offer a more accurate representation of real-world conditions, which will be essential when comparing the simulation results to the data collected during the laboratory experiments.

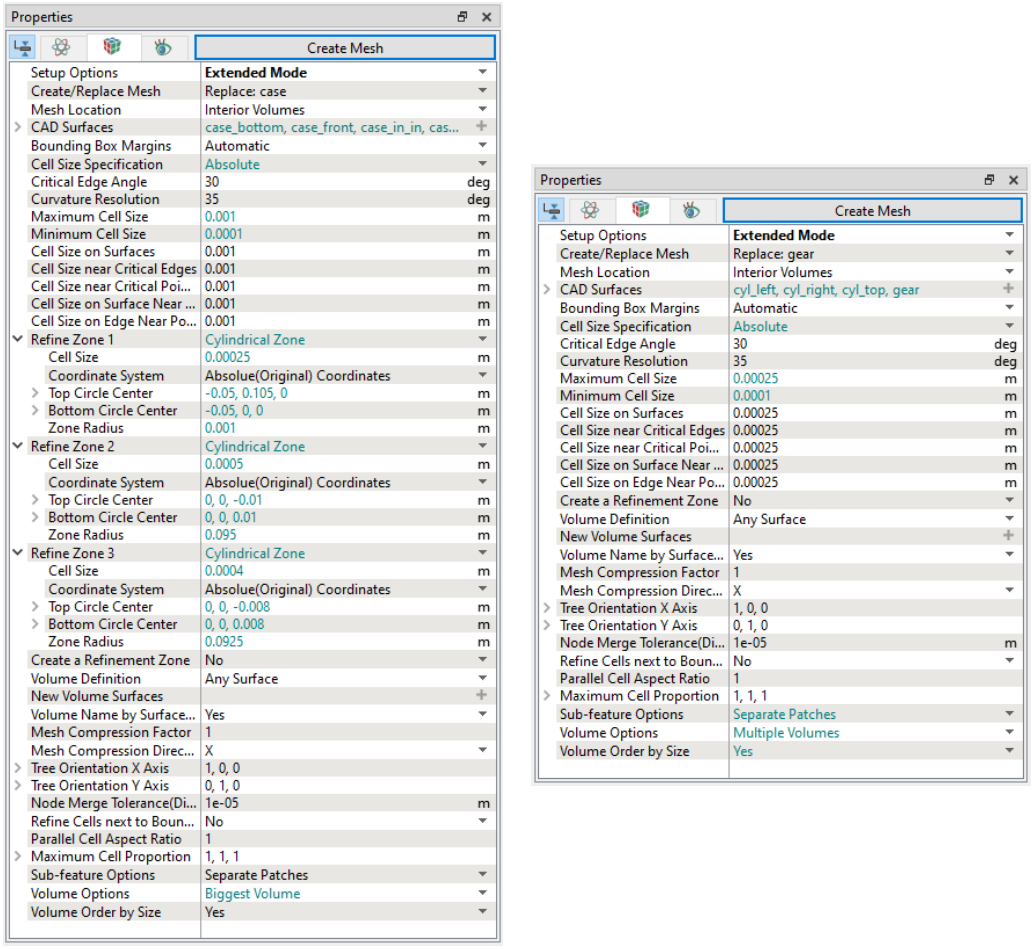

Figure 3.20: Mesh settings of the complete simulations

Despite the reduction in the domain size, this complete simulation approach still provides a robust dataset that can be used for the final analysis and validation. The results of these simulations, once compared with the experimental data, will offer critical insights into the predictive capabilities of the CFD model and the Simerics MP+ software, particularly in its application to gear lubrication studies. Additionally, the results will help identify any remaining limitations or discrepancies, allowing for further refinement of both the simulation setup and the experimental configuration in future research.

Chapter 4

Results and Discussion

The simulations described in the previous chapter formed the basis for a series of studies aimed at understanding how different key parameters influence the operating conditions, most notably the average resistive torque experienced by the rotating gear. The first phase of this investigation focused on utilizing the partial simulations, which were designed to quickly evaluate critical factors in a simplified domain before moving on to the full gear system. This step-by-step approach helped identify potential challenges and allowed for the optimization of simulation settings before conducting the final experiments.

One of the key challenges encountered early in the simulations was related to the oil jet mesh crossing, particularly at the mismatched grid interface (MGI) between the mesh of the rotating gear and the stationary enclosure. This region required special attention due to the complex interaction between the rotating and stationary domains, which often led to simulation instabilities or inaccuracies if not handled properly. The MGI plays a crucial role in coupling the mesh of the rotating gear with the stationary mesh of the surrounding enclosure. Specifically, the MGI allows for the exchange of information, such as pressure, velocity, volumetric flow rate, and other relevant flow variables, across the two distinct domains.

The key function of the MGI is to manage the seamless transfer of data between the rotating and stationary meshes while minimizing the computational overhead that more complex techniques, such as dynamic re-meshing, would introduce. Despite this advanced capability, there are critical limitations that must be considered

when designing the simulation. One of the most important factors is ensuring that the mesh density across the MGI is comparable on both sides of the interface. Large discrepancies between the mesh sizes can lead to information loss at the interface, which in turn compromises the accuracy of the flow variables being passed between the domains.

During the initial attempts, the mesh near the gear teeth and the surrounding enclosure was too dissimilar, leading to poor performance in the oil jet crossing. Specifically, the simulation failed to maintain constant the volumetric flow rate across the interface. Figure 4.1 reports the issue, manifested in results that resembled a partial obstruction of the oil flow as if the oil was passing through a coarse filter. Consequently, the resistive torque was inaccurately calculated because the flow interaction with the gear teeth was not properly captured.

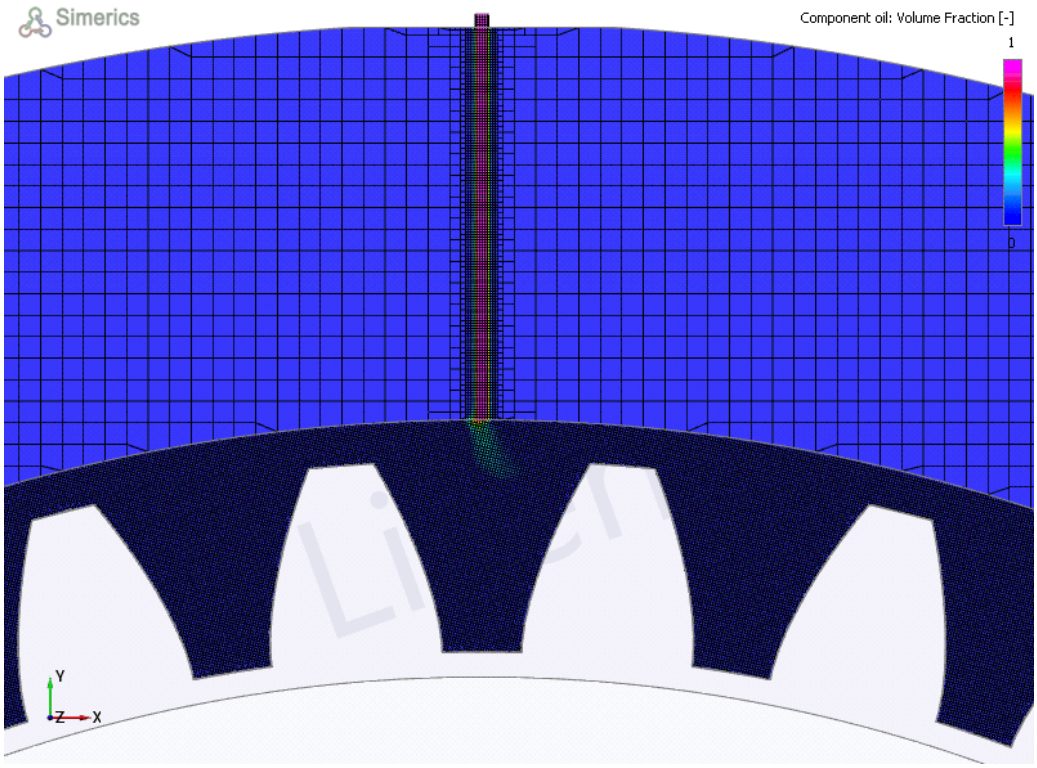

Figure 4.1: Oil jet flow obstruction at MGI interface

In addition to mesh refinement, time step selection played a significant role in the success of the simulation. A large time step would cause inaccuracies in data transfer between the meshes, leading to errors in the computed resistive torque and fluid dynamics behavior. This issue is well described by the Courant number, a dimensionless parameter that governs the stability and accuracy of computational fluid dynamics (CFD) simulations.

The Courant number (C_o) is defined by Equations 4.1.

$$C_o = \frac{u \cdot \Delta t}{\Delta x} \tag{4.1}$$

Where:

u: is the local fluid velocity [m/s],

Δt: is the time step size [s],

Δx: is the spatial grid size [m].

The Courant number expresses the ratio between the movement of the fluid during a single time step and the size of the grid cells.

If $Co \leq 1$: the simulation remains stable because the fluid moves within a single grid cell, ensuring accurate data transfer.

If $Co > 1$: the simulation becomes unstable, leading to inaccuracies or even divergence of the solution.

In the case of Simerics MP+, the software employs an algorithm that dynamically adjusts the time step to ensure that the Courant number remains within an acceptable range. If the chosen time step is too large, Simerics MP+ automatically subdivides it to maintain stability and prevent loss of information at critical interfaces such as the MGI.

Once these initial challenges with mesh crossing and time step selection were resolved, the simulation results became more reliable, and it was possible to move

forward with evaluating the influence of different parameters on the average resistive torque. The following sections summarize the analysis performed, focused on how changes in different parameters affect the average resistive torque.

Mesh Dimension Sensitivity: The effect of varying mesh resolution, particularly near the MGI and gear teeth, on the accuracy of the average resistive torque. Finer meshes provided more precise capture of the fluid-gear interaction, improving torque calculations, but also increased computational load. Coarser meshes, while computationally faster, often resulted in less accurate torque measurements due to a lack of detail in capturing fluid behavior near critical regions.

Time Step Sensitivity: The influence of time step size on the ability of the simulation to accurately predict resistive torque. Larger time steps tended to miss finer details in the interaction of the fluid with the gear, leading to inaccurate torque predictions, especially in high-speed rotations. Smaller time steps, on the other hand, helped in capturing the fluid dynamics more precisely, resulting in more stable and accurate torque values, particularly when dealing with rapid fluid-structure interactions.

Jet Position Sensitivity: How the position of the oil jet relative to the gear influenced the average resistive torque. Changes in jet distance and angle, obtained through jet offset, significantly affected how the oil interacted with the gear teeth, with more distant positions leading to higher resistive torques.

Flow Rate Sensitivity: The relationship between different volumetric oil flow rates and the resulting resistive torque. Higher flow rates generally increased the resistive torque, as more oil impacted the gear surface. Lower flow rates led to reduced torque, indicating that there is an optimal flow rate range for maximizing lubrication while reducing the resistive torque.

Temperature Effects (Controlled): While the temperature was kept constant during the simulations, it is important to consider that variations in temperature could affect the viscosity of the oil, and hence, the resistive torque. Future studies allowing for temperature changes could provide insights into how thermal variations influence the lubrication process and torque behavior.

The partial simulations provided valuable insights into the overall behavior of the system, helping to refine the setup for the complete simulations and laboratory

experiments. These initial findings allow to understand the influence of oil jet interaction on the resistive torque of the gear and identify potential issues in mesh quality and time step selection that were crucial for accurate simulations. The results obtained here were instrumental in guiding the choice of operating conditions for the full gear simulations, ensuring a smoother transition from the virtual to the physical testing phase.

4.1 Sensitivity Analysis of Mesh Resolution

In this section, the influence of mesh dimension on resistive torque was studied through a series of simulations. The objective was to assess how varying the mesh size impacts both the computational load, in terms of cell count and simulation time, and the accuracy of the results, particularly regarding the resistive torque acting on the gear. For this purpose, the partial simulation method was employed, as previously discussed in earlier sections.

To investigate the impact of mesh dimension, both the case and the gear domains were meshed with progressively finer grids. The cell sizes used in the simulations ranged from 0.0005 mm to 0.00005 mm. Additionally, different combinations of volume mesh and surface mesh sizes were tested to evaluate the effect of refining the mesh only on the surface of the gear. The results of these simulations are summarized in the Table 4.1.

simulation	mesh size [mm]	min mesh size [mm]	surface mesh size [mm]	total number of cells [-]	simulation time [h]	max torque [Nm]	average torque [Nm]	average torque [%]	average torque variation [%]
1	0.0005	0.0001	0.0005	43346	0.08	3.90	0.3063	111.49	11.49
2	0.0002	0.00005	0.0002	388156	0.78	4.07	0.2892	105.26	5.26
3	0.0002	0.00005	0.00005	1933252	4.75	4.18	0.2846	103.59	3.59
4	0.0001	0.00002	0.0001	3099450	13.75	4.12	0.2825	102.84	2.84
5	0.0001	0.00002	0.00002	29750901	108.00	4.19	0.2836	103.21	3.21
6	0.00005	0.00001	0.00005	24056686	51.50	4.15	0.2747	100.00	0.00

Table 4.1: Simulation settings and results of mesh resolution analysis

As expected, reducing the cell size resulted in a significant increase in the total number of cells within the computational domain, from the initial 43 thousand to over 24 million. However, this increase was not proportional, as the relationship between cell size and the number of cells follows a non-linear hyperbolic behavior. This non-linearity arises because the computational domain is three-dimensional.

When the mesh is refined, the reduction in cell dimension occurs across all three spatial axes: length, width, and height. Consequently, any reduction in the cell size affects the total number of cells in all three dimensions simultaneously. As a result, the total number of cells in the domain increases approximately by the cube of the reduction factor in cell size. In other words, when the size of each cell is halved, the number of cells increases by a factor of eight.

This cubic growth in the number of cells is critical to understanding the computational cost associated with finer meshes. While reducing the mesh size improves spatial resolution, it also dramatically increases the number of cells that need to be processed by the solver. The plot in Figure 4.2 clearly illustrates this hyperbolic relationship between cell size and cell count, emphasizing the importance of optimizing the mesh resolution. Striking the right balance between cell size and the total number of cells is crucial for managing computational resources effectively. A mesh too coarse may result in inaccurate results due to poor spatial resolution, while a mesh too fine will lead to exponentially increased computational time and memory requirements, making the simulation inefficient or even unfeasible.

This observation underscores the importance of mesh optimization, where one must find the ideal compromise between mesh refinement and computational efficiency. The diminishing returns on accuracy after a certain level of mesh refinement must be weighed against the exponential increase in computational cost. Therefore, choosing an optimal mesh size is essential to ensure both the accuracy of the results and the feasibility of the simulation in terms of time and computational resources.

The relationship between the number of cells N_{cells} and the cell dimension L_{cells} can be described by Equation 4.1.

$$N_{cells} \propto \left(\frac{1}{L_{cells}}\right)^3 \tag{4.2}$$

Where:

N_{cells}: is the number of cells $[-]$,

L_{cells}: is the cells size $[mm]$,

This mathematical relationship expressed in Equation 4.1 was confirmed by the trend observed in Figure 4.2, where the number of cells increased sharply as the mesh became finer.

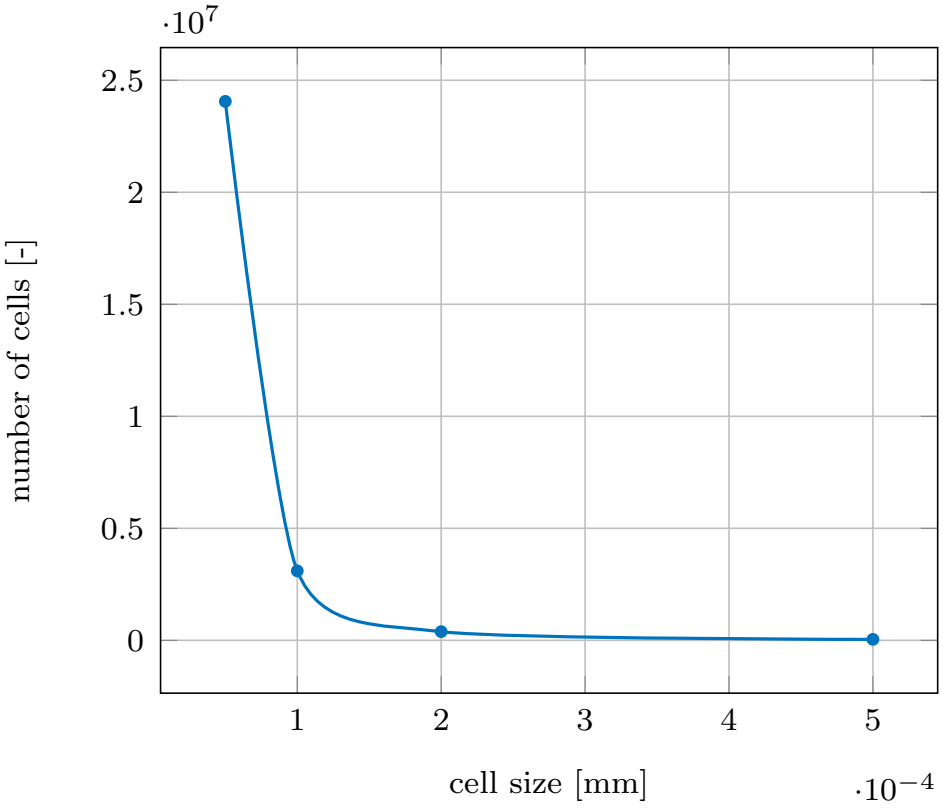

Figure 4.2: Number of cells as a function of cell size

4.1.1 Impact on Simulation Time

The relationship between mesh resolution, defined by cell size or the total number of cells, and simulation time is critical to understanding the trade-offs in computational fluid dynamics (CFD) simulations. An increase in the number of cells directly influences the simulation time, as each cell represents a discrete volume within the computational domain where the governing conservation equations (for mass, momentum, and energy) must be solved. This inherently leads to a proportional increase in the number of equations that must be computed, which consequently lengthens the overall computational time.

As expected, when the mesh is refined (i.e., when cell size is reduced, thereby increasing the total number of cells), the simulation time increases. This is primarily because each additional cell introduces more degrees of freedom that must be accounted for in the numerical solver. Thus, the more cells present, the more extensive the computational workload becomes, requiring more processing power and time to achieve convergence. This is a fundamental aspect of CFD simulations, particularly in gear lubrication modeling, where detailed flow phenomena are of interest.

However, the increase in cell count has a beneficial impact on the spatial resolution of the simulation. A finer mesh enables the capture of smaller-scale fluid flow details, such as boundary layer effects, localized vortices, and detailed pressure gradients that may be critical for accurately resolving the fluid dynamics within the lubricated contact zones of gears. This higher resolution provides more precise insights into the behavior of the lubricant and the interactions between moving parts. Therefore, selecting an appropriate mesh size becomes a delicate balance: while a finer mesh provides more detailed results, it also significantly increases simulation time and computational cost.

In addition to spatial resolution, temporal accuracy plays a critical role in simulations involving transient phenomena, such as the dynamic behavior of lubricant flow between rotating gears. A finer mesh often necessitates a reduction in the simulation time step to maintain numerical stability and accuracy, as governed by the Courant-Friedrichs-Lewy (CFL) condition. The Courant number ensures that the physical propagation of information (such as the movement of fluid) within a single time step does not exceed the distance covered by one computational cell. As the cell size decreases, the time step must also be reduced to satisfy this criterion, further compounding the simulation time. Thus, the computational expense increases not

only due to the increased number of cells but also because of the smaller time steps required for maintaining solution accuracy.

Moreover, as the number of cells increases, the interactions between neighboring cells become more complex. The numerical solver must calculate the interactions between adjacent cells at each time step, which involves solving additional fluxes and gradients across the cell faces. These interactions contribute to the overall simulation workload, especially in cases where there is significant variation in fluid properties or complex geometrical features within the domain, such as the gear teeth in the lubrication model. As a result, the increase in simulation time as a function of cell count is often nonlinear, as multiple factors, including spatial resolution, time step size, and inter-cell interactions, all contribute to the computational cost.

The results obtained from the simulations demonstrate this nonlinearity. The relationship between simulation time and the number of cells is not purely proportional; rather, the computational time increases at an accelerating rate as the number of cells grows. This is evident from the results presented in Figure 4.3, which shows a steep rise in simulation time as mesh refinement increases. This trend highlights the diminishing returns of excessively refining the mesh, as the computational cost grows significantly without a corresponding improvement in simulation accuracy beyond a certain point. Therefore, a sensitivity analysis of mesh resolution is essential for optimizing CFD simulations, especially in complex lubrication models like those encountered in gear systems. This allows for identifying the optimal mesh size that balances the need for detailed flow resolution with the computational feasibility of the simulation. All these factors contribute to the non-proportional relationship between the number of cells and simulation time.

As shown, the simulation time does not scale linearly with the number of cells, due to factors such as solver efficiency, nonlinear convergence behavior, and data handling complexities. For example, the use of turbulence models and nonlinear solvers in computational fluid dynamics (CFD) often introduces additional computational load, making the increase in simulation time greater than what would be expected purely from cell count. Moreover, parallel computing environments introduce inefficiencies in data input/output (I/O) and memory usage, leading to diminishing returns in simulation speed as mesh refinement progresses.

In three-dimensional simulations, the number of cells increases cubically with mesh refinement, resulting in a rapid rise in simulation time. Additionally, increased memory requirements and I/O operations may become bottlenecks, further exacer-

bating the growth in computational time. In summary, the relationship between simulation time and cell count generally follows a cubic trend, especially in 3D simulations with complex physical models.

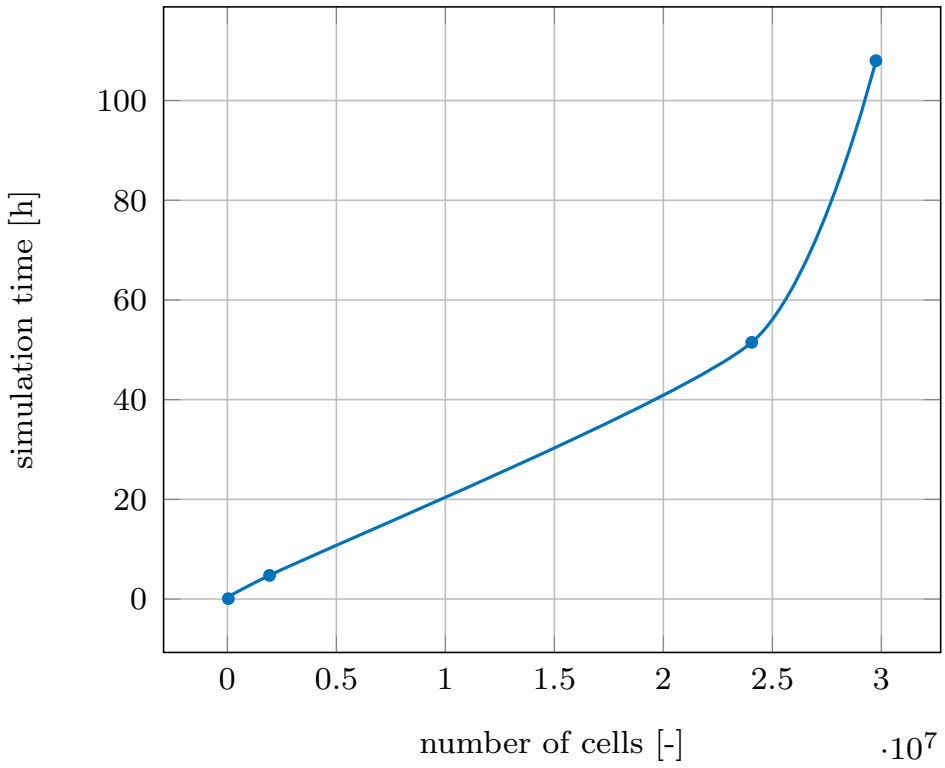

Figure 4.3: Simulation time as a function of number of cells

In these simulations, the time step was kept constant, isolating the impact of cell count on simulation time and eliminating the influence of varying time steps.

In summary, while finer mesh resolutions improve the accuracy of CFD simulations by capturing more detailed fluid dynamics, they also impose a significant burden on computational resources. The increase in cell counts leads to a longer simulation time due to the higher number of equations, smaller time steps, and more intricate inter-cell interactions that must be computed. The non-proportional relationship between cell number and simulation time underscores the importance of selecting an appropriate mesh resolution that achieves the desired accuracy without excessively increasing computational costs.

4.1.2 Impact on Simulation Accuracy

In addition to affecting simulation time, the number of cells also influences the accuracy of the simulation. To quantify this effect, Figure 4.4 displays the average resistive torque on the gear for various mesh sizes.

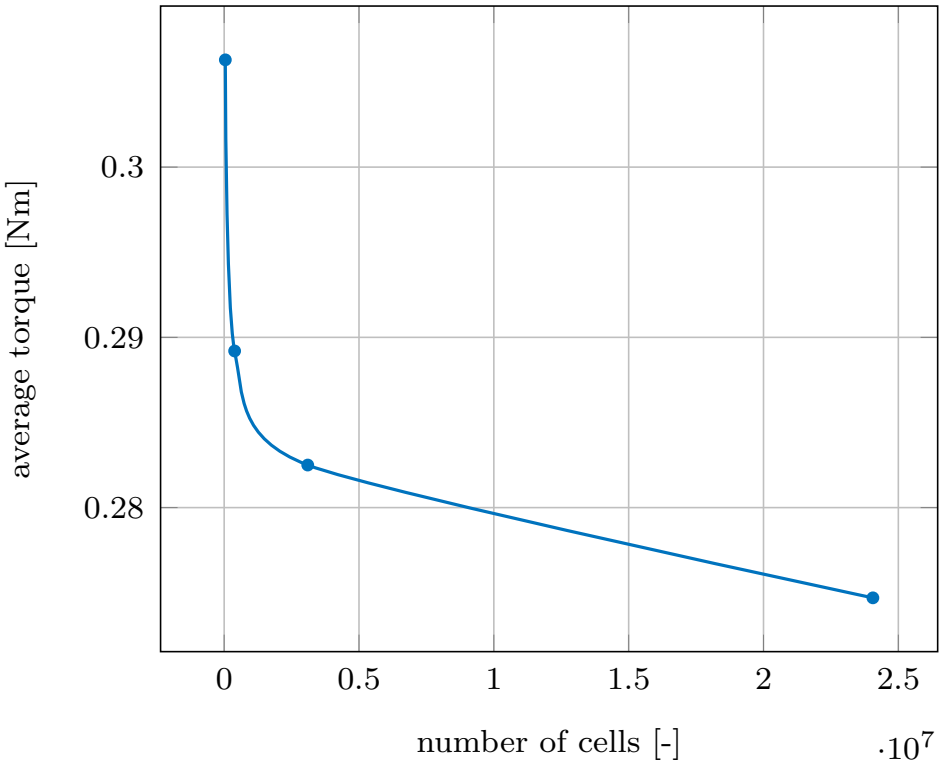

Figure 4.4: Average resistive torque as a function of number of cells

As the graph shows, increasing the number of cells led to a reduction in the average resistive torque. More importantly, the results converged to a final value as the number of cells increased. This convergence suggests that after reaching a certain cell count, further refinement yields diminishing returns in terms of accuracy. Initially, reducing the mesh size dramatically improves the accuracy of the results, but beyond a certain threshold, the benefits of additional refinement become marginal.

In this study, a significant drop in resistive torque was observed early on, with smaller and smaller reductions occurring as the mesh became finer. This behavior

indicates a point of diminishing returns, where increasing the number of cells has only a minimal impact on the accuracy of the results but significantly increases the computational time. For this particular case, using a mesh with fewer than half a million cells was identified as the best trade-off between accuracy and computational cost. Therefore, for future simulations, a cell size of 0.0002 mm has been selected. This choice results in a deviation of 5% from the optimal results, which is slightly worse than the 3% deviation observed with a cell size of 0.0001 mm. However, it allows saving almost 13 hours of simulation time, reducing it from nearly 14 hours to less than 1 hour, making the 2% increase in deviation a worthwhile trade-off.

Nevertheless, it is important to underscore the accuracy of the software, even when considering the varying dimensions of the cell size used in the simulations. Despite the fact that different mesh resolutions can lead to variations in results, the software has demonstrated a high level of accuracy. Specifically, the difference in the resistive torque calculated between the simulations using the smallest and largest cell sizes is only 11.50%. This discrepancy, although present, is relatively small and does not significantly affect the overall reliability of the results. Moreover, this variation in torque corresponds to a substantial reduction in computational resources: more than 24 million cells were eliminated by using a larger cell size, which in turn led to a reduction of 51 hours in the total simulation time. This time-saving makes the choice of a larger cell size a practical trade-off, ensuring that the simulation process is much more efficient without compromising the precision of the results to a large extent.

This initial study on the sensitivity of resistive torque to mesh dimension provided valuable insights into optimizing the mesh size for future simulations. The findings highlight the critical importance of balancing mesh refinement with computational efficiency in order to achieve reliable results within a reasonable time frame. Properly selecting mesh dimensions is essential to ensure both accuracy and efficiency, two crucial factors in CFD simulations for gear lubrication studies.

Additionally, it is worth noting that factors like solver convergence, parallel computing architecture, and data handling can have a significant impact on overall simulation performance, beyond the basic influence of cell count. Therefore, these aspects should be considered in future studies to optimize the simulation workflow further. This analysis forms the basis for establishing optimal meshing strategies for future simulations, where a balance between simulation time and result accuracy is crucial for successful CFD analyses in automotive engineering applications.

4.2 Sensitivity Analysis of Time Step

The second factor analyzed in this study is the effect of the time step on the average resistive torque and its influence on the overall simulation time. The results of this analysis are summarized in Table 4.2.

simulation	mesh size [mm]	time step per tooth gap [-]	total time steps [-]	degree per time step [°]	total number of cells [-]	simulation time [h]	average torque [Nm]	average torque [%]	average torque variation [%]
1	0.0002	25	110	0.3789	3099450	1.00	0.2706	95.64	-4.36
2	0.0002	50	220	0.1895	3099450	1.83	0.2781	98.31	1.69
3	0.0002	100	440	0.0947	3099450	3.26	0.2810	99.32	-0.68
4	0.0002	200	880	0.0474	3099450	6.13	0.2825	99.88	-0.12
5	0.0002	400	1760	0.0237	3099450	10.00	0.2834	100.19	0.19
6	0.0002	800	3520	0.0118	3099450	15.95	0.2833	100.13	0.13
7	0.0002	1600	7040	0.0059	3099450	29.93	0.2829	100.00	0.00

Table 4.2: Simulation settings and results of time step analysis

As visible in Table 4.2, the time step per tooth gap is increased from 25 up to 1600, doubling the previous value for every new simulation. This change caused an increase in the total number of time steps present in a full rotation of the gear, from 110 to 7040, and a consequent reduction in the degree contained in each step, from 0.3789° to 0.0059°. The biggest result that these changes caused was the increase in simulation time that passed from one hour to almost thirty, while the average resistive torque value maintained a good consistency. This is also possible thanks to the adaptive algorithm present in Simerics MP+, called the adaptive Courant number method, where intermediate time steps are added locally to respect the CFL condition.

4.2.1 Impact on Simulation Time

As previously discussed, the time step is a critical parameter for the accuracy and efficiency of the simulation. If the time step is too large, the information exchange between computational cells becomes inaccurate, leading to potential failure of the simulation. On the other hand, choosing a time step that is too small significantly increases computational time. This is due to the direct relationship between the size of the time step and the number of iterations required. A smaller time step results in a higher number of time steps, each requiring a complete recalculation of the system variables. This creates a cumulative effect, where the increase in computational time is directly proportional to the decrease in time step size. Unlike the mesh refinement, where the computational demand per time step increases, here the increase in computational load is driven by the sheer number of time steps needed, making it proportional to the time step size.

The graph in Figure 4.5 clearly illustrate this relationship. As the time step decreases, the simulation time increases linearly. This is expected, as reducing the time step means that more steps are required to cover the same simulation period, with each step demanding a fixed amount of computational resources.

Although the increase in computational time due to smaller time steps is not as dramatic as the impact caused by mesh refinement, it is still significant. It is essential to strike a balance in selecting the time step to avoid excessive computational costs while ensuring accurate simulation results. The time step must be small enough to satisfy the Courant–Friedrichs–Lewy (CFL) condition, ensuring numerical stability and convergence of the simulation. It is also important to note that whenever the cell size is reduced, the time step should be adjusted accordingly to maintain this stability.

However, the Simerics MP+ software offers an advantage in this regard by implementing an adaptive algorithm, called the adaptive Courant number method, that adjusts the time step locally to meet the required CFL condition. This feature allows for larger time steps than would typically be permissible, while still maintaining compliance with the CFL condition. As a result, the simulation can achieve a balance between computational efficiency and numerical accuracy, optimizing the time step without compromising the overall quality of the simulation.

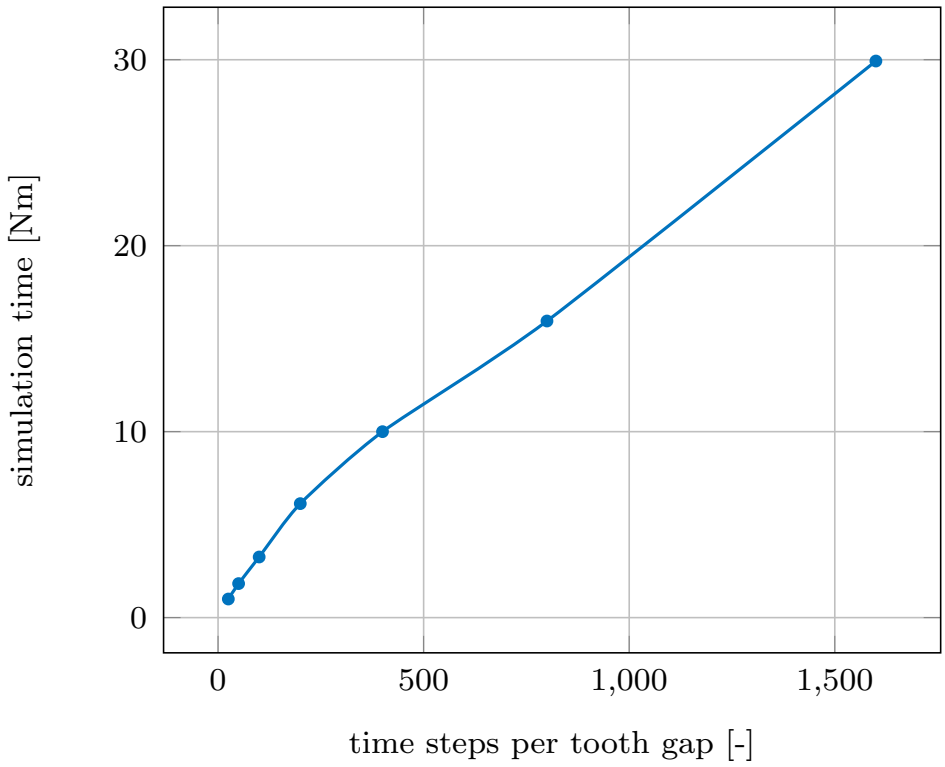

Figure 4.5: Simulation time as a function of time steps per tooth gap

As presented in Figure 4.5, the simulation time is directly proportional to the number of time steps. For instance, increasing the number of time steps between two consecutive gear teeth results in a corresponding increase in simulation time. This is an anticipated outcome, as a greater number of time steps means that more simulations are required to cover the same degree of rotational movement. Essentially, as the number of time steps increases, so does the computational load, since the system must calculate more intermediate states during the same angular displacement.

In Figure 4.6, the relationship between the degree of rotation per time step and simulation time reveals an inversely proportional relationship, resulting in a hyperbolic pattern. As the time step size decreases, the simulation time sharply increases, highlighting the non-linear nature of this relationship. Larger time step sizes drive the simulation time closer to zero, while smaller time steps cause the simulation time to approach infinity. This behavior is expected because, with larger time steps, fewer iterations are needed to simulate a given rotation, thus reducing the computational

effort. Conversely, smaller time steps require exponentially more iterations, which drastically increases simulation time.

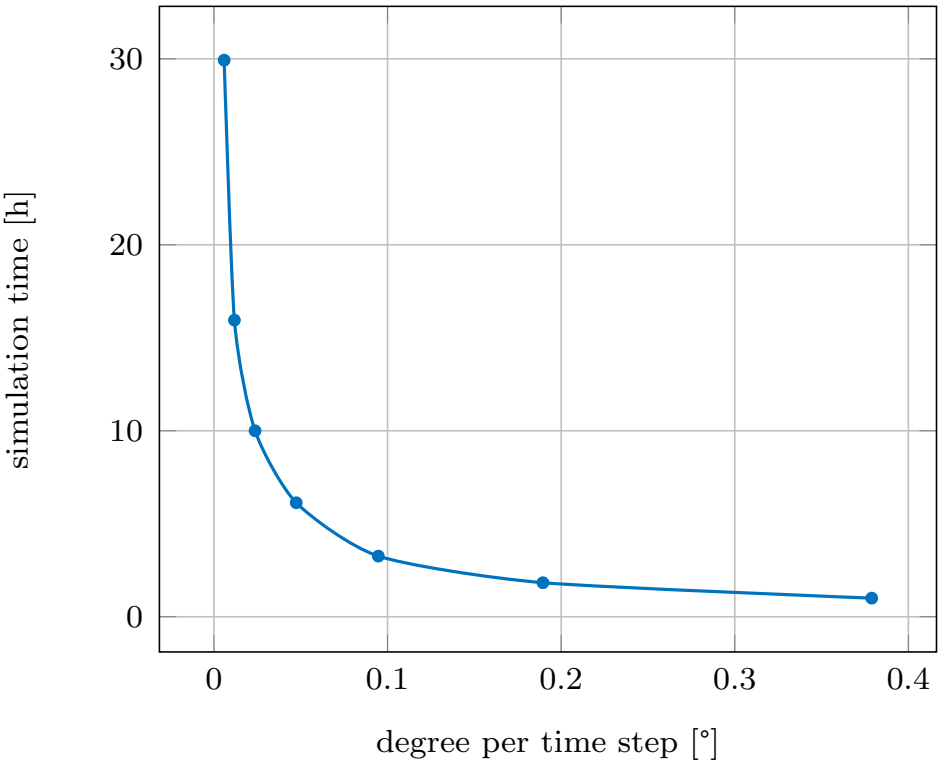

Figure 4.6: Simulation time as a function of degree per time step

The optimal balance can be found in the region closest to the origin of the hyperbola, where the time step size achieves a compromise between accuracy and computational efficiency. In this region, the time step is small enough to capture the necessary details of the dynamics of the system without excessively prolonging the simulation. Achieving this balance is critical for maintaining an efficient simulation process, as it minimizes the risk of either excessive computational time or inaccurate results. By carefully selecting a time step that operates in this optimal zone, it is possible to ensure that the simulation remains both accurate and computationally feasible.

4.2.2 Impact on Resistive Torque

The effect of reducing the time step on the average resistive torque is illustrated in the Figure 4.7. As the number of time steps between two gear teeth increases (i.e., as the time step size decreases), the resistive torque value initially rises, showing a sharp increase for very small changes in time step size. This steep rise occurs in the early stages when the time step is significantly reduced, reflecting the sensitivity of the system to fine time resolution. After this initial surge, the torque values gradually level off, eventually stabilizing as the system approaches its final resistive torque value.

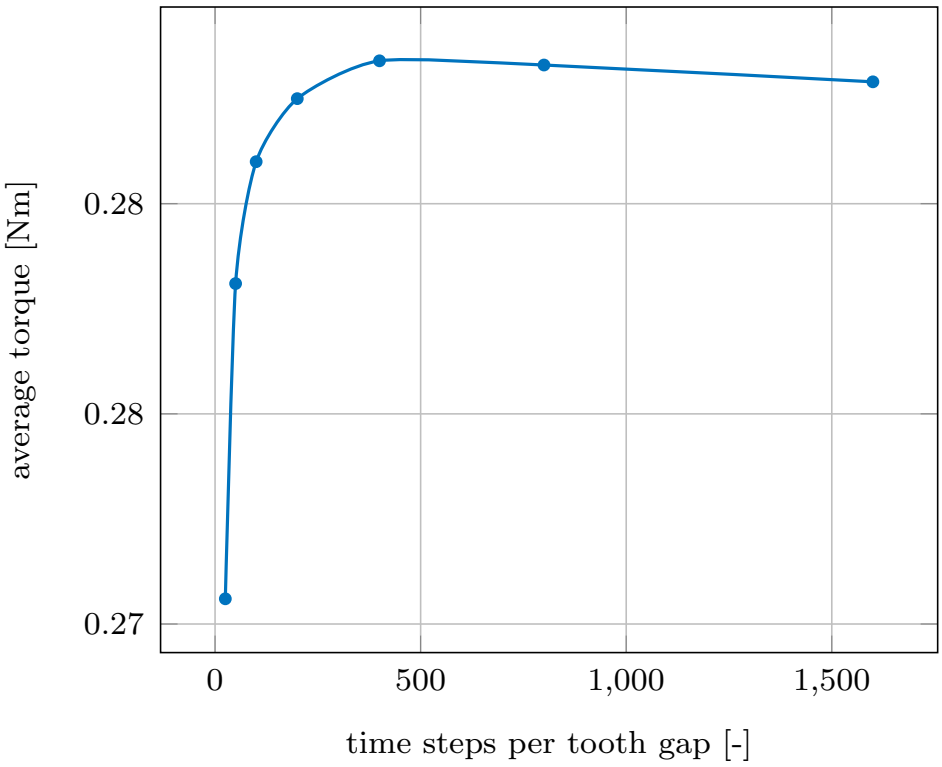

Figure 4.7: Resistive torque as a function of time steps per tooth gap

It is crucial to highlight that, despite this initial increase, the overall variation in resistive torque between the maximum and minimum values remains relatively small, within a 5% range. This limited variation is largely attributed to the adaptive Courant number algorithm implemented in Simerics MP+, which dynamically

adjusts the time step. By allowing the use of larger time steps while still maintaining the stability and accuracy of the numerical solution, the algorithm ensures that computational resources are used efficiently. Consequently, simulations benefit from faster processing times without a significant loss in accuracy, even when larger time steps are employed.

From as early as 100 time steps per gear tooth gap, the resistive torque value closely approaches its asymptotic limit. The difference between the torque value at 100 time steps and the final stabilized value is less than two thousandths, suggesting that this range is an optimal point for balancing accuracy and efficiency. Increasing the number of time steps beyond 100 provides diminishing returns in terms of accuracy, as the resistive torque stabilizes, and further reductions in time step size offer minimal additional benefit. This behavior indicates that the ideal range for the time step lies between 100 and 400 time steps per gear tooth gap. Beyond this threshold, the increase in simulation time outweighs the negligible gains in accuracy, making it inefficient to reduce the time step any further.

The plot in Figure 4.8 shows a clear trend where the average resistive torque increases with a smaller time step size and decreases with larger time steps. However, from 200 time steps onwards, the difference in the resulting torque is minimal and not worth the extra simulation time required. The curve suggests that while smaller time steps lead to more accurate torque measurements, the difference becomes negligible beyond a certain threshold. Therefore, careful analysis is required to select a time step size that balances computational efficiency and accuracy, avoiding unnecessary reductions in the time step that would only increase simulation time without significantly improving results.

Given the minimal influence of the time step size on the resistive torque once a certain threshold is reached, the selection of the time step for future simulations was based primarily on its effect on simulation time rather than on the torque values. As the resistive torque stabilizes with only slight variation beyond a certain number of time steps, the focus shifts to optimizing computational efficiency. Based on this evaluation, the optimal number of time steps between two gear teeth was determined to be 100. This value strikes a balance, ensuring that the resistive torque results are accurate while keeping simulation times within a reasonable range for future analyses. The difference in torque with respect to the 1600 time steps simulation is only 0.68%.

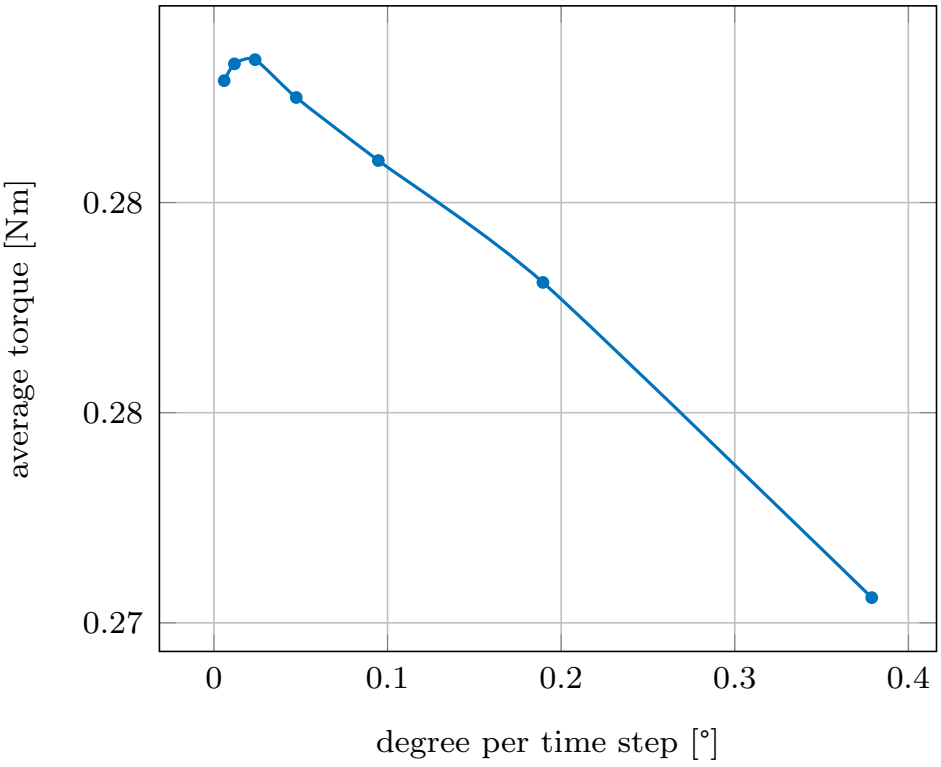

Figure 4.8: Average resistive torque as a function of degree per time step

4.3 Sensitivity Analysis of Inlet Jet Position

From the results obtained in the previous sets of simulations regarding the average resistive torque, it became evident that a method to increase the output torque was necessary to produce a viable experimental setup. A threshold of 1 Nm had been established for the minimum required output torque, which needed to be measured by the torque meter to ensure that the experiment yielded meaningful results. However, it was clear from the previous simulations, that the output torque was insufficient to meet this threshold. Given that the rotational speed of the gear system had already reached the operational limit of the test bench, increasing the speed was not a feasible option. This left the volumetric flow rate as the primary factor to manipulate in order to increase the torque. Yet, increasing the flow rate would have introduced complications, such as reducing the visibility of the phenomenon due to the higher amount of oil entering the chamber. Thus, it became necessary to explore an alternative method for maximizing the output torque.

One viable approach was to investigate the effect of the oil jet angle. In the basic configuration adopted up to now the oil jet was always directed perpendicular to the center of the gear. However, it could also be possible to direct the jet with an angle to the teeth of the gear. The easiest method to obtain this angle is to offset the oil jet nozzle with respect to the center gear axle; this solution was chosen mainly to simplify the physical realization of this component in the experiment setup. For this reason, the off-centering of the oil jet has been studied in this chapter.

By adjusting the position of the jet, the objective was to determine at which point the maximum resistive torque would be achieved without significantly affecting other aspects of the performance of the system. The rationale behind this approach is based on the expectation that changing the jet position could affect how the oil impacts the gear teeth, thereby influencing the torque output. Specifically, if the oil jet could be directed at the leading face of the tooth gear, increasing the angle at which the jet impacts the surface and the duration of this interaction, an increase in torque was expected. This is because the interaction between the first face of the tooth is the one creating the resistive torque.

Figure 4.9 shows how the offset has been applied; having imposed a clockwise rotating motion to the gear, the jet was moved to the left trying to obtain an increase in torque by raising the resistance of the gear motion. The offset has been measured in mm and it is applied starting from the center of rotation of the gear.

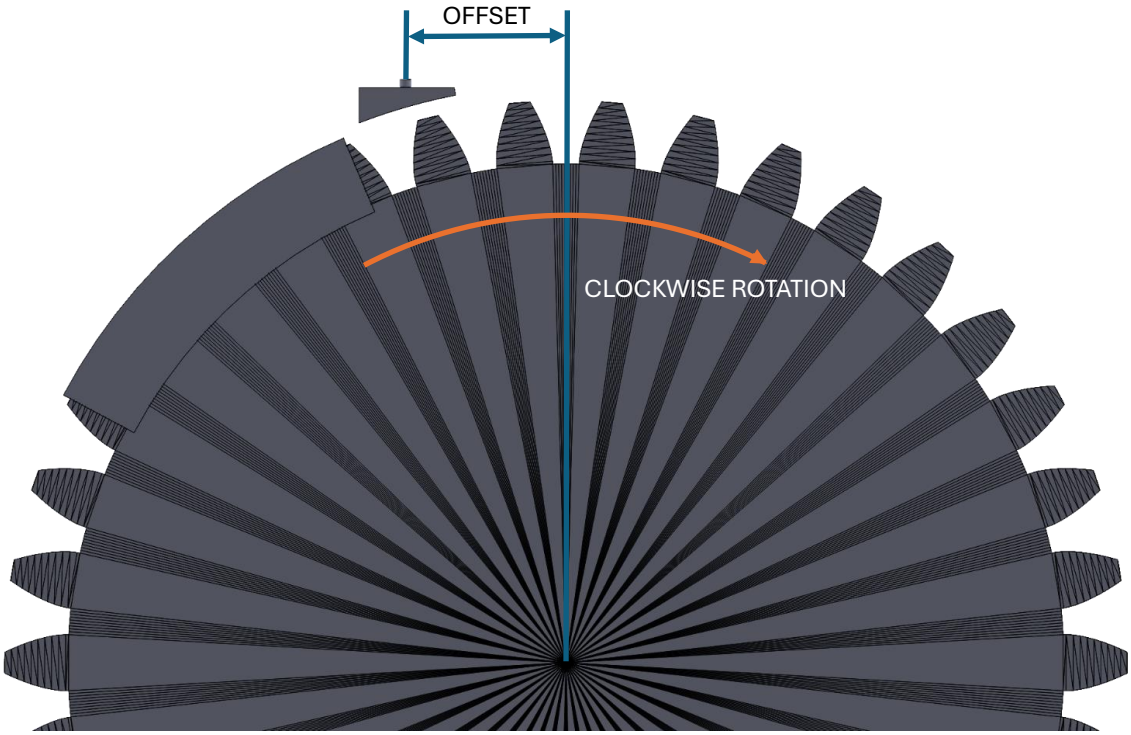

Figure 4.9: Jet offset definition

The results of this investigation are summarized in Table 4.3, which shows how the jet offset has been changed from the center position at 0 mm up to the maximum distance of 69 mm where the contact between the oil jet and the tooth is perfectly perpendicular and at mid-tooth heigh. The increases in offset distance were 10 mm each and some refined steps were done around the 60 mm mark, where an unexpected reduction in torque was encountered. In fact, looking at the table an increase in resistive torque has been obtained for almost every offset, except for that region, with increasing value for higher offset values.

simulation	mesh size [mm]	time step per gap [-]	jet offset [mm]	average torque [Nm]	average torque [%]	average torque variation [%]
1	0.0002	100	0	0.1412	100.00	0.00
2	0.0002	100	10	0.1496	105.89	5.89
3	0.0002	100	20	0.1577	111.67	11.67
4	0.0002	100	30	0.1609	113.93	13.93
5	0.0002	100	40	0.1609	113.96	13.96
6	0.0002	100	50	0.1684	119.26	19.26
7	0.0002	100	55	0.1597	113.11	13.11
8	0.0002	100	60	0.1375	97.38	-2.62
9	0.0002	100	65	0.1782	126.21	26.21
10	0.0002	100	69	0.1738	123.05	23.05

Table 4.3: Simulation settings and results of inlet jet position analysis

The graph in Figure 4.10 illustrates the effect of varying the oil jet position on the average resistive torque. As hypothesized, increasing the offset of the oil jet from the gear center leads to a corresponding increase in resistive torque. This behavior can be attributed to several factors. First, as the jet is moved farther from the gear center, the lever arm through which the force of the jet acts on the gear teeth becomes longer, resulting in greater torque. This is a direct consequence of the torque formula, where torque is the product of force and the perpendicular distance from the pivot point.

Additionally, the offset jet position causes the oil to strike the leading face of the tooth for a longer duration. The first face of the gear tooth, which is responsible for generating the resistive torque, experiences more prolonged exposure to the oil stream. Moreover, the angle at which the oil impacts the tooth is increased, meaning that the oil strikes the surface more directly and efficiently. These combined factors contribute to the observed increase in resistive torque as the jet offset increases.

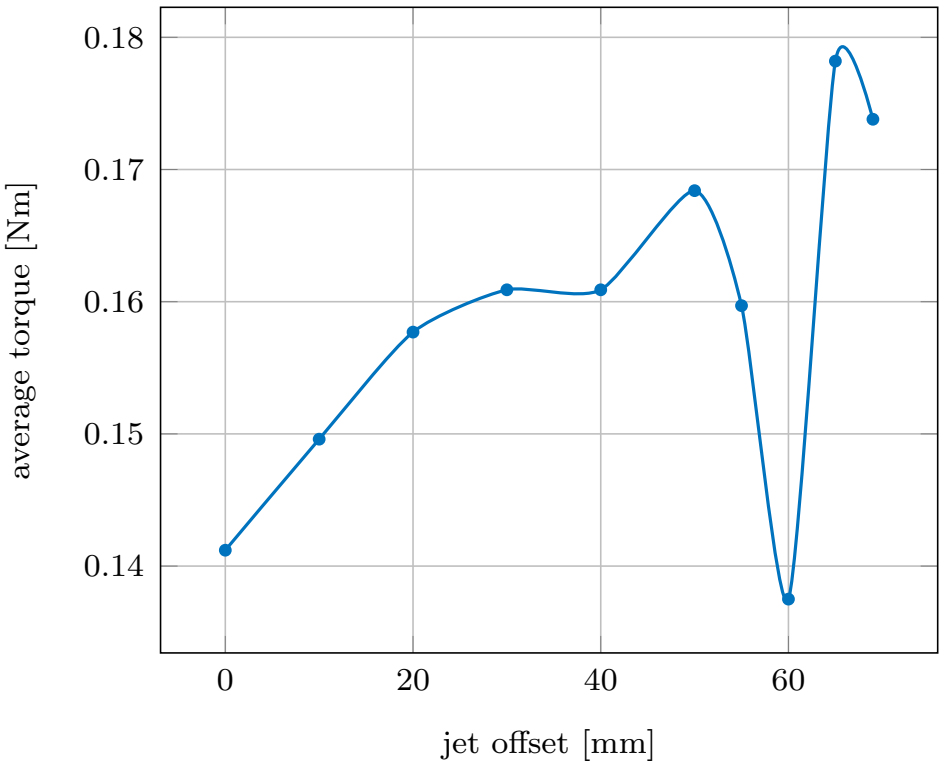

Figure 4.10: Average resistive torque as a function of jet offset

However, beyond a certain point, further increases in the offset distance lead to a sharp decline in the resistive torque, up to values lower than those recorded when the jet was positioned at the center of the gear. This unexpected reduction in torque is due to geometric factors. Specifically, when the jet offset is set to a distance of 60 mm, during the rotation of the gear, the tooth that first encounters the oil stream moves out of range, significantly shortening the length of the oil jet. This causes the need for additional time before the jet can impact the next tooth effectively.

As the first tooth moves past the jet, the vertical distance between the oil stream and the next tooth increases significantly. Consequently, the oil jet has to travel a greater distance to reach the next tooth, reducing the duration and effectiveness of the impact. Moreover, the oil jet is able to penetrate for a very limited distance in the teeth gap so only the top part of the tooth is in contact with the oil jet and for a very short time. The result is a drastic reduction in the resistive torque, as the

oil stream no longer sustains a strong, continuous collision with the gear teeth. In Figure 4.11 is reported the graph of the instantaneous resistive torque for 50 mm and 60 mm offset, and it is visible how the torque is reduced in duration and amplitude for the 60 mm offset.

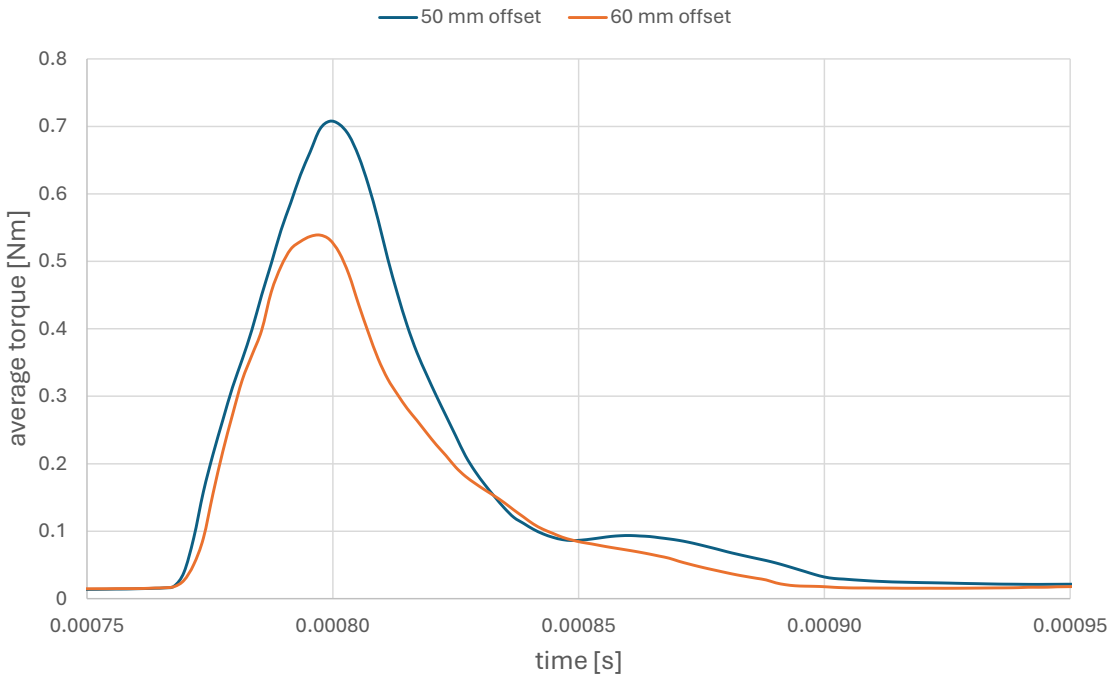

Figure 4.11: Resistive torque as a function of time for different jet offset

Figure 4.12 illustrates two frames for the 50 mm offset case (top) and two frames for the 60 mm offset case (bottom). From the initial frames, a significant difference in the behavior of the oil jet can already be observed. In the bottom view, the oil jet is more dispersed, indicating that a smaller quantity of oil enters the tooth gap effectively.

In the subsequent frames, it becomes evident that, for the 60 mm offset case, the oil jet barely enters the tooth gap, with only a minimal amount of oil making contact with the tooth surface. While the angle of impact of the oil jet on the tooth surface is more optimal, the reduced quantity and duration of the oil impact result in diminished lubrication efficiency. Consequently, the 60 mm offset leads to a decrease in resistive torque.

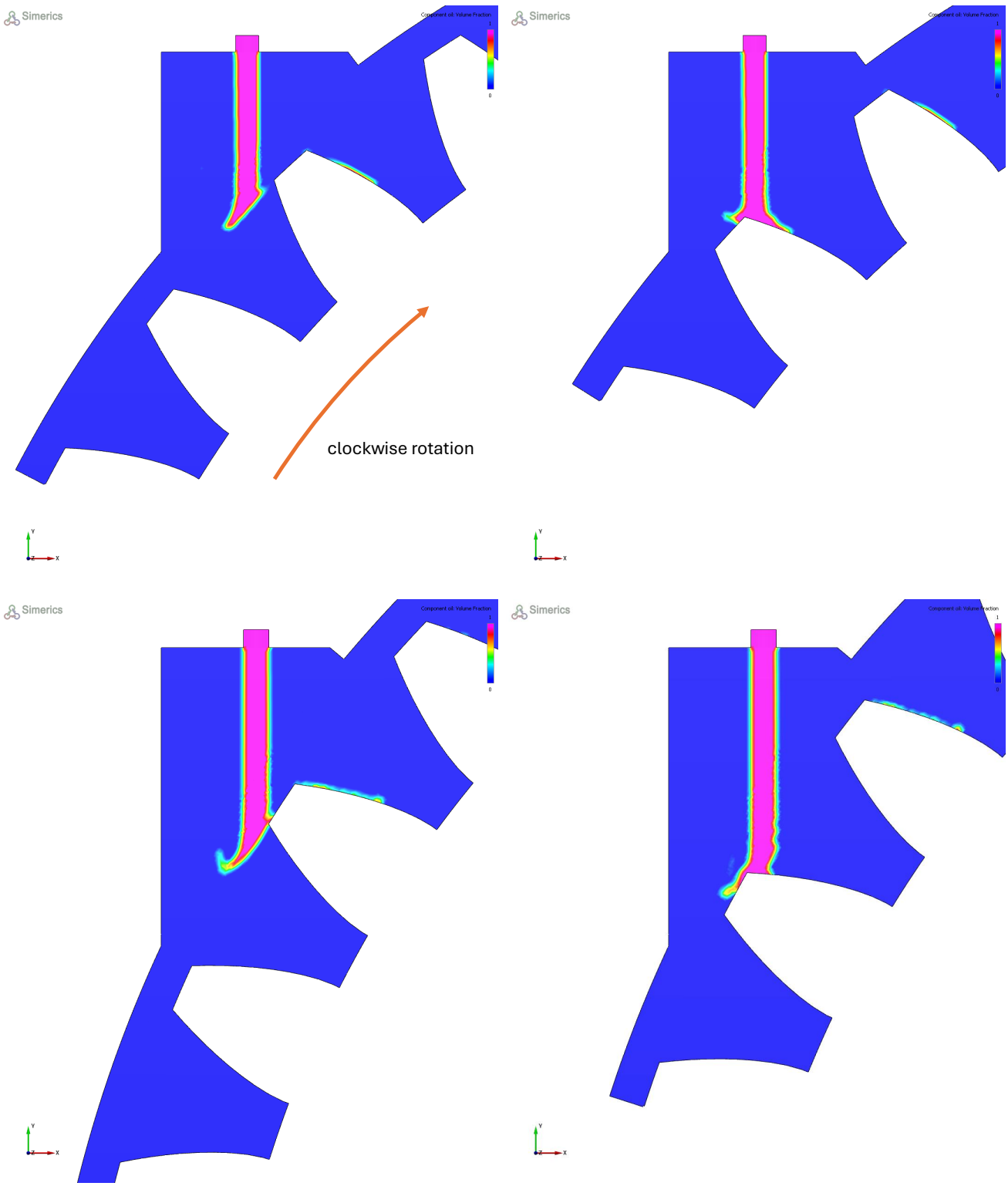

Figure 4.12: Section view of the oil volume fraction at mid-gear thickness for a jet offset of 50 mm (top) and 60 mm (bottom)

After the deep in the resistive torque is possible to highlight the increase, up to the maximum, for bigger offset distances. These results indicate that the maximum resistive torque is achieved when the oil jet is nearly tangent to the gear surface. At this position, the oil strikes the first surface of the tooth, which is responsible for generating resistive torque, in a manner that is nearly perpendicular to the face of the tooth. This creates an ideal impact angle, allowing the oil stream to exert maximum force on the tooth in the direction that generates resistive torque. This results in a localized maximum torque when the oil jet is directed tangentially on the pitch circumference of the gear. The problem with this position is that the lubrication is not as effective as before and a higher amount of nebulization is present due to the bigger velocity difference between jet and tooth.

After thoroughly analyzing the data from this sensitivity study, an offset value of 50 mm was chosen for future simulations and experiments. This offset was selected as it provided a significant increase in resistive torque, almost 20%, without introducing the negative side effects observed at larger offsets. Specifically, it maximized the torque output while maintaining a balance between efficiency and practical considerations, avoiding the sharp reductions in torque seen at higher offset distances like 60 mm. This value represents an optimal compromise, ensuring that the resistive torque is enhanced as much as possible while minimizing the risk of undesirable secondary effects such as inefficient oil collisions or excessive simulation complexity due to high oil nebulization. Unfortunately, this change was not sufficient to reach the target torque.

4.4 Sensitivity Analysis of Volumetric Flow Rate

The final set of simulations was conducted to determine the optimal volumetric flow rate required to achieve a measurable and reliable resistive torque for the experimental tests. The primary objective was to identify the flow rate that would result in a resistive torque exceeding 1 Nm, ensuring that the torque could be accurately measured by the torque meter. To this end, seven simulations were performed, and the results are summarized in Table 4.4.

simulation	mesh size [mm]	time step per tooth gap [-]	jet offset [mm]	volumetric flow rate [L/min]	jet diameter [mm]	jet velocity [m/s]	average torque [Nm]	average torque [%]	average torque variation [%]	upstream pressure [bar]
1	0.0002	100	0	2.50	1.40	27.07	0.1412	100.00	0.00	6.10
2	0.0002	100	0	12.00	1.40	129.92	0.5995	424.48	324.48	72.88
3	0.0002	100	0	20.00	1.40	216.54	0.9994	707.66	607.66	169.05
4	0.0002	100	50	3.00	1.40	32.48	0.2111	149.44	49.44	7.32
5	0.0002	100	50	5.00	1.40	54.13	0.4115	291.40	191.40	16.56
6	0.0002	100	50	9.00	1.40	97.44	0.9761	691.12	591.12	46.81
7	0.0002	100	50	10.00	1.40	108.27	1.1418	808.51	708.51	56.81
8	0.0002	100	50	5.00	1.00	106.10	0.5949	421.26	321.26	59.86

Table 4.4: Simulation settings and results of volumetric flow rate analysis

From the analysis, it was determined that to reach the desired average resistive torque of over 1 Nm, the minimum volumetric flow rate should be 10 L/min. At this flow rate, the oil jet achieves a velocity of 108.27 m/s, and the system requires an upstream pressure of 47.90 bar. These parameters are achievable with the available equipment in the laboratory, making this flow rate a practical option for the experimental setup. The tangential velocity of the gear is 67.02 m/s so a ratio of 1.62:1 is present in the final configuration between jet and gear speed.

As shown in Table 4.4, the average resistive torque increases with higher volu-

metric flow rates, as anticipated. This is due to the greater quantity of oil that is colliding with the gear teeth, generating higher resistive torque. The relationship between flow rate and resistive torque is directly proportional, as the increased flow rate delivers more oil to the gear, thereby exerting a greater force and generating higher torque. This aligns with the theoretical expectation that more oil volume will result in a higher momentum transfer to the gear, leading to an increase in resistive torque.

Interestingly, simulations with a smaller nozzle, which increases both the jet velocity and upstream pressure, did not yield a proportional increase in resistive torque. While the smaller nozzle does result in a higher jet velocity, and consequently a greater impact force on the gear teeth, the increase in resistive torque is more modest than expected. This can be explained by the fact that, although the velocity increase of the jet, the total volume of oil delivered to the gear remains constant. When compared to a bigger jet diameter with the same jet velocity the increase in velocity alone does not compensate for the reduced oil quantity, and therefore, the increase in torque is limited. The momentum of the oil jet rises with velocity, but the overall impact on resistive torque is less significant because the volume of oil, which is a key factor in force generation, does not increase.

Moreover, for the system to achieve an acceptable final value of resistive torque using a smaller nozzle, the required upstream pressure would have to exceed the operational limits of the available equipment. In fact, the simulations indicated that pressures higher than what is obtainable from the supply line would be necessary to attain the desired torque values with smaller nozzles. This poses a significant safety concern, as operating at excessively high pressures could risk equipment failure or damage. Therefore, after careful consideration of these factors, a nozzle with a radius of 1.4 mm was chosen as the optimal configuration for the final experimental tests. This nozzle size strikes a balance between achieving the necessary resistive torque and maintaining safe operating pressures.

To further understand the influence of jet position and nozzle size on the required volumetric flow rate and upstream pressure, two additional simulations were performed with the jet centered in its original position and using a 1 mm nozzle. The results of this study show that, to obtain a resistive torque within the target range, the oil jet would need to achieve a velocity of 216.54 m/s, which would require an upstream pressure of 188.57 bar. This pressure far exceeds the capabilities of the current laboratory setup and is not feasible for safe operation. These findings further emphasize the importance of selecting a nozzle size and jet offset that balances the

need for sufficient resistive torque with the practical constraints of the experimental system.

The graph in Figure 4.13 illustrates that the average resistive torque is directly proportional to the volumetric flow rate. Therefore, to increase the average torque, it is sufficient to increase the volumetric flow rate accordingly. For different jet diameters, the plot retains this proportional relationship, but with variations in slope. Specifically, a smaller diameter results in a steeper slope, while a larger diameter produces a shallower slope. This effect is highlighted by the results reported in Table 4.4, where the 1 mm nozzle diameter achieves higher oil jet velocity and average resistive torque compared to the 1.4 mm nozzle diameter. This behavior can be attributed to the increased jet velocity associated with smaller nozzles. The plot also highlights the increase in average resistive torque when transitioning from the no-offset to the 50 mm offset configuration.

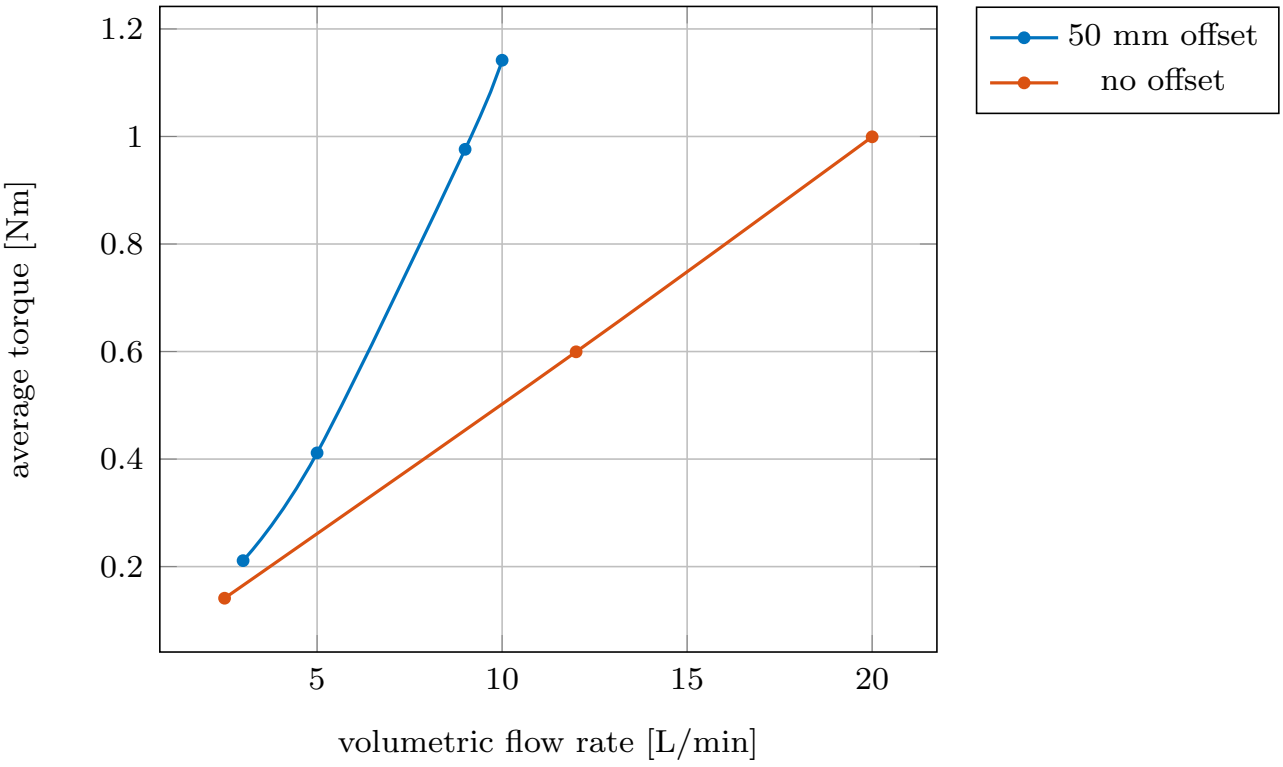

Figure 4.13: Average resistive torque as a function of volumetric flow rate for a nozzle diameter of 1.4 mm and different jet offset

Figure 4.14 highlights how the upstream pressure increases with the volumetric flow rate. Although it is not immediately obvious from the plot, this relationship follows a quadratic trend, meaning that doubling the volumetric flow rate results in a fourfold increase in upstream pressure. This indicates that careful attention must be given to the volumetric flow rate, and it should be limited as much as possible to prevent the upstream pressure from reaching unsafe levels.

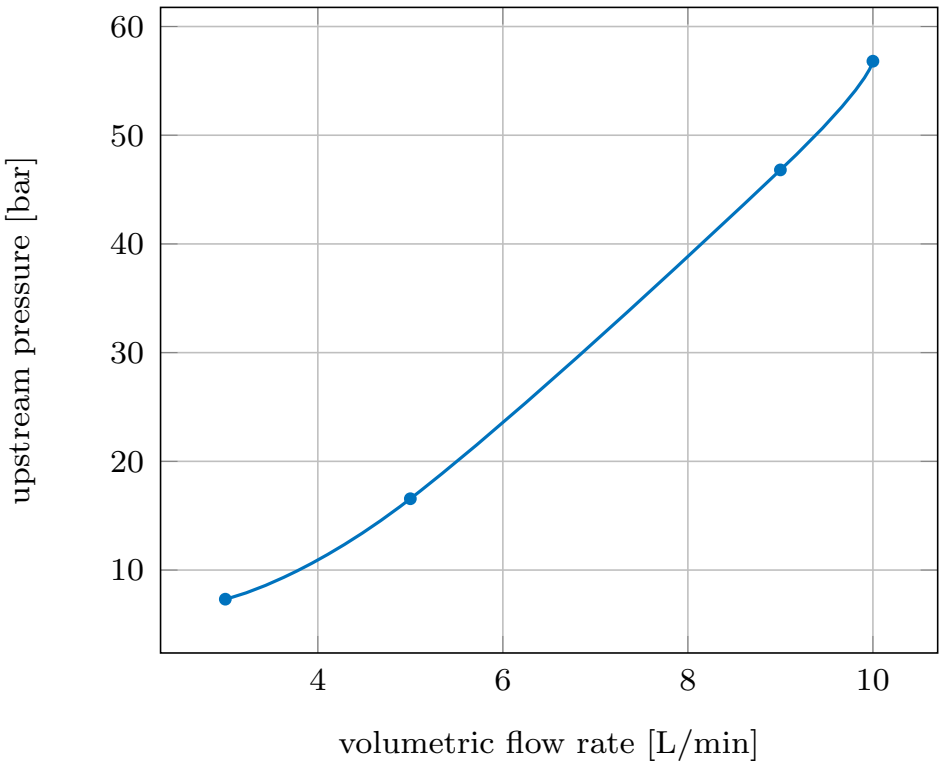

Figure 4.14: Upstream pressure as a function of volumetric flow rate for a nozzle diameter of 1.4 mm

Finally, Figure 4.15 illustrates the increase in average resistive torque as the upstream pressure rises. It also highlights how jet offsetting increases the average resistive torque for the same upstream pressure, making it easier and safer to achieve 1 Nm of torque due to the lower upstream pressure required. Additionally, it is important to note that the no-offset configuration would exceed the pressure limit of the hydraulic oil delivery system, rendering the experiments unfeasible.

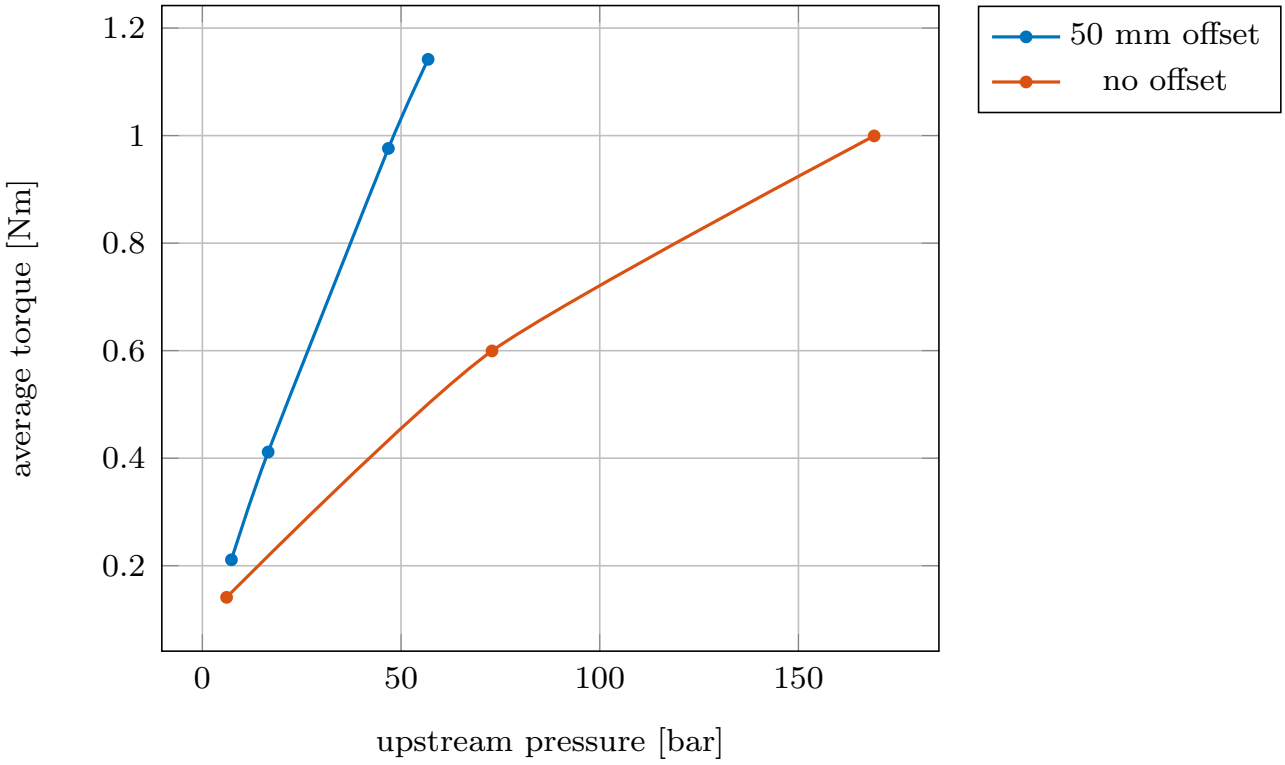

Figure 4.15: Average resistive torque as a function of upstream pressure for a nozzle diameter of 1.4 mm and different jet offset

The study of volumetric flow rate and jet parameters revealed that a flow rate of 10 L/min, paired with a 1.4 mm nozzle radius, offers the best compromise between performance and safety. This configuration allows the system to reach the necessary resistive torque while keeping pressures within safe and achievable limits. Any attempt to increase torque through higher flow rates or smaller nozzles would either yield diminishing returns or require pressures beyond the safe threshold, making the selected configuration the most practical solution for the experimental tests.

4.5 Partial Simulations Results

Figure 4.16 shows a series of frames illustrating the magnitude of oil flow velocity for oil volume fractions greater than 1% during a partial simulation. In this case, an oil jet with a diameter of 1.0 mm and a volumetric flow rate of 2.5 L/min was used, with no offset applied.

In the first frame (time = 0.000411 s), the oil jet is seen impacting the first tooth of the gear. This impact covers the front and top faces of the tooth with a thin layer of oil. However, as the jet progresses over the top, it detaches from the tooth surface. This detachment indicates that the rear face of the tooth is left almost entirely without lubrication; the simulation results show no visible oil film on this part, which could imply an area of insufficient lubrication in real-world conditions.

As the gear rotates, the oil jet elongates, penetrating further into the gaps between the teeth. This extension of the jet is accompanied by two side oil streams, visible on either side of the main jet. These streams form as the initial impact disperses the oil outward, which is then dragged along by the motion of the gear. When the jet encounters a new tooth surface, it impacts around mid-height and immediately begins to spread over the front surface, while simultaneously accelerating to match the rotational speed of the gear.

In the second frame (time = 0.000444 s), this interaction is even more pronounced. Here, the oil jet, initially traveling at a speed of 56 m/s, is shown to accelerate to 100 m/s upon impact with the tooth due to the rotational motion of the gear. After this initial impact, the oil begins to spread across the surface of the tooth, and its velocity decreases to match the tooth speed, as it has lost its momentum in the negative Y direction and now adheres to the motion of the gear.

By the third frame (time = 0.000493 s), two distinct wakes are visible on either side of the tooth, each exhibiting a velocity of around 80 m/s. These wakes represent regions where the oil has been directed outward due to the impact dynamics and the subsequent shearing effect of the rotating tooth.

In the final frame (time = 0.000526 s), these wakes continue to expand as they exit the tooth surface, gradually dissipating as they move away from the gear. From the partial simulations, it is not possible to determine how this oil will behave once it exits the axial thickness of the gear; this is why complete simulations were performed.

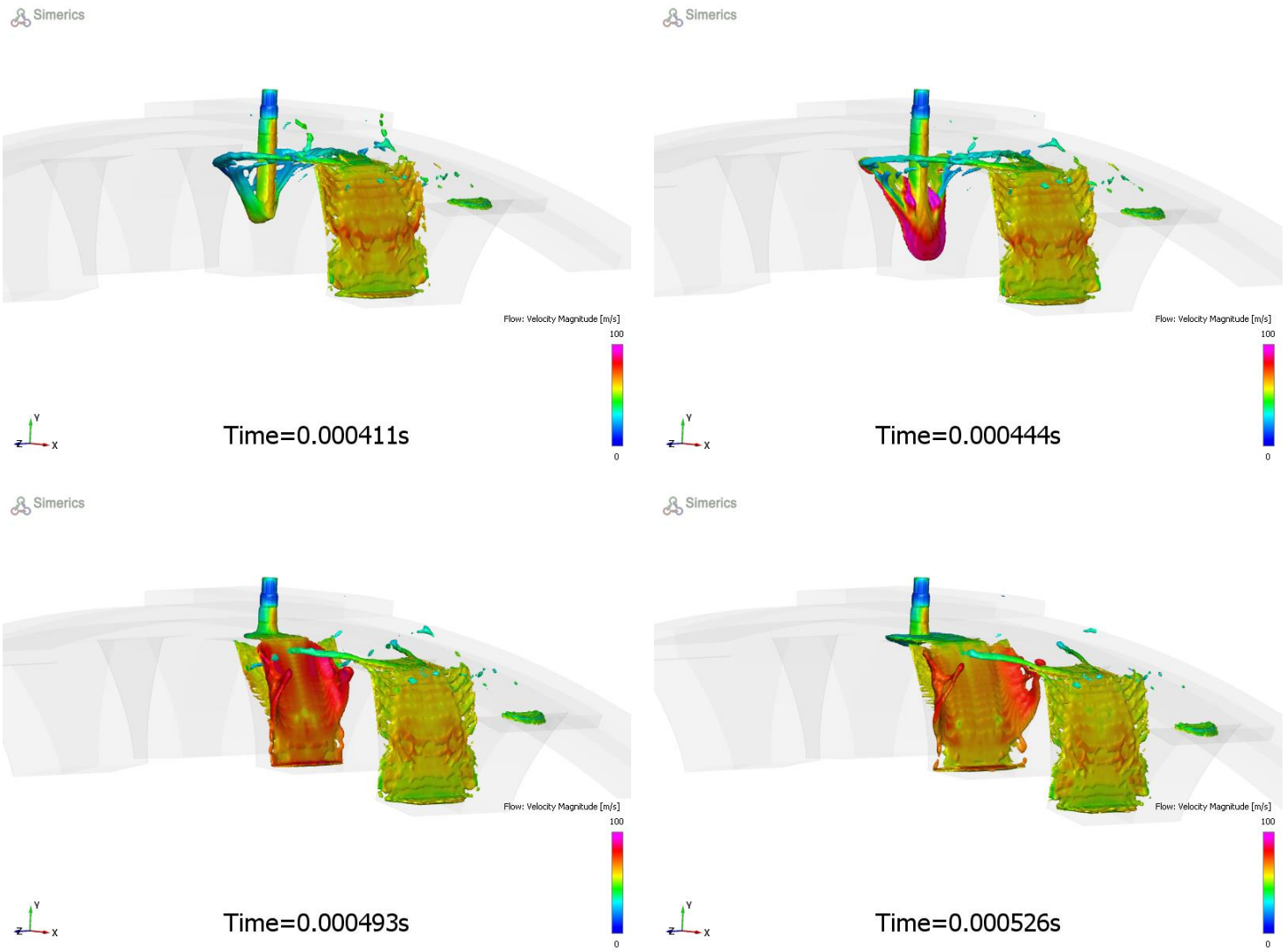

Figure 4.16: View of the partial simulation illustrating the oil flow velocity magnitude for oil volume fractions greater than 1%

Figure 4.17 shows a series of frames displaying the mid-thickness section of the gear, illustrating the oil volume fraction over time from the same simulation as in the previous figure. In these images, the blue areas represent regions with an oil concentration of 0%, and so air, while the purple areas indicate regions with a concentration of 100% oil.

Observing the oil jet, it is evident that the central portion of the jet, which corresponds to the diameter of the nozzle, is composed entirely of oil. Surrounding this core, there is a thin outer layer where a gradient is visible, transitioning from pure oil to pure air as it moves outward.

In the first frame (time = 0.000345 s), the oil jet is seen impacting the right side and top surface of the first tooth. This impact leaves a thin film of oil on these surfaces, with some oil reaching the lower part of the tooth gap. It is noticeable that the jet does not impact the left surface of the tooth; however, within a very short time, the oil jet has already entered the tooth gap.

In the second frame (time = 0.000411 s), the oil jet has penetrated further into the tooth gap, nearing the point of contact with the next tooth. The oil film on the right side of the first tooth remains attached, providing consistent lubrication across the surface.

The third frame (time = 0.000444 s) shows the initial contact between the oil jet and the new tooth. Here, the oil begins to spread immediately over the lower part of the tooth, rapidly covering the surface. By the fourth frame (time = 0.000477 s), the oil has quickly reached the base of the tooth gap, demonstrating efficient coverage along this surface.

In the fourth and fifth frames (times = 0.000477 s and 0.000493 s, respectively), the oil jet fully covers the right side and begins to spread across the top surface of the tooth as it is compressed by the rotating gear. This compression distributes the oil across the entire top surface, ensuring a comprehensive oil film.

Finally, in the sixth frame (time = 0.000526 s), the oil jet is observed leaving the tooth, with an established oil layer on the tooth surfaces that were in contact. This sequence demonstrates the continuous oil coverage achieved by the jet impact and the flow dynamics as the oil spreads to maintain lubrication on key gear surfaces.

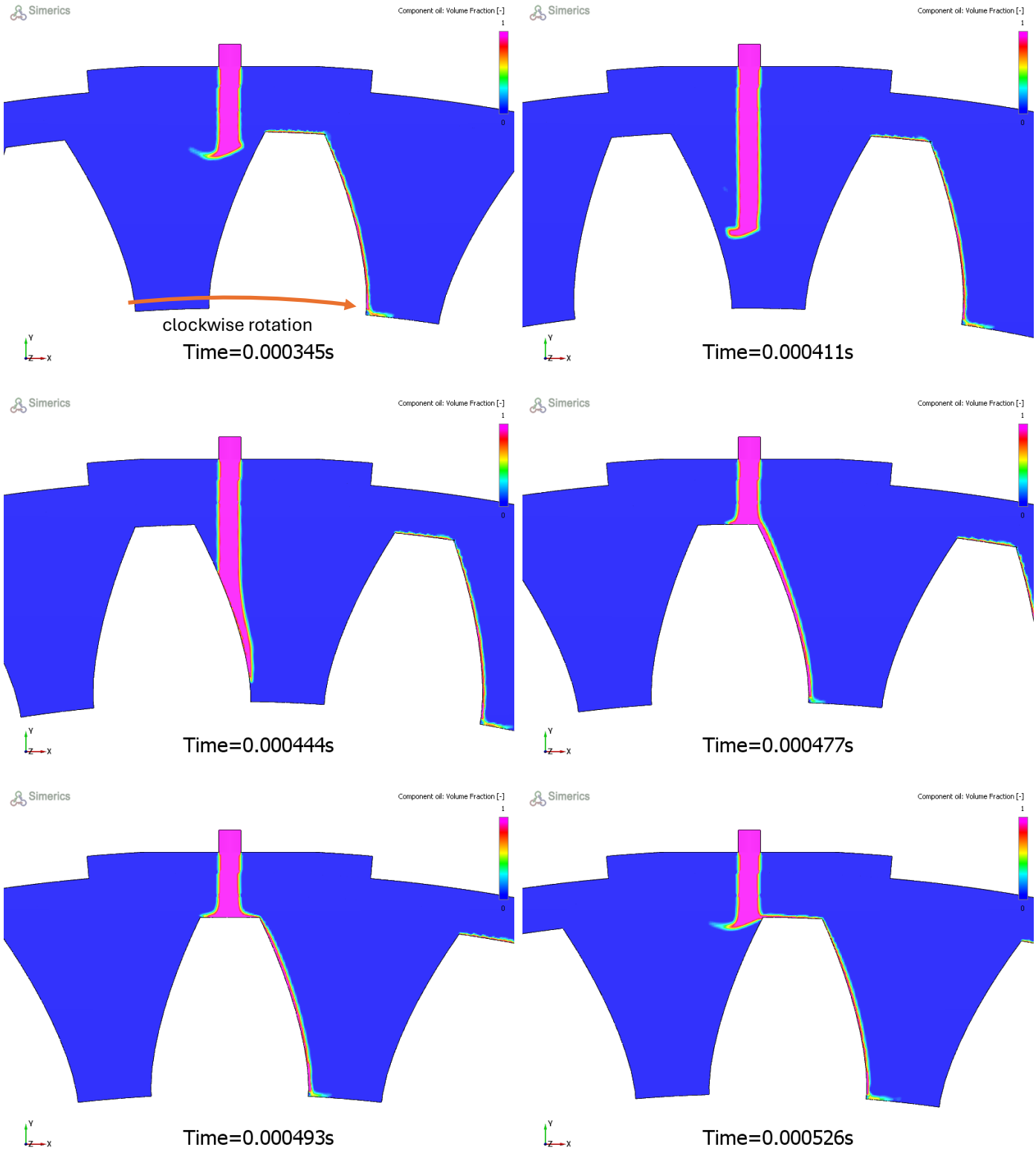

Figure 4.17: Section view of the partial simulation at mid-gear thickness illustrating the oil volume fraction

Figure 4.18 displays the average and instantaneous resistive torque values from the simulations discussed earlier, represented by the orange and blue lines, respectively. The instantaneous resistive torque reveals distinct peaks that occur each time the oil jet impacts the correct surface of the teeth. These peaks are periodic, with consistent timing, though slight fluctuations in their maximum values are observed. After the first impact, the simulation achieves stable accuracy, making extended simulations unnecessary and demonstrating the effectiveness of partial simulations for this study. The average resistive torque calculated for this simulation is 0.2810 Nm.

At the start of the simulation, an initial peak is observed due to air acceleration as the system initializes. However, these peaks quickly stabilize and drop almost to zero. The first tooth impact is excluded from the torque average calculation to eliminate the influence of these transient effects. Although the average resistive torque value is relatively low, instantaneous torque peaks exceed 1 Nm. Unfortunately, these instantaneous values cannot be captured during laboratory experiments due to their transient nature.

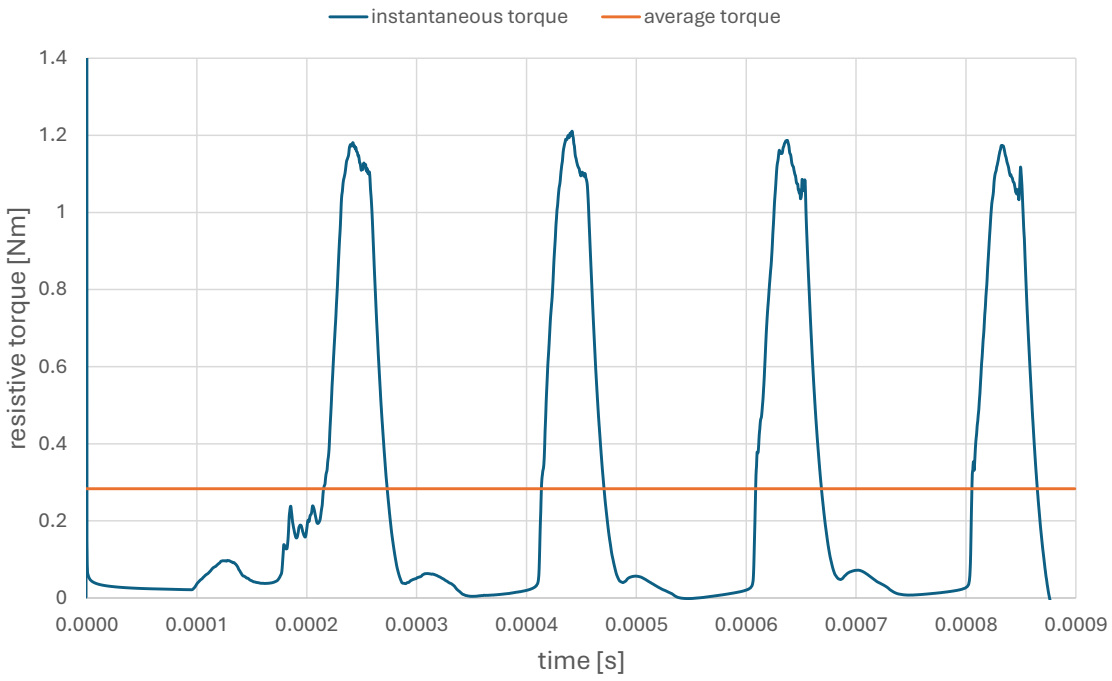

Figure 4.18: Instantaneous resistive torque as a function of time in partial simulation

4.6 Full Simulations Results

In the following figures, the results of a complete simulation are presented. Specifically, the simulation is set up with an oil jet diameter of 1.4 mm, a 50 mm offset, and a volumetric flow rate of 10 L/min.

Figure 4.19 displays the flow velocity magnitude for both air and oil at the mid-gear height section. In this image, the color gradient represents different velocity magnitudes, with blue areas indicating velocities close to 0 m/s, essentially regions where the air is almost stationary. On the opposite end, purple areas represent the highest velocities, reaching up to 150 m/s. The gradient in between corresponds to intermediate velocities between these two extremes.

From the figure, can be observed that the corners of the enclosure contain regions of nearly stagnant air, while the tooth gaps display significantly higher velocities for both air and oil. In these gaps, the air and oil trapped between the teeth are pushed forward by the rotating motion of the gear, creating zones of increased velocity. The gear tip velocity itself is approximately 67 m/s; however, the air and oil in the tooth gaps reach even higher velocities. This increase is due not only to the translational movement induced by the motion of the gear but also to lateral and outward flows caused by air and oil displacement around the gear.

In the top-left region of the image, the oil jet is visible as it enters the enclosure through a cylindrical inlet. The jet velocity here is around 108 m/s, highlighting its high momentum as it penetrates the system. To the left of the oil jet, the high-velocity air is visible. This velocity causes the air to collide with the oil jet, resulting in the initial breakup of the oil stream.

In the top-right portion of the gear, there is a prominent high-velocity region. This is primarily due to oil detachment from the gear surface, creating localized areas of dense oil accumulation. This detached oil is eventually propelled toward the top and right sides of the enclosure, where it contributes to the elevated presence of oil in these zones.

At the bottom of the case, under the gear, there is an opening where the oil can exit the enclosure. This feature facilitates circulation and helps maintain pressure equilibrium within the system.

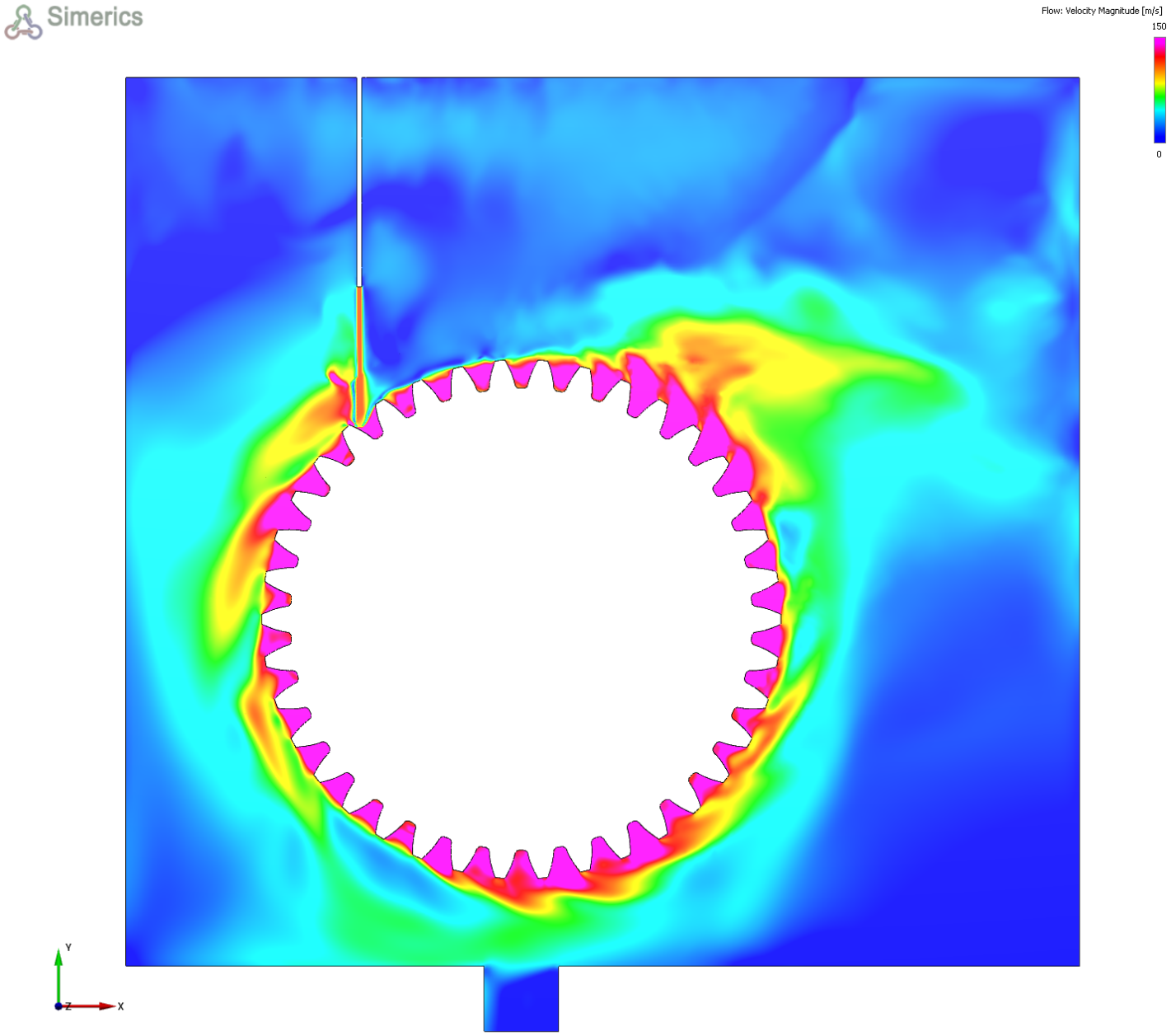

Figure 4.19: Frontal section view at mid-gear thickness of the complete simulation illustrating the flow velocity magnitude

In Figure 4.20, the lateral section from the same simulation shown previously in Figure 4.19 is illustrated, with a focus on the flow velocity magnitude. This side view provides a clearer perspective on the dynamics of the oil jet as it enters the enclosure. Observing from this angle, it becomes evident that the oil jet progressively widens as it travels from the injection point toward the impact area on the gear teeth. This expansion is primarily due to the interaction between the oil jet and the surrounding air, which induces instabilities and promotes the dispersion of the jet.

Upon reaching the gear teeth, the oil jet partially rebounds, creating two distinct wakes that are visible on the right and left sides at the top of the gear. These wakes indicate regions where the oil disperses and partially atomizes, forming fine droplets. Eventually, this dispersed oil exits from the front and rear walls of the gear enclosure. However, due to the limited axial domain in the simulation, it is not possible to fully capture the lateral spread and behavior of the oil beyond this section.

To address this in real-world applications, the enclosure was designed with a front window positioned at a considerable distance from the gear. This design choice was intentional, aiming to minimize the likelihood of oil droplets splashing onto the front window and obstructing visibility within the enclosure, a critical consideration for the high-speed slow-motion recordings.

In the lower region of the gear, a detachment zone is visible, where a portion of the oil separates from the gear surface and enters the return line. This detachment zone is significant for directing excess oil away from the gear and back into the lubrication system, facilitating efficient oil recirculation and preventing excessive accumulation of oil around the gear. Moreover, this exit is necessary for maintaining constant pressure inside the enclosure.

Additionally, it is worth noting that the air in front of and behind the gear remains relatively still, indicating minimal airflow in these regions. However, near the top of the enclosure, some movement is visible along the wall above the jet, where splashed oil causes localized air movement. This area represents a zone of higher air velocity, likely resulting from the interaction between the wall and the dispersed oil droplets, which contributes to a slight airflow in this otherwise stagnant region.

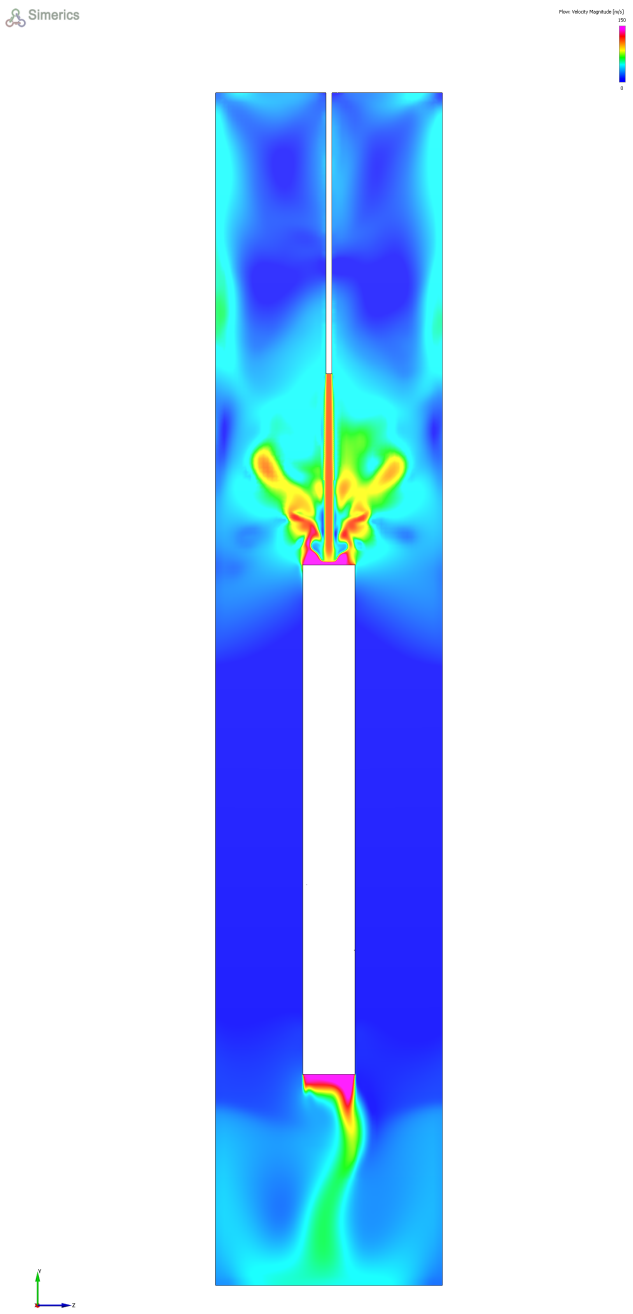

Figure 4.20: Lateral section view at mid-gear height of the complete simulation illustrating the flow velocity magnitude

In Figures 4.21 and 4.22, the distribution of oil within the enclosure is illustrated, derived from the same simulation previously discussed. These images focus on areas where the oil volume fraction exceeds 1%, with color gradients representing the velocity of the oil. Specifically, the blue areas indicate near-zero velocity (0 m/s), while the purple regions denote velocities approaching 150 m/s. This visual representation allows for a detailed analysis of the velocity and dispersion of the oil within the enclosure.

From these figures, it is evident that the outer regions of the oil jet exhibit lower velocities than the central core. This result aligns with expectations, as the external portion of the jet is composed predominantly of air, about 99%, which surrounds the core of the oil jet. Although this surrounding air is accelerated by the momentum of the jet, it does not achieve the same velocity as the core of the jet. Instead, this layer of entrained air decelerates the jet, contributing to the gradual breakup of the oil jet as it disperses. This interaction between the jet and surrounding air plays a significant role in the destabilization and atomization of the oil, essential for effective lubrication distribution.

Within the tooth gaps, a considerable amount of oil is visible as it exits both laterally and across the tops of the teeth. The high-velocity droplets of oil are tangentially propelled toward the right side of the enclosure, where they retain a significant speed until they make contact with the lateral wall. Other droplets, though moving at a lower velocity, ascend to the upper regions of the enclosure, impacting the ceiling of the enclosure. Fortunately, these dispersed droplets pose no risk of obstructing visibility, as there are no windows directly at the height of the gear on the top part of the enclosure. The windows on the right side, which may encounter some oil impact, serve primarily as secondary light entry points, with no critical function for observation or monitoring.

A particularly interesting feature of these images is the formation of oil droplets as they are expelled from the tooth surfaces due to the centrifugal force generated by the rotation of the gear. These droplets, propelled at high speeds, create an arched trajectory as they leave the tooth surface. This arched pattern is the result of the combined effects of gear rotation and tooth shape, which accelerate the oil particles to high velocity creating the previously mentioned wake at the right of the gear where most of the oil is detached and propelled to the right side wall.

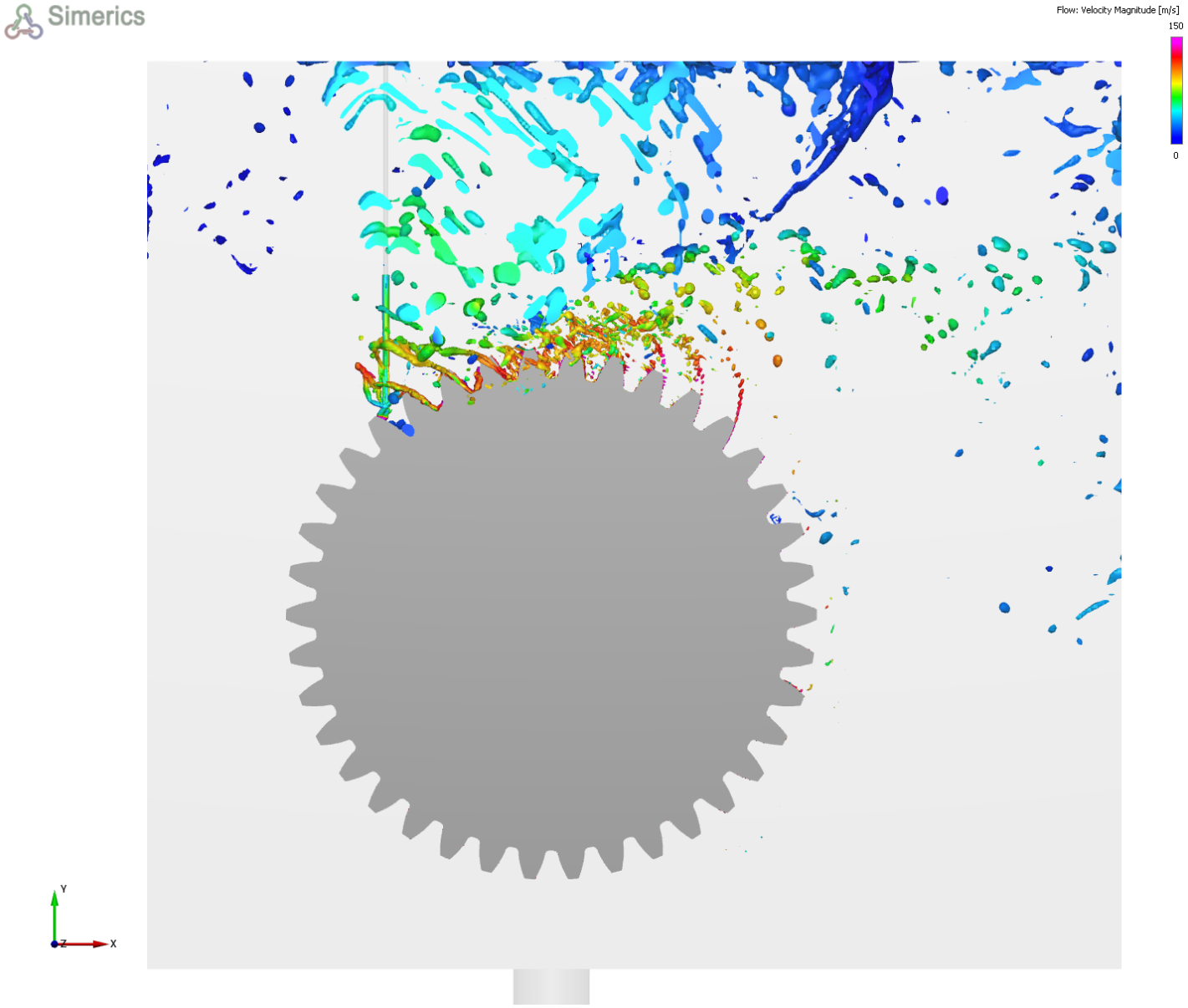

Figure 4.21: Frontal view of the complete simulation showing the oil flow velocity magnitude for oil volume fractions greater than 1%

No oil is visible in the lower part of the enclosure in these images. This is due to the limited duration of the simulation, which covers only a single gear rotation, or approximately 0.0075 seconds. If the simulation were extended for a longer period, it would likely show oil splashing against the enclosure walls and eventually settling at the bottom. This settled oil would then flow into the return line, completing the recirculation cycle within the lubrication system.

Finally, it is worth noting that the boundary layer effects are not accurately captured in this simulation. This limitation arises because a standard mesh template was applied to the gear, which does not account for the detailed boundary layer behavior. The choice for the general mesh template was due to sub-optimal performance in the simulation of the oil jet behavior. Unfortunately, unlike a specialized gear mesh, this general template does not allow for the boundary layer to be accurately represented, which may lead to minor discrepancies in the simulation results, especially near surfaces where boundary layer effects are prominent.

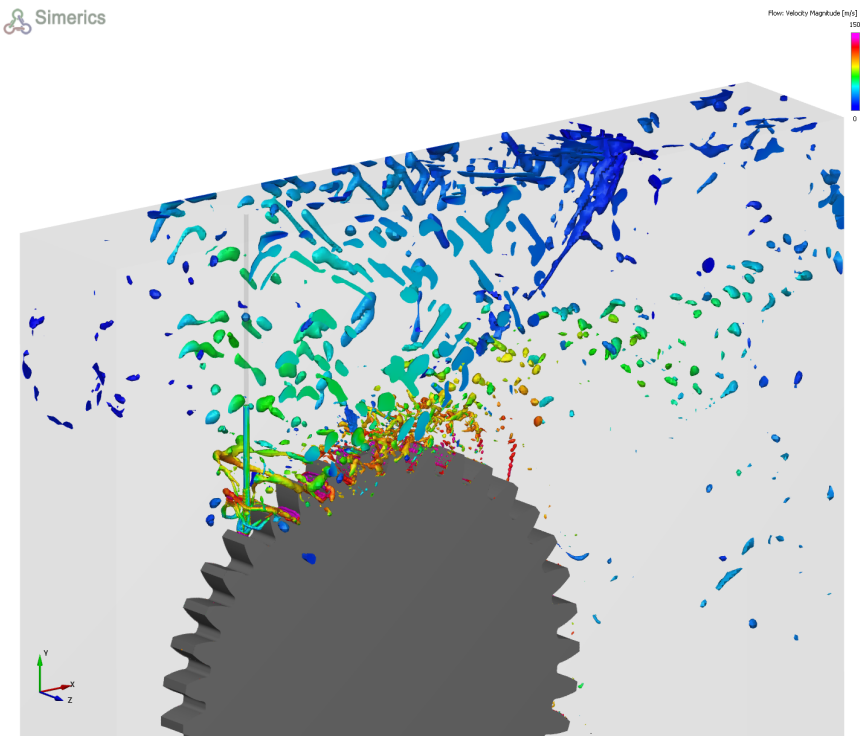

Figure 4.22: View of the complete simulation showing the oil flow velocity magnitude for oil volume fractions greater than 1%

In Figure 4.23, the average and instantaneous values of resistive torque are shown for the previously discussed simulations, represented in orange and blue, respectively. The plot focuses on a specific time interval, from 0.0070 s to 0.0100 s, to better illustrate the torque trend. The instantaneous resistive torque reveals that each time the oil jet impacts the right surface of the teeth, a peak is generated. These peaks have a constant period, although there is a slight fluctuation in the maximum values from one peak to the next. The average resistive torque for this simulation is 1.25 Nm, showing a minimal increase over the partial simulation result of 1.14 Nm, which underscores the effectiveness of the initial, partial simulations. As expected, a small discrepancy exists between the two, but the partial simulations provided a very accurate approximation.

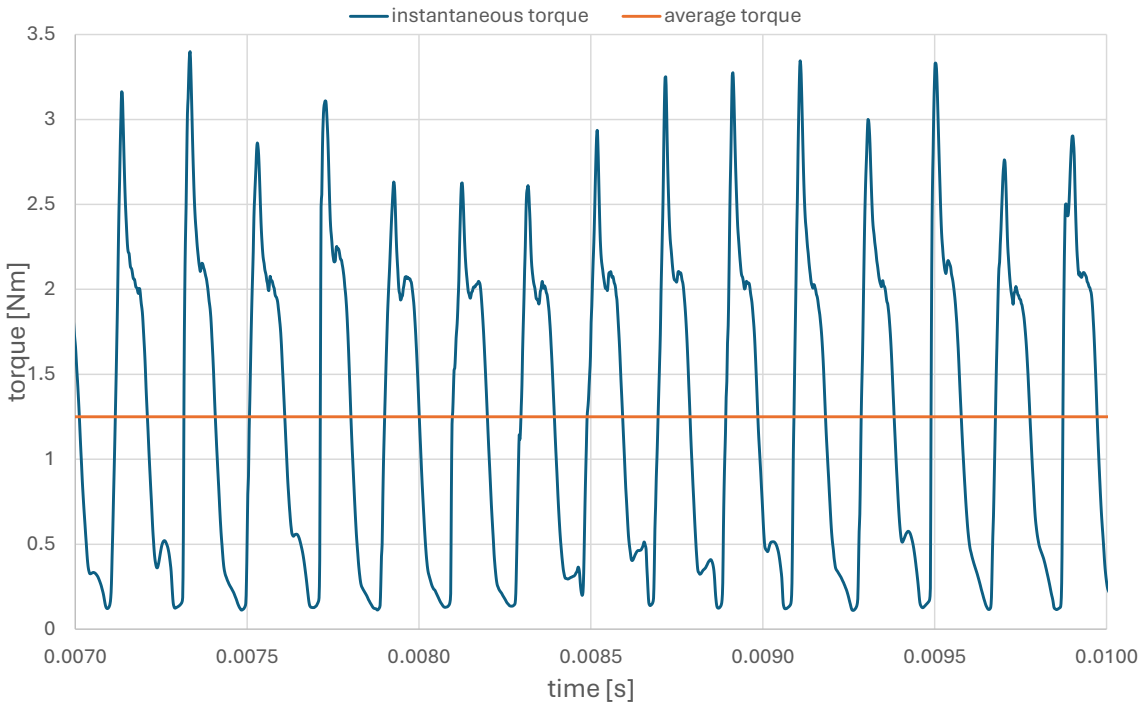

Figure 4.23: Instantaneous resistive torque as a function of time in complete simulation

Chapter 5

Design of Components for Laboratory Experiment

Based on the data collected from the simulations, the design of the various components for the laboratory experiment has been carefully refined and optimized. The objective of this design process was to replicate real-life operating conditions as closely as possible to the simulated scenario. However, it is essential to acknowledge that accurately reproducing all simulation parameters in a physical experiment presents significant challenges. Many factors in a laboratory setting, such as material tolerances, environmental fluctuations, and equipment limitations, may affect the ability of the experiment to match the simulation perfectly.

Given these challenges, it becomes crucial to focus on key parameters that directly influence the behavior of the system. During the experiment, these critical parameters will be meticulously measured to capture the actual operating conditions. Once the experimental data is collected, a new set of simulations will be conducted, incorporating the precise measurements obtained from the physical setup. This iterative approach allows for a more accurate comparison between the experimental results and the outcomes predicted by the simulation. By closely analyzing the deviations between real-world data and simulated results, the accuracy and reliability of the simulation software can be thoroughly assessed, providing valuable insight into its capabilities and limitations.

In this way, the experiment not only validates the design and operation of the components but also serves as a feedback mechanism for improving the simulation models. Ultimately, this iterative refinement of both physical and virtual models ensures that the laboratory setup closely aligns with theoretical expectations, leading to more reliable and meaningful conclusions in the study of gear lubrication dynamics.

The main components designed for this experiment are:

1. **Gear**: The primary object of study, housed within a controlled environment.
2. **External Enclosure**: Encloses the experiment, preventing oil from splashing outside, allowing for components mounting and maintaining controlled conditions.
3. **Threaded Rod**: Facilitates precise positioning of the oil jet at varying offsets and distances from the gear.
4. **Drive Shaft**: Secures the gear to the laboratory test bench spindle.
5. **Centering Plates**: Aligns the threaded rod and prevents oil splashes from escaping the case.
6. **Lexan Windows and Frames**: Seals the openings while allowing visual observation of the experiment.

5.1 Gear

The gear was modeled based on the parameters used in the simulation. The key design parameters have been summarized in Table 3.1. While Figure 5.1 illustrates the understudy gear geometry.

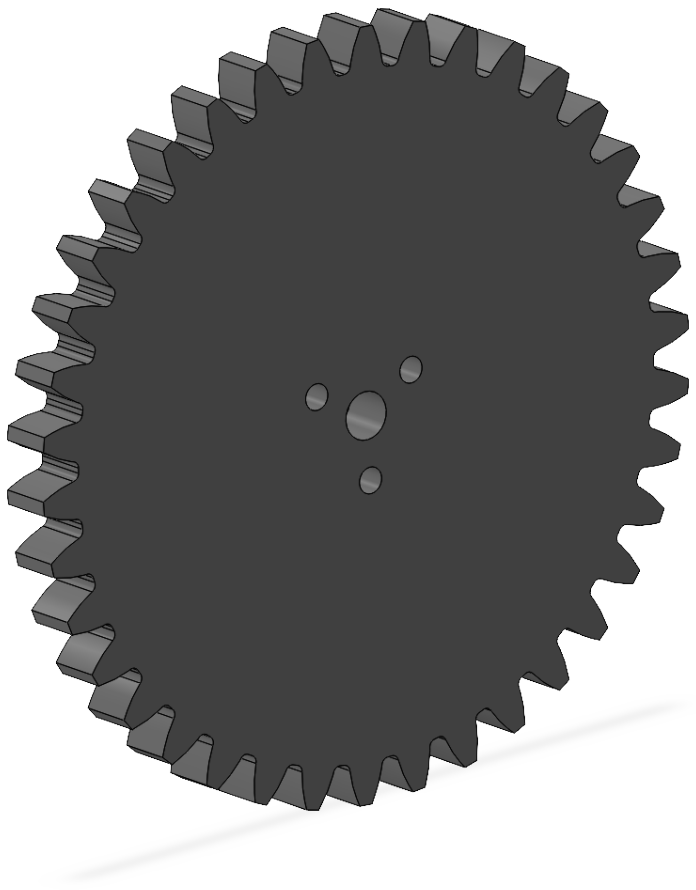

Figure 5.1: CAD model of the gear

5.2 External Enclosure

The external enclosure is constructed from stainless steel sheets with a thickness of 3 mm. Its front section has a height of 280 mm and a width of 300 mm, while the depth measures 265 mm. The overall depth was specifically chosen so large to ensure an adequate distance between the oil droplets and the observation windows. This design consideration helps keep the windows clean for extended periods, allowing longer time for capturing high-quality slow-motion video footage without obstruction.

At the top of the case, there is a slot designed to accommodate the threaded rod. This rod can be moved horizontally along the slot to adjust the position of the jet, enabling precise control of the jet offset relative to the gear. Additionally, the case is equipped with four strategically placed windows, the main one on the front, one on the top, and two on the sides. These windows provide ample illumination for the gear using LED lighting, which is critical for capturing high-speed slow-motion footage.

The rear of the case is equipped with four mounting holes that allow it to be securely attached to the test bench using M10 screws. A larger hole is also present to enable the passage of the test bench spindle. To ensure a proper seal between the case and the mounting surface, a gasket will be installed between the back of the case and the spindle mount.

In the lower section of the case, a cylinder with an internal G 1/2" threading is welded to allow the fastening of the oil return line, which directs the oil back to the reservoir. For ease of window installation, all openings are surrounded by threaded holes, allowing the windows to be fastened securely to the case. This design ensures both functionality and ease of maintenance during the experiment. A detailed image of the case is shown in Figure 5.2.

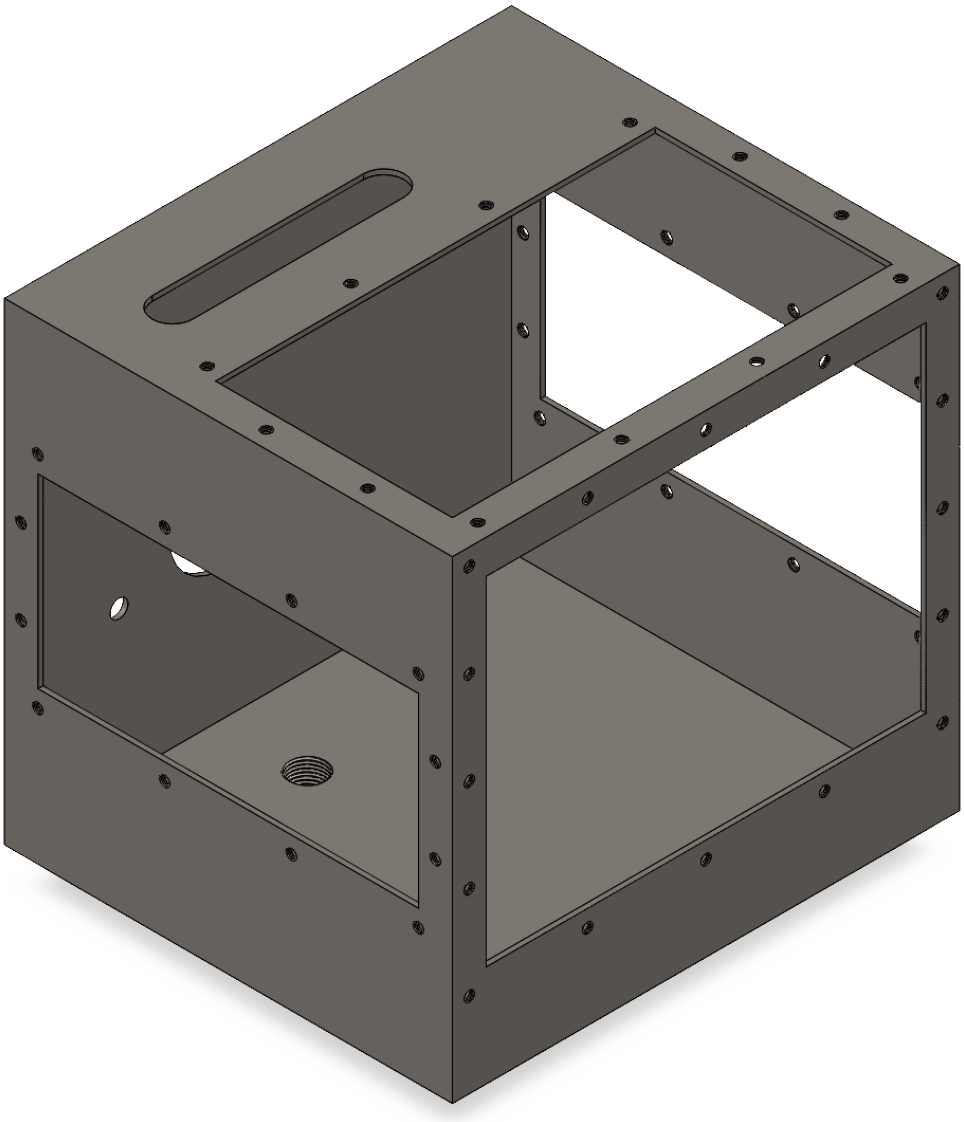

Figure 5.2: CAD model of the external enclosure

5.3 Threaded Rod

The threaded rod is manufactured by milling a 30 mm thick hexagonal stainless steel bar, creating two threaded sections while retaining a hexagonal shape in the middle to function as a nut to tighten the fitting connector and to have a flat surface for the pressure sensor mounting. One end of the rod features a shorter G 1/2" thread, designed for connecting a quick-release fitting that attaches the threaded rod to the main oil supply. The opposite end of the rod is 165 mm long and uses a standard M20x2.5 threading. This part is used to control the distance between the oil jet and the gear. The rod is positioned to the external case using two centering plates, whose primary function is to cover the unused portion of the case slot, preventing oil from splashing out. Additionally, two nuts with washers are used to fasten the rod in place. By adjusting the position of the top nut, the extent to which the rod is inserted into the case can be fine-tuned, thereby controlling the precise distance between the oil jet and the gear.

The threaded rod is hollow to allow oil to flow through its center. At its end, there is an M6x1.0 threaded hole where the nozzle nut is attached. This configuration allows for the flexibility of changing the nozzle nut, enabling the use of different jet sizes to meet the specific experimental requirements. Furthermore, one of the hexagonal faces of the rod has a threaded M5x0.8 hole designed to mount a pressure sensor, which will monitor the pressure upstream of the nozzle. The volumetric flow rate will be directly measured through the oil supply line, ensuring precise control of the oil flow during the experiment. Figure 5.3 shows the detailed structure of the threaded rod in a section view.

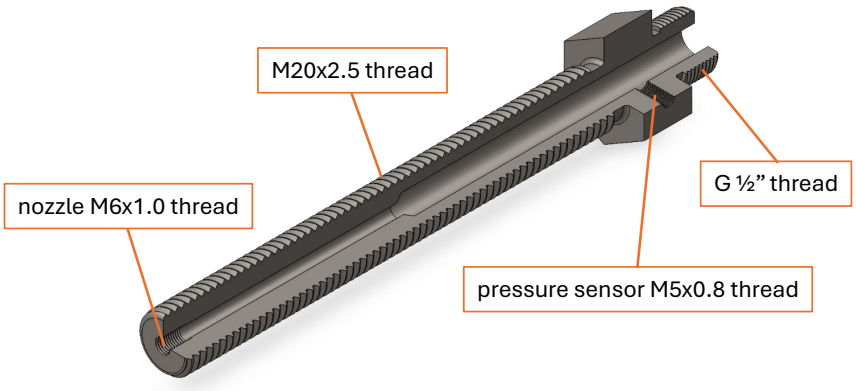

Figure 5.3: CAD model of the threaded rod

5.4 Drive Shaft

The drive shaft is made entirely of stainless steel and serves the critical function of fastening and securing the gear to the spindle of the laboratory test bench. This component includes a cylindrical section with a 20 mm diameter, which is designed to center the drive shaft on the spindle. Two lateral keys are integrated into this section, ensuring a rigid connection between the drive shaft and the spindle, thereby securing their synchronized rotation. To fix the drive shaft in place within the spindle, two lock nuts are employed. These lock nuts prevent the drive shaft from loosening or disengaging from the spindle during operation, ensuring the stability of the assembly.

On the opposite end of the drive shaft, there is another cylindrical section whose top surface serves as the backing face for the gear. This surface ensures that the gear is properly supported during the experiment. Additionally, this section is equipped with three threaded M5 holes, which are used to securely fasten the gear to the drive shaft, ensuring it remains fixed in position during rotation.

Finally, a smaller cylindrical section is present, specifically designed to center the gear on the drive shaft with high precision. This ensures the alignment and balance of the gear during operation, minimizing any risk of misalignment that could affect the experimental results. A picture of the drive shaft is shown in Figure 5.4.

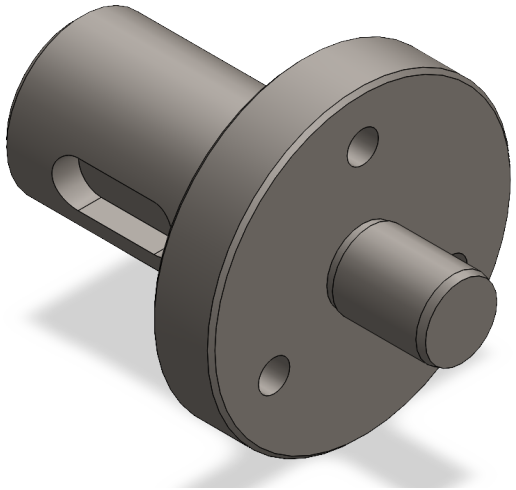

Figure 5.4: CAD model of the drive shaft

5.5 Centering Plates

As mentioned in the section on the threaded rod, centering plates are utilized to position the rod within the slot in the top part of the enclosure. These plates are made from 3 mm thick stainless steel, and two are used simultaneously, one on the outside and one on the inside of the enclosure. Their primary function is to position the threaded rod while also preventing oil from splashing out through the unused portion of the slot.

The top plate remains the same across all configurations and is designed to be sufficiently long so that it always covers at least 10 mm over the slot in both directions, regardless of the position of the rod. This ensures that no gaps are left exposed, effectively containing any oil within the case.

For the internal or bottom plate, it was not feasible to use a single, uniform plate due to the proximity of the slot to the side of the case. As a result, several different bottom plates were designed, each covering a 16 mm range of positions. This modular approach allows for precise adjustment while maintaining proper sealing, even in tight spaces. The outer and inner plates are shown in Figure 5.5.

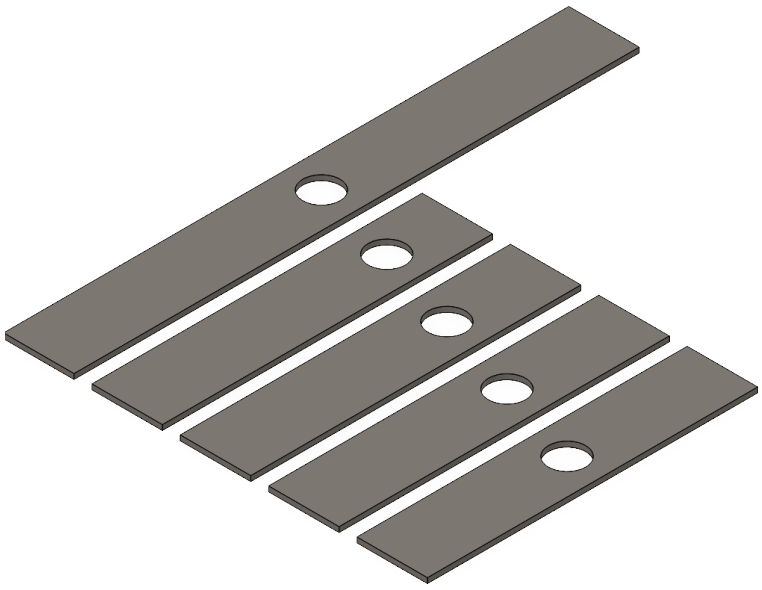

Figure 5.5: CAD model of the centering plates

5.6 Windows

To enable visual observation of the internal components during operation and to allow for high-speed, slow-motion video recording, several openings were incorporated into the enclosure. Some of these openings are designated for the camera, while others are for the LED lighting required for proper illumination. To prevent oil from splashing out into the laboratory environment and to ensure safety, these openings are sealed using a highly impact-resistant plastic material. For this purpose, an 8 mm thick Lexan sheet is employed. Lexan is a fully transparent material, making it ideal for maintaining visibility while also ensuring the internal components are well-lit. In addition to its optical clarity, Lexan offers excellent durability and can withstand significant impact forces, providing an added layer of protection in the event of a catastrophic failure within the experimental setup.

The Lexan windows are designed with a 20 mm margin surrounding each opening to allow for secure fastening. A gasket is placed between the Lexan sheets and the case to ensure a tight seal, preventing any potential oil leakage during the experiment. This arrangement ensures both safety and functionality, allowing for uninterrupted monitoring and data capture without the risk of oil contamination in the surrounding laboratory space. The three Lexan windows are illustrated in Figure 5.6.

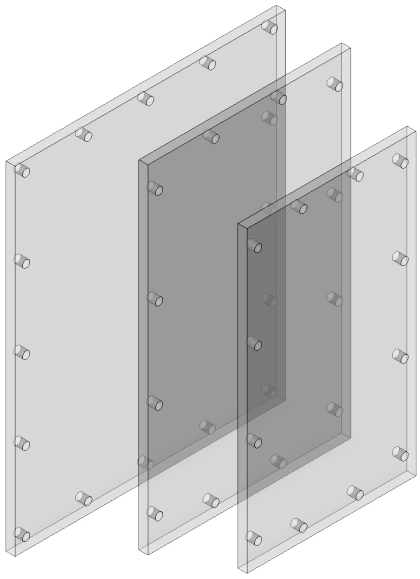

Figure 5.6: CAD model of the Lexan windows

5.7 Window Frames

To securely fasten the Lexan windows to the case, custom external frames were designed for each window. These frames are fabricated from 3 mm thick stainless steel sheets, offering both strength and durability. Each frame is carefully dimensioned to a width of 20 mm, ensuring that there is no obstruction of the openings or interference with visibility through the windows. This design consideration allows for a clear view of the internal components while providing robust support to the Lexan sheets.

The primary function of the frames is to distribute the clamping pressure from the bolts evenly across the surface of the Lexan windows. By doing so, the frames prevent the formation of localized stress points that could lead to cracks or material failure, particularly during the assembly or disassembly of the front window. The heads of the bolts make direct contact with the stainless steel frames, which helps in spreading the force evenly, thereby protecting the Lexan from damage and ensuring a long service life for the windows.

The frames not only contribute to the structural integrity of the entire assembly but also enhance the overall safety and reliability of the experimental setup. The three window frames are shown in Figure 5.7. These frames play a vital role in maintaining the stability of the window installation while allowing for clear observation of the test environment without compromising the strength of the case.

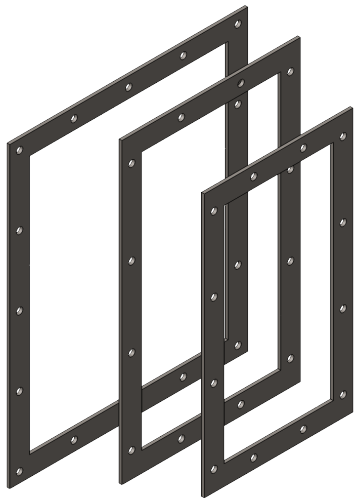

Figure 5.7: CAD model of the window frames

5.8 Final Assembly

After mounting all the components described in the previous sections, the complete test environment is assembled, as shown in Figure 5.8, which illustrates the positioning of all key components. This final configuration brings together the gear, external case, threaded rod, drive shaft, centering plates, windows, and their respective frames, creating a fully functional setup for conducting the laboratory experiment.

In the assembly, the gear is positioned inside the case, slightly offset to the left. This offset is intentional, as the gear will rotate clockwise during the experiment, and the majority of the oil is expected to end up on the right-hand side. By positioning the gear in this way, the setup ensures optimal exposure of the gear to the oil jet while minimizing any unnecessary contact with other parts of the apparatus.

A significant design consideration is the distance between the gear and the front Lexan window, which is maintained at over 150 mm. This substantial gap serves a critical purpose: it helps prevent excessive oil from splashing onto the window during testing. Keeping the window clear of oil buildup for a longer period, allows for better visibility inside the case, especially important for high-speed video recording and visual observation during the experiment.

The threaded rod, which controls the position of the oil jet, is securely fastened to the top of the enclosure using the centering plates and nuts. These components ensure that the rod remains stable throughout the test, allowing for precise adjustments to the position of the oil jet relative to the gear, further enhancing the accuracy and repeatability of the experiment.

Overall, the fully assembled setup weighs approximately 12 kg, making it light enough to be directly mounted to the laboratory test bench and manageable for adjustments and maintenance.

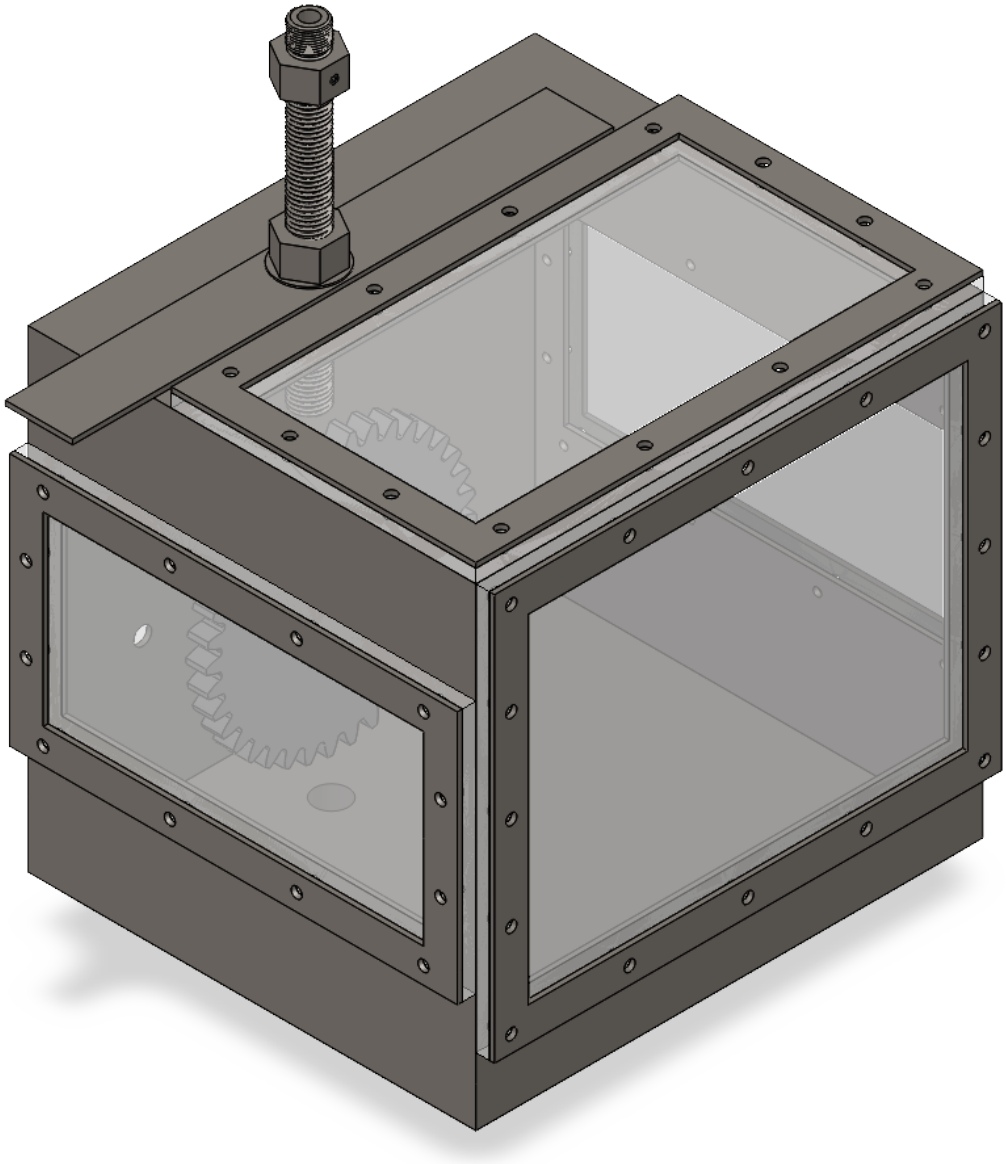

Figure 5.8: CAD model of the final test setup assembly

5.9 Test Fit of FDM Printed Parts

The previously modeled gear, drive shaft, case, and threaded rod were test-fitted on the laboratory test bench using physical models produced through the Fused Deposition Modeling (FDM) process with PLA plastic. As shown in Figure 5.9, the drive shaft is properly dimensioned to connect and support the gear on the test bench spindle. As described earlier, the gear is attached to the drive shaft using three M5x0.8 screws, while the drive shaft is secured to the spindle with two set screws, one on each side, and rotationally linked by two lateral keys. A section of the case was also mounted on the test bench to verify the dimensions and positioning of both the gear and the threaded rod mounted on top of the case.

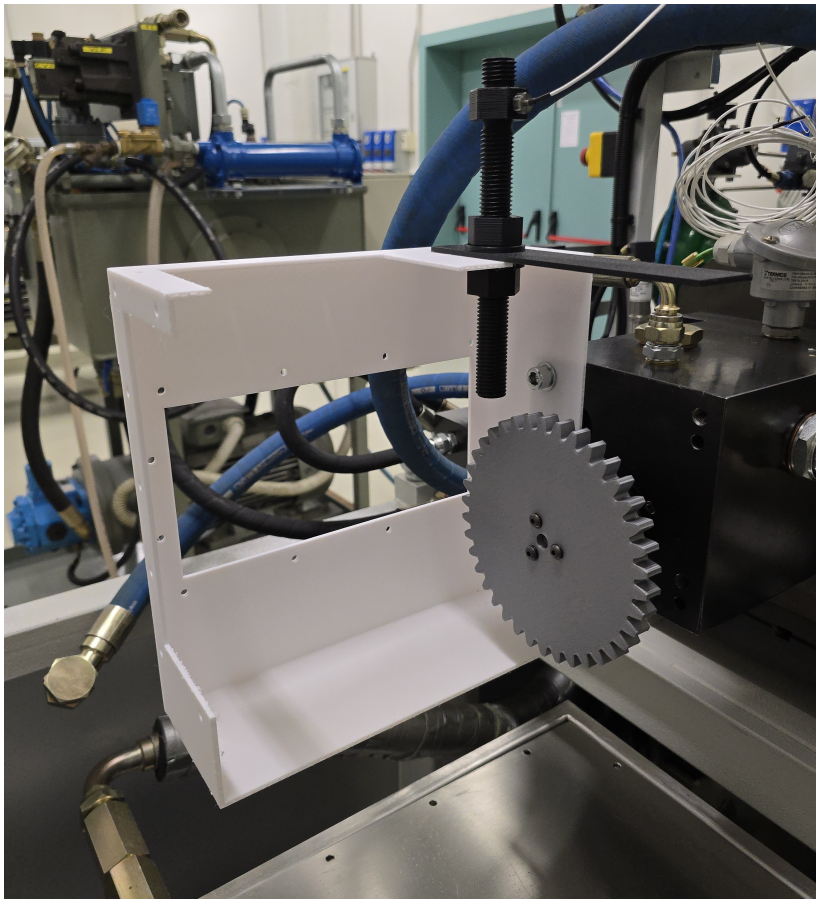

Figure 5.9: Test fit of 3D printed components

Chapter 6

Additional Study on Splash Lubrication

In this chapter, additional studies to explore different lubrication methods employed in automotive gearbox systems were conducted, in particular splash lubrication. Splash lubrication is widely regarded as one of the most prevalent methods for lubricating transmission gear systems in the automotive sector. Its popularity stems from several factors, including its inherent simplicity, reliability, and cost-effectiveness.

This investigation builds upon the findings of our previous study, with simulations designed to facilitate a seamless transition into laboratory experiments. This approach allows anyway for the realization in the real world of experiments based on the simulations and for a comprehensive comparison between simulated results and actual experimental data. While there is currently no confirmation whether this study will be replicated in a laboratory experiment, it would be interesting to observe the differences in resistive torque, and consequently efficiency, between the two lubrication methods.

The configuration of a splash lubrication system is relatively straightforward. The essential components required for conducting experiments include a gear to be analyzed, an oil bath to provide the lubricant, and a suitable container for carrying out the experiment. Notably, the system does not necessitate complex features such as inlets, outlets, or intricate positioning mechanisms, making it simple to realize a possible future experimental test.

The primary objective of this study, mirroring that of the previous investigation, was to identify the critical parameters and their effect on the resistive torque in gear systems under splash lubrication.

A schematic representation of the fundamental principles and geometry of a splash lubrication system is illustrated in Figure 6.1.

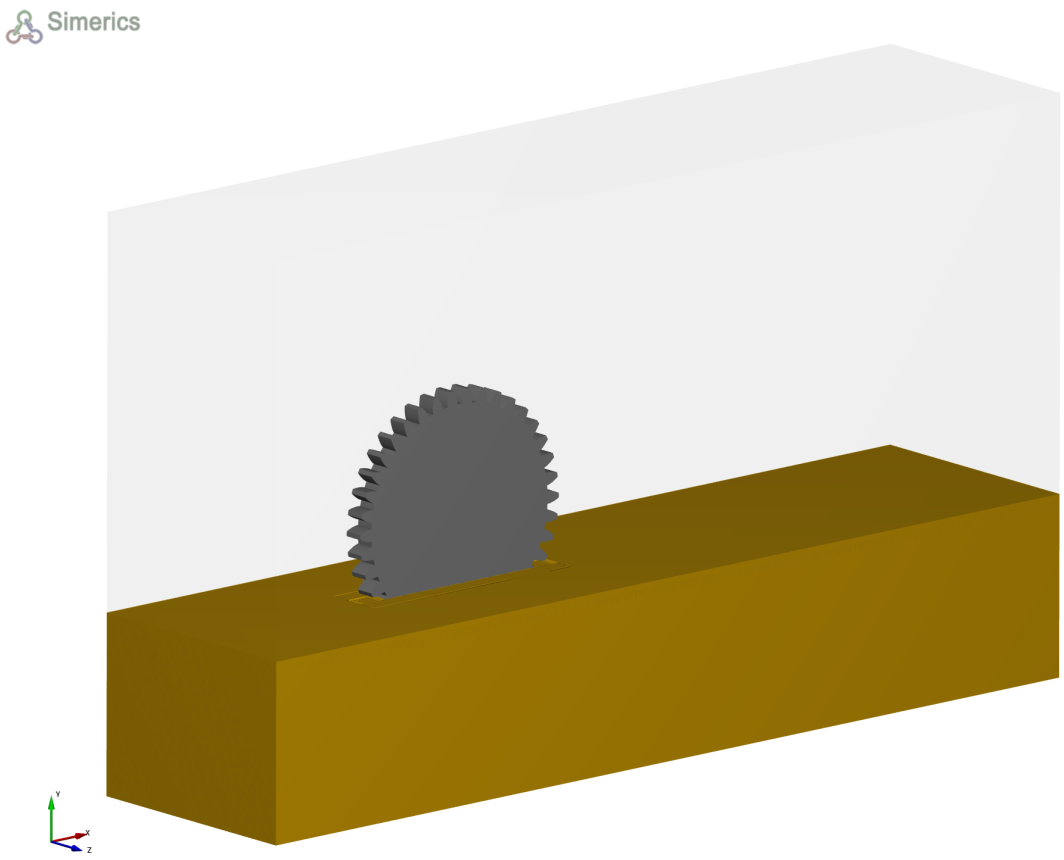

Figure 6.1: Splash lubrication system

6.1 Methodology

Based on the initial considerations, a simple experimental setup was developed. The test container is a simple rectangular box with dimensions of 200 mm in height, 400 mm in length, and 150 mm in width. The oil is deposited at the bottom of the container, with the oil level specified according to the length of the gear that is intended to be immersed. For the gear, a model based on a chain drive gear already available in the laboratory was utilized.

The key design parameters of the gear have been summarized in Table 6.1 and the CAD model of the gear is reported in Figure 6.2.

Chain drive gear parameters	
tooth number [−]	26
module [mm]	9.535
pitch circle diameter [mm]	79.02
outer circle diameter [mm]	83.00
tooth diameter [mm]	6.35
thickness [mm]	5.30

Table 6.1: Chain drive gear parameters

Building on the insights gained from the earlier simulations, the only variables altered in this study were the oil level and the rotating speed of the gear. The primary objective, similar to the previous investigation, was to determine the minimum oil level and speed at which the resistive torque generated by the gear exceeded 1 Nm.

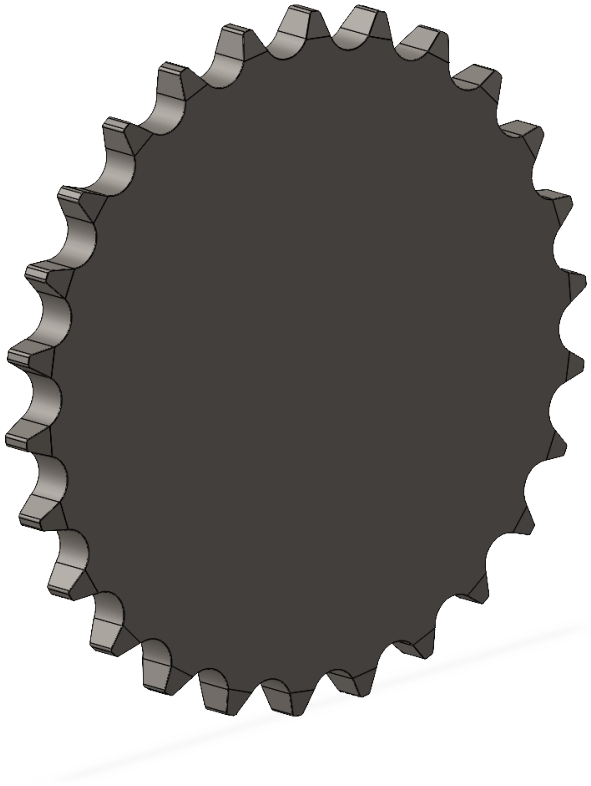

Figure 6.2: CAD model of the chain gear

6.1.1 CAD Geometry Model

The geometry of the simulations has been created starting from the gear and then adding all the parts necessary to simplify the mesh creation. In Figure 6.3 it is possible to see the cylindrical shell used for the gear mesh definition, the two cylinders for creating a medium-sized mesh between the gear and the case mesh, and finally, the enclosure domain for the case mesh. The various entities are disconnected from each other to simplify the model import and mesh creation in Simerics MP+. In fact, the domains will be repositioned inside the software before the meshing process. The gear has been positioned on the left side of the enclosure, as it rotates counterclockwise. This arrangement anticipates that most of the oil splashing and wake will occur on the right side of the container. More space was left on the right side to minimize wall interaction and prevent oil from bouncing back onto the gear. This design choice helps to reduce disturbances that could affect the accuracy of the results. No inlet or outlet was required for the experiment, which significantly simplified the CAD geometry.

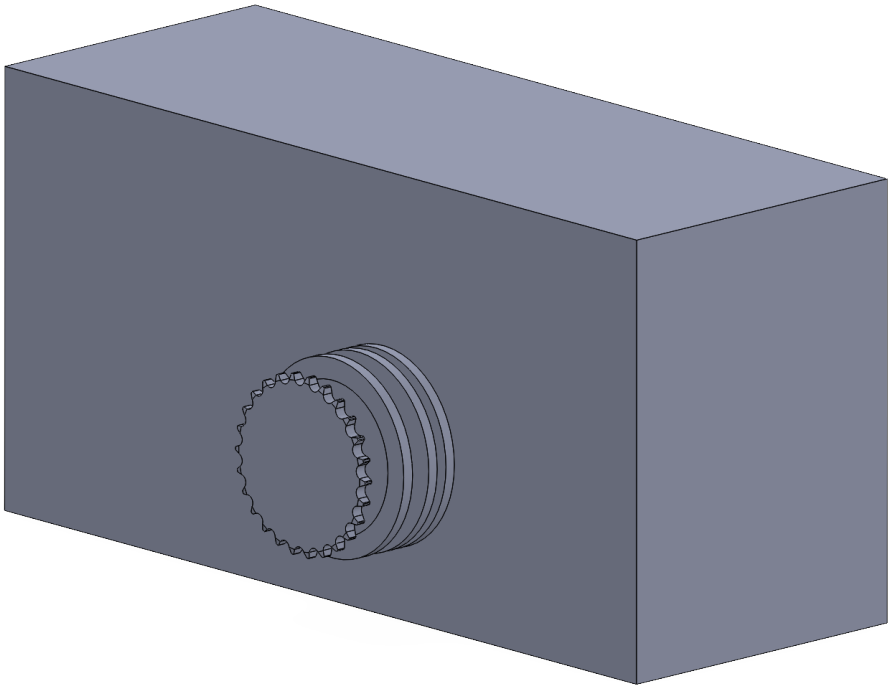

Figure 6.3: CAD model of the splash lubrication simulations

6.1.2 Meshing and Simulation Setup

For this study, the domain was divided into two parts: the gear mesh and the enclosure mesh, both created using the general mesh template. Several refinement zones were introduced within the case mesh. The first zone is at the free oil film surface, with a thickness of 10 mm, 5 mm above, and 5 mm below it. The second zone is located in the right region of the gear, where the oil wake is expected. The last zone is centered on the gear and is used to create a more gradual transition between the small cell size in the gear mesh and the larger cells in the enclosure mesh.

The final result of the meshed domain is shown in Figure 6.4, with a more detailed view of the meshes near the gear in Figure 6.5. The meshed domain primarily consists of two meshes and three distinct refinement zones:

1. **Rotating gear mesh**: This mesh follows the rotational movement of the gear. As shown in the figure, it is created using the gear tooth profile and the cylinder added in the CAD model. During the simulation, this mesh rotates rigidly around the center of the gear, while its external surfaces maintain constant contact with the internal faces of the case mesh. The mesh was generated using the general mesh template.
2. **Fixed case mesh**:This mesh remains stationary throughout the entire simulation, and its primary function is to replicate the real-world environment around the gear. Its internal surface always maintains contact with the rotating gear mesh and was generated using the general mesh template, with dimensions larger than those of the gear mesh.
3. **Refinement zone around the gear**: This part of the case mesh is refined to a size comparable to that of the gear mesh. It surrounds the gear mesh and is designed to prevent issues when the oil passes between the two different meshes, ensuring a smooth transition in cell size.
4. **Refinement zone at the free oil film**: This part of the case mesh is a refined zone at the level of the free oil film and is primarily used to better visualize the behavior of the free oil layer.
5. **Refinement zone along the oil wake**: This part of the case mesh is refined to have a higher mesh resolution in the wake region, allowing for better capture of the wake behavior

As for the previous study the two meshes are always in contact with each other. For this reason, it is important to correctly define these common surfaces as a mismatched grid interface (MGI) in the software. Defining an MGI enables the exchange of information between the different meshes and is essential for the success of the simulation. The MGI must be defined for both the stationary and moving meshes.

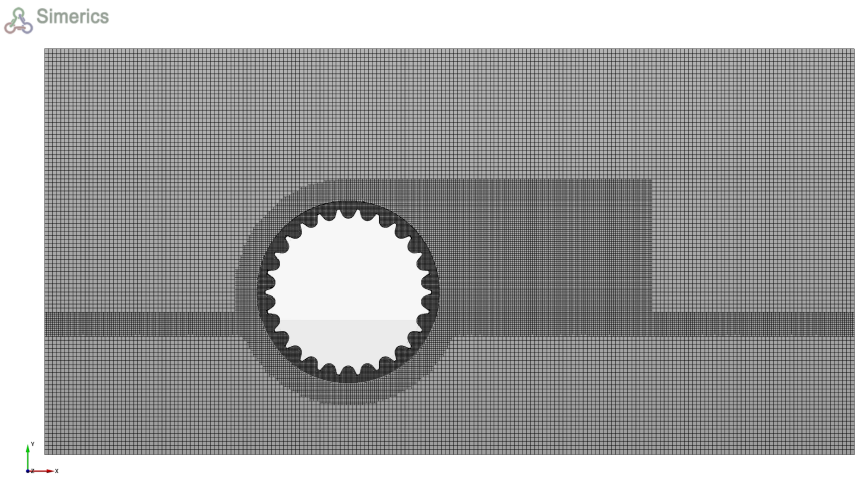

Figure 6.4: Mesh of the splash lubrication simulations

The basic parameter maintained constant for all the simulations have been reported in Table 6.2.

Constant simulation parameters	
oil density $[km/m^3]$	860
air density $[km/m^3]$	1.1766
ambient pressure $[Pa]$	101325
oil viscosity $[Pa \cdot s]$	0.06
oil surface tension $[N/m]$	0.04
gravity force $[m/s^2]$	9.81

Table 6.2: Constant simulation parameters

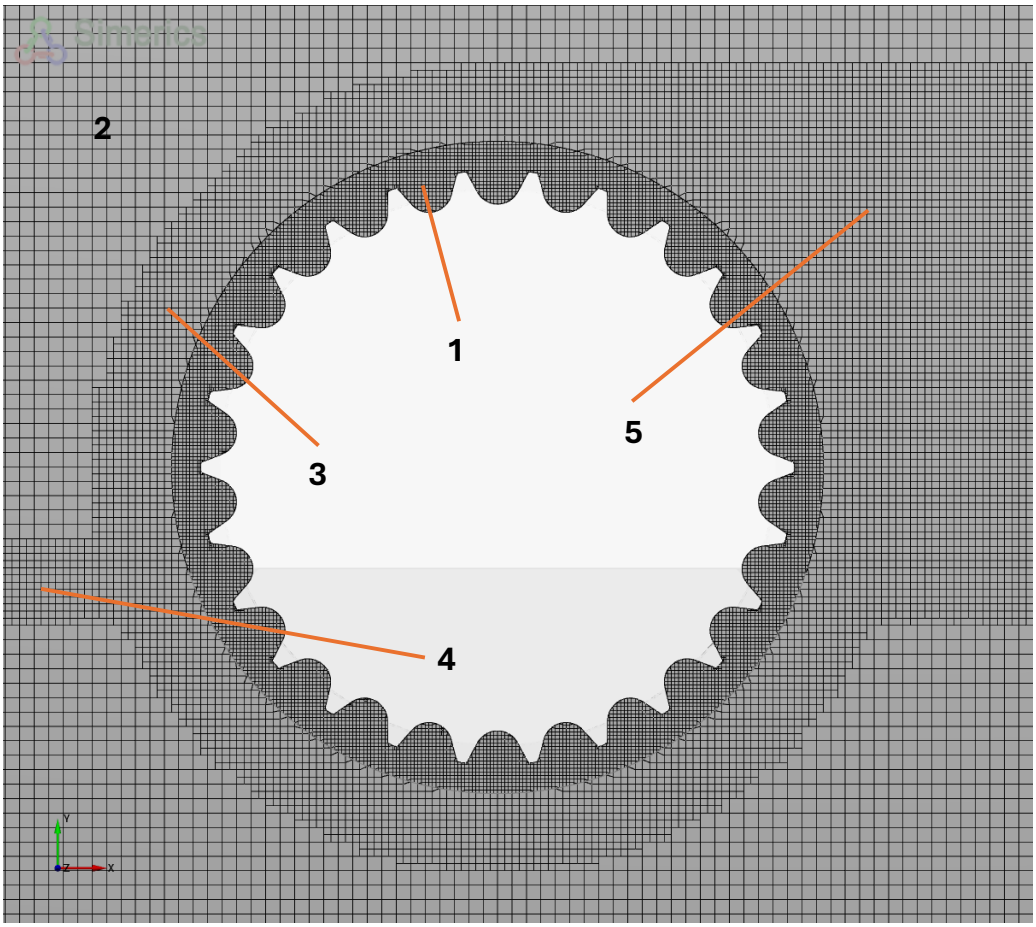

Figure 6.5: Mesh details of the splash lubrication simulations

Figure 6.6 contains screenshots from Simerics MP+ showing the settings used in the meshing process for the splash lubrication simulation. On the left, the case mesh is shown with the three refinement zones, while on the right, the settings for the gear mesh are presented.

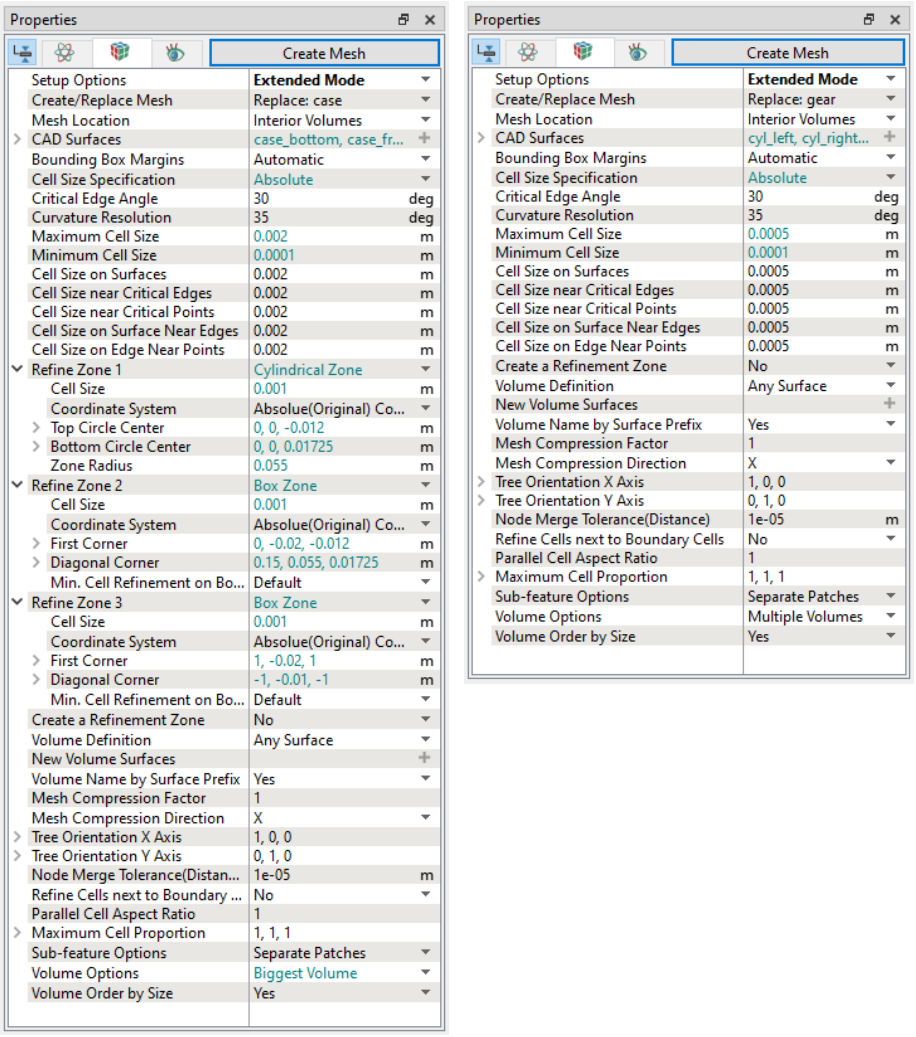

Figure 6.6: Mesh settings of the splash lubrication simulations

6.2 Results

6.2.1 Sentitivity Analysis on Oil Level

The sensitivity of the average resistive torque to the oil level has been the first parameter study conducted on the new simulation setup. The run simulations have been reported in Table 6.3. As can be seen from the table the oil level was changed from 31 mm, where the gear is immersed only for 10 mm, up to -51 mm, where the gear is completely submerged in the oil. The negative values lose their meaning in real-world application, since the gear will never be immersed more than half in the oil, let alone fully submerged. Nevertheless, these simulations were run to see if was even possible to reach the requested torque with this gear. As expected the resistive torque increases with increasing oil level.

simulation	oil distance from gear center [mm]	oil level [mm]	gear rotational speed [rpm]	total number of cells [-]	simulation time [h]	average torque [Nm]	average torque [%]	average torque variation [%]
1	31.00	49.00	2000	3904520	29.58	0.0159	100	0
2	21.00	59.00	2000	3881392	20.76	0.0352	221	121
3	11.00	69.00	2000	3859909	21.66	0.0572	359	259
4	1.00	79.00	2000	3860452	19.17	0.0823	517	417
5	-11.00	91.00	2000	3874485	18.95	0.1275	800	700
6	-21.00	101.00	2000	3877063	20.04	0.1600	1004	904
7	-31.00	111.00	2000	3866336	19.50	0.1911	1199	1099
8	-41.00	121.00	2000	3873639	19.21	0.2405	1509	1409
9	-51.00	131.00	2000	3937756	18.95	0.3243	2035	1935

Table 6.3: Simulation settings and results of oil level analysis

Figure 6.7 shows the increase in resistive torque when the oil level is increased. It can also be noticed that the graph has a proportional trend up to the mid-gear height and then starts to increase faster. Even in the more extreme cases the torque never reached the requested value.

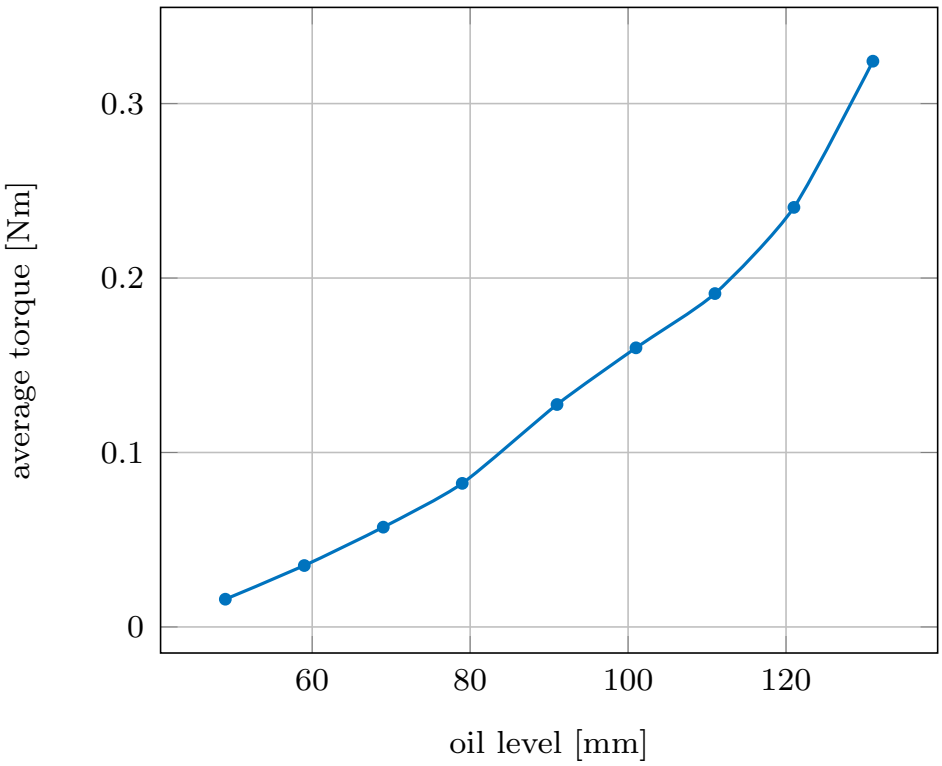

Figure 6.7: Average resistive torque as a function of oil level

6.2.2 Sensitivity Analysis on Gear Rotation Speed

The sensitivity of the average resistive torque to the gear rotating speed has been the second parameter study conducted on the new simulation setup. The run simulations have been reported in Table 6.4.

In this Set of simulations, the rotating speed of the gear has been increased from 2000 rpm to 8000 rpm with 2000 rpm increments. As expected increasing the speed also the resistive torque is increased. From 2000 rpm to 8000 rpm an increase in resistive torque of 300% is present, this is a huge increase even if it is not sufficient to reach the wanted result.

simulation	gear speed [rpm]	oil distance from gear center [mm]	oil level [mm]	total number of cells [-]	average torque [Nm]	average torque [%]	average torque variation [%]
1	2000	15	65	2615744	0.0528	100	0
2	4000	15	65	2615744	0.0898	170	70
3	6000	15	65	2615744	0.1592	302	202
4	8000	15	65	2615744	0.2101	398	298

Table 6.4: Simulation settings and results of gear rotational speed analysis

Figure 6.8 highlights how the average resistive torque increases with the increase in the rotating speed of the gear. The trend exhibits a proportional behavior, allowing for the prediction of the resistive torque at higher rotational speeds, even though the available test bench is not capable of reaching those higher speeds.

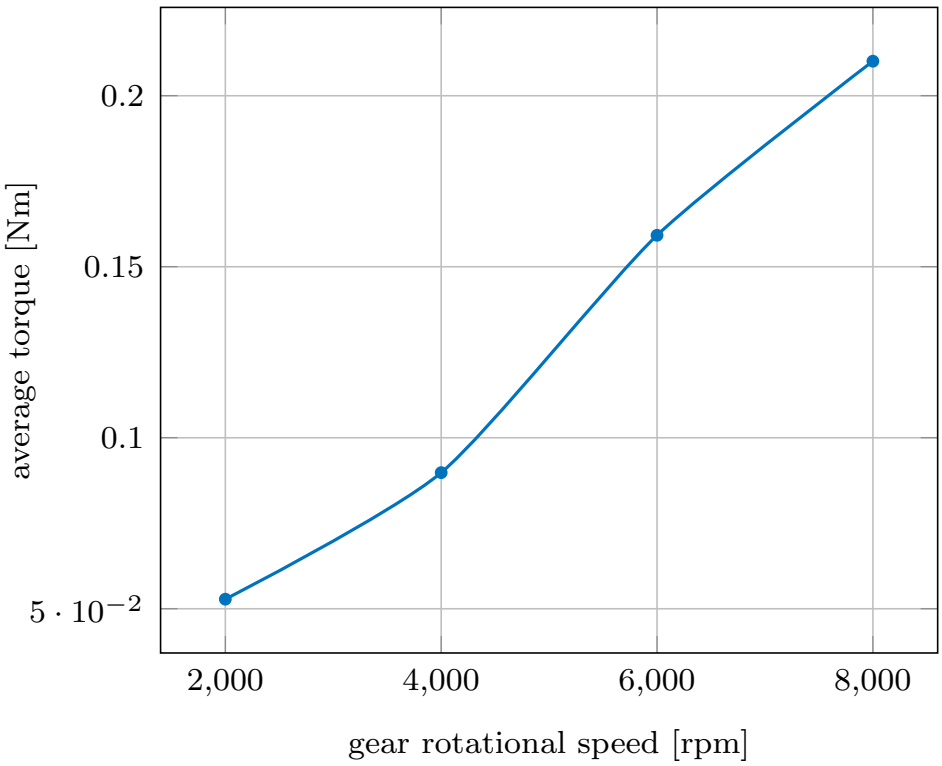

Figure 6.8: Average resistive torque as a function of gear rotational speed

6.2.3 Splash Lubrication Simulation with Original Gear

After evaluating the influence of simulation parameters and observing the low resistive torque generated by the chain drive gear, an analysis of splash lubrication was conducted using the original gear designed for the jet lubrication study. This choice was made due to the gear's different geometry, featuring a larger diameter and greater thickness, which was expected to produce a higher torque.

The same procedure as in the previous simulations was followed, with the only exception being the definition of the gear mesh. Specifically, the geometry of the gear enabled the use of a specialized meshing template in Simerics MP+, known as the general gear mesh. This template divides the mesh based on the specified number of axial, tangential, and radial elements, while also allowing for the definition of boundary layer thickness. Although this mesh presented challenges when applied to the oil jet analysis, it proved to be highly effective for the splash lubrication study. A detailed view of the resulting mesh generated by the general gear mesh template is shown in Figure 6.9.

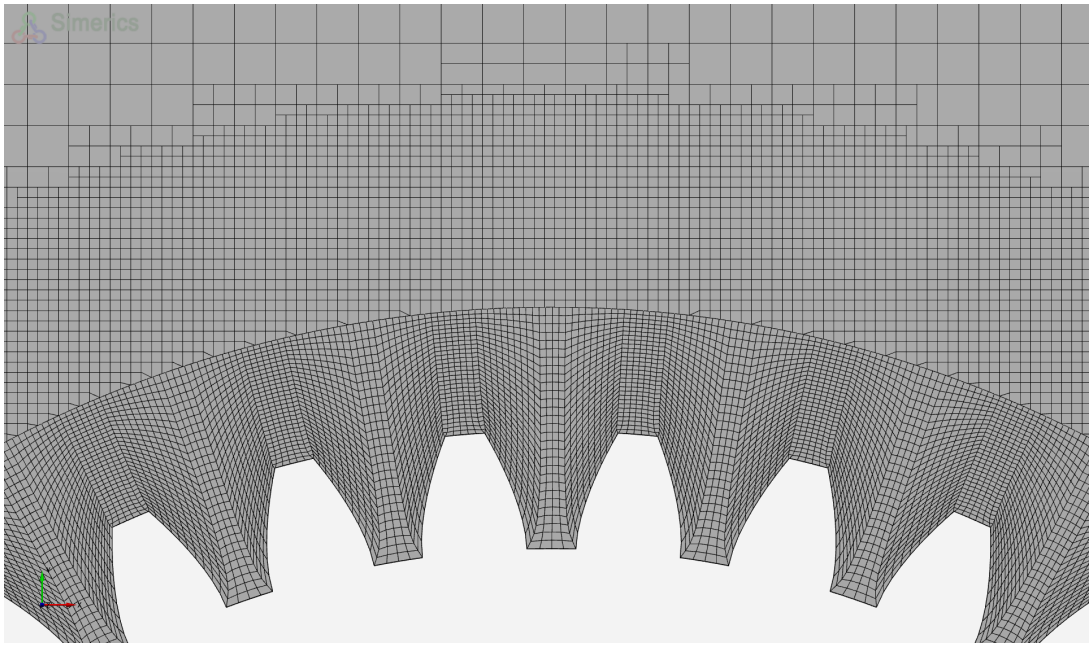

Figure 6.9: Mesh details of the splash lubrication simulations with the original gear

The oil level has been set as low as possible to reduce the total weight that must be supported by the test bench, as well as to minimize splashing. For speed, the opposite approach was taken: the speed was increased as much as possible to achieve the required torque with the lowest amount of oil. It is important to note that these simulations were relatively long, primarily due to the long time needed to reach steady-state conditions. As shown in Table 6.5, to exceed 1 Nm the gear must rotate at 8000 rpm with the gear immersed to a depth of 25 mm in oil.

simulation	gear speed [rpm]	gear oil immersion depth [mm]	average torque [Nm]
1	8000	5	0.6
2	8000	10	0.8
3	8000	25	1.6

Table 6.5: Simulation settings and results of original gear oil level analysis

Figure 6.10 illustrates the results of the simulation conducted with the original gear operating at 8000 rpm and a 25 mm gear oil immersion depth. Oil volume fractions exceeding 1% are visualized, with their color corresponding to the flow velocity magnitude. The fastest oil is observed adhering to the gear teeth, followed by the oil in the upper region of the rear wake.

As expected, a significant oil wake is present on the right side of the gear, splashing oil onto the top and rear surfaces before it trickles back into the oil bath. Additionally, smaller wakes can be observed at the front of the gear, caused by the teeth impacting the oil's free film. Over a longer simulation time, these smaller wakes are expected to diminish significantly.

This visualization also highlights the advantages of using the generic gear template in Simerics MP+, which effectively captures the oil boundary layer that remains attached to the gear profile, enhancing the accuracy and fidelity of the simulation.

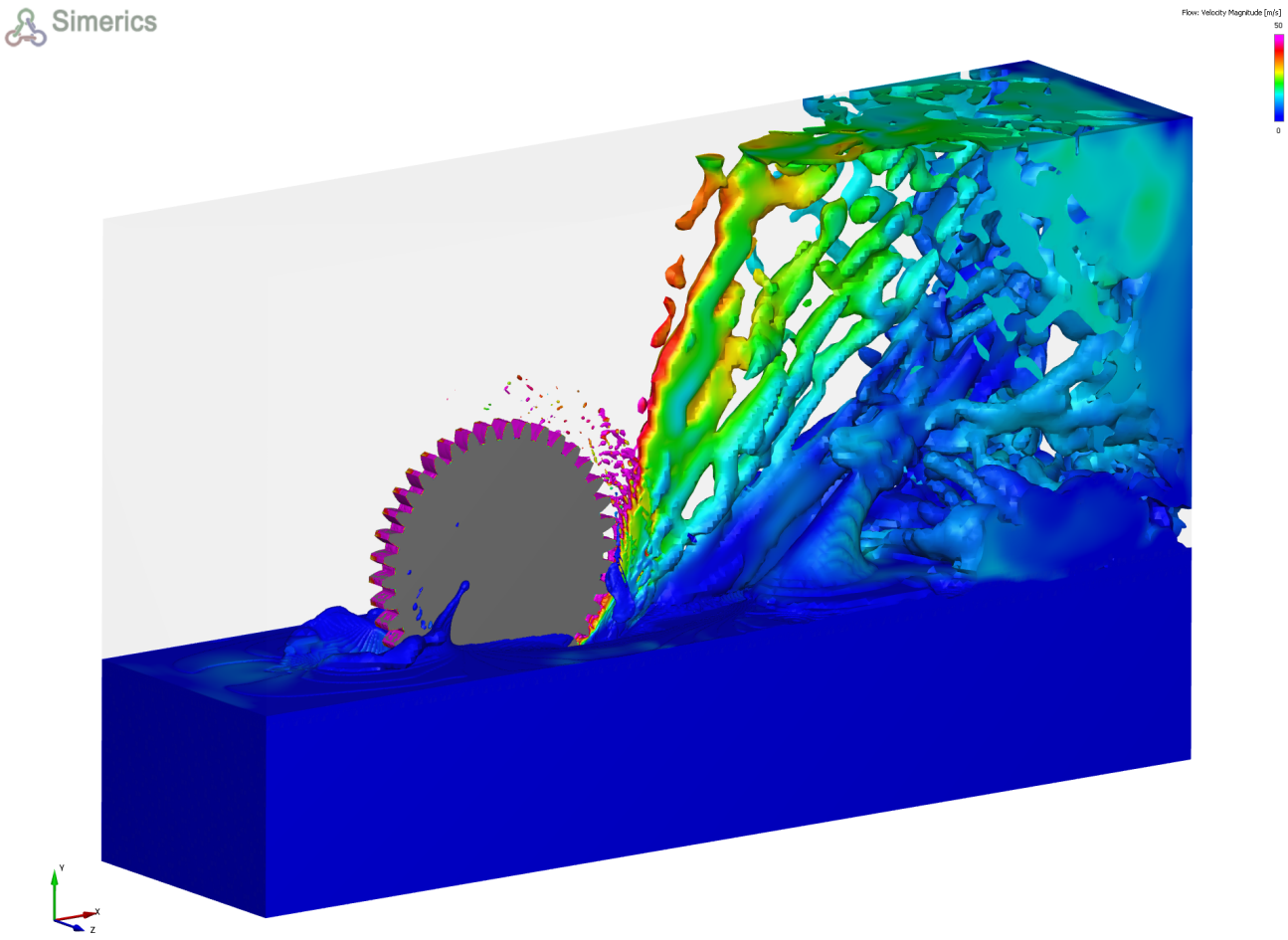

Figure 6.10: View of the splash simulation with the original gear showing the oil flow velocity magnitude for oil volume fractions greater than 1%

As shown in Figure 6.11, the resistive torque exhibits a proportional relationship with the increase in the oil level. By immersing the original gear to a depth of 25 mm in oil, a torque value of 1.6 Nm is eventually reached. Since the plot shows a proportional trend, it is possible to extrapolate the minimum oil level required to achieve the desired resistive torque. In this case, immersing the gear to a depth of 15 mm should result in a resistive torque slightly greater than 1 Nm.

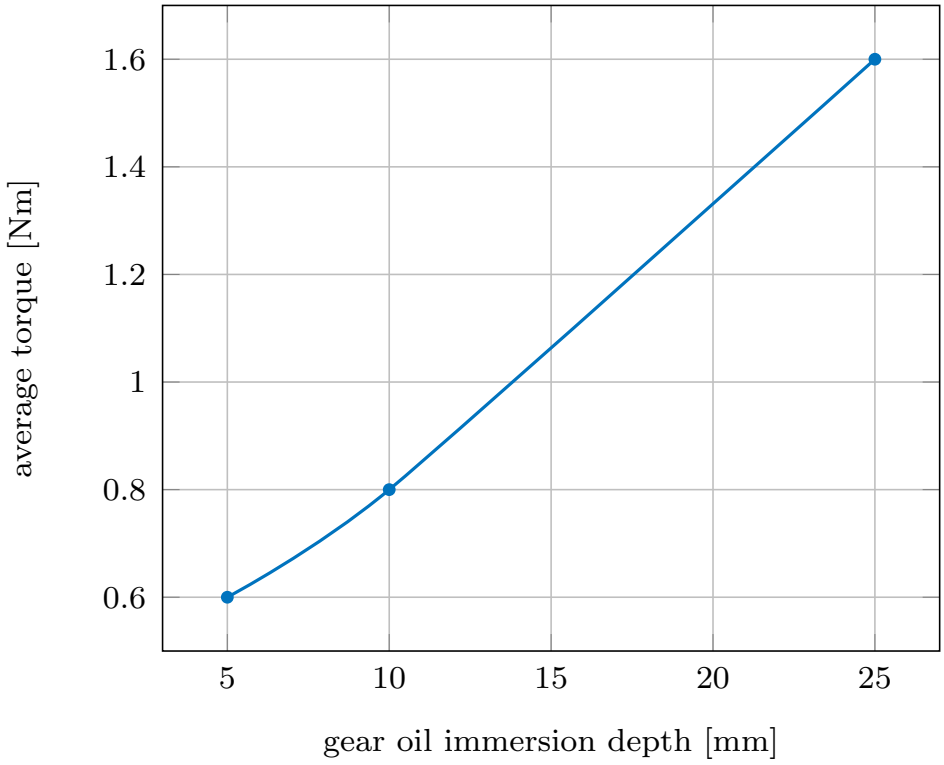

Figure 6.11: Average resistive torque as a function of gear oil immersion depth

Figure 6.12 presents the instantaneous resistive torque for the splash lubrication simulation with a gear oil immersion depth of 25 mm. As evident from the plot, the torque initially exhibits a high value that gradually decreases over time. This initial spike is caused by the gear having to accelerate a significant amount of stationary oil when rotation begins.

As the simulation progresses, the oil is splashed onto the rear wall of the enclosure, causing the oil level within the bath to decrease until a steady state is achieved. At

this steady state, the amount of oil falling back into the bath equals the amount splashed out by the rotating gear. Despite reaching this equilibrium, some oscillations around the final value remain.

However, this process is time-consuming, and the simulation analyzed covers only the first 0.035 seconds. While the torque appears to have approached its steady-state value within this timeframe, extending the simulation would be necessary to confirm this with certainty. Notably, the transition phase in this splash lubrication simulation is considerably longer compared to the oil jet simulations.

Closer inspection of the torque curve reveals small periodic peaks, which occur each time a new gear tooth impacts the oil film and enters the oil bath.

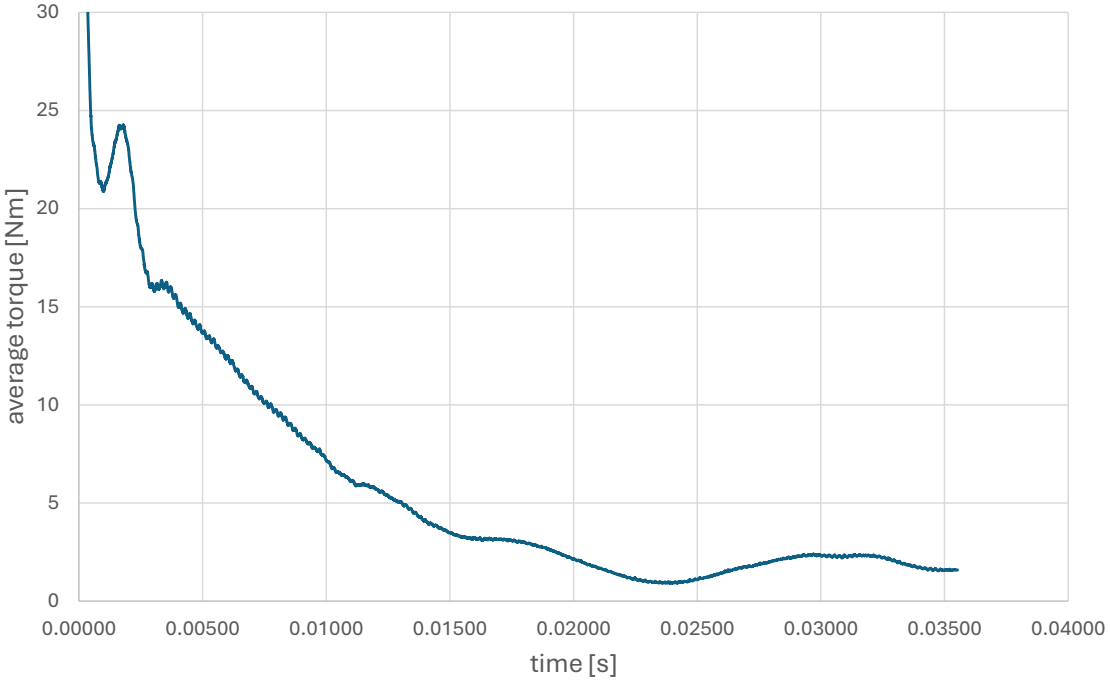

Figure 6.12: Instantaneous resistive torque as a function of time in splash lubrication simulations

Chapter 7

Conclusions

The primary objective of this thesis was to design an experiment based on the forced lubrication method for rotating gears to validate the CFD software Simerics MP+. The study focused on understanding the effects of different parameters on simulation results and identifying the most significant ones. A smaller-scale study on splash lubrication systems was also conducted.

The research findings revealed that simulation outcomes are highly sensitive to setup configurations. Sensitivity analyses indicated that cell size directly affects simulation time and accuracy. While smaller cell sizes increase computational time, they also improve reliability, highlighting the need to strike a balance between accuracy and efficiency. This analysis was crucial in determining an optimal cell size for subsequent studies. Time step sensitivity analysis showed that although reducing the time step lengthens simulation time, its impact on accuracy remained minimal due to the ability of the software ability to self-regulate the time step when needed. This analysis was crucial in determining an optimal time step that maintained a reasonable simulation time.

Once the simulation parameters were optimized, the focus shifted to studying physical parameters for defining the experimental setup. Key findings included identifying the optimal jet position for forced lubrication and determining the necessary flow rate to achieve the desired resistive torque.

The design phase then involved creating CAD models of the experimental com-

ponents, including the external enclosure, drive shaft, threaded rod with centering plates, Lexan and frame windows for recording and observations.

Additionally, a preliminary study on oil bath lubrication was conducted. Using an existing gear, simulations were run to analyze the sensitivity of oil levels and gear speed, which were found insufficient for achieving the desired torque. The study then switched to using the gear designed for forced lubrication, determining the necessary oil level for the required torque output.

As the physical experiment is yet to be conducted, a final comparison between experimental and simulated results is pending, and therefore, a definitive validation of Simerics MP+ cannot be provided at this stage. However, the components for the experiment are currently under production, and future results will allow for a comprehensive comparison.

This research offers a valuable foundation for future studies on gear lubrication and lubrication systems in general. Once the experiment is completed and the results compared, it will be possible to confirm the reliability of Simerics MP+ for future research applications. This validation is critical, as Simerics MP+ provides several advantages over competing software, and understanding its capabilities can streamline future studies.

Despite the positive outcomes, certain limitations were encountered, particularly computational constraints that restricted mesh and domain resolution, reducing simulation accuracy. Future research could aim to enhance CFD models to capture more detailed transient phenomena and explore alternative lubrication methods. Comparing different lubrication methods could also be useful to understand the advantages and disadvantages of each methodology and determine which is the most efficient. Additionally, refining experimental setups and incorporating advanced measurement techniques would allow for improved accuracy by recalibrating simulations with precise experimental data.

Overall, this study demonstrates the effectiveness of Simerics MP+ in simulating gear lubrication and provides practical recommendations for optimizing simulation strategies. These findings pave the way for future research using this software to study lubrication systems.

References

[1] L. S. Akin, D. P. Townsend, and J. J. Mross. Study of lubricant jet flow phenomena in spur gears. *TechnicalMemorandumTM X-71572, NASA*, 1974.

[2] E. Burberi, T. Fondelli, A. Andreini, B. Facchini, and L. Cipolla. Cfd simulations of a meshing gear pair. *Proceedings of ASME Turbo Expo 2016: Turbomachinery Technical Conference and Exposition*, 2016.

[3] C. N. Eastwick and G. Johnson. Gear windage: a review. *Journal of Mechanical Design*, 130(3), 2008.

[4] T. Fondelli, D. Massini, A. Andreini, B. Facchini, and F. Leonardi. Three-dimensional cfd analysis of meshing losses in a spur gear pair. *Proceedings of ASME Turbo Expo 2018: Turbomachinery Technical Conference and Exposition*, 2018.

[5] Tommaso Fondelli, Antonio Andreini, Riccardo Da Soghe, Bruno Facchini, and Lorenzo Cipolla. Numerical simulation of oil jet lubrication for high speed gears. *International Journal of Aerospace Engineering*, 2015.

[6] Tommaso Fondelli, Antonio Andreini, Riccardo Da Soghe, Bruno Facchini, and Lorenzo Cipolla. Numerical simulation of oil jet lubrication for high speed gears. *Hindawi Publishing Corporation International Journal of Aerospace Engineering*, 2015.

[7] Tommaso Fondelli, Daniele Massini, Bruno Facchini, and Federico Leonardi. Three-dimensional cfd analysis of meshing losses in a spur gear pair. *Proceedings of ASME Turbo Expo 2018 Turbomachinery Technical Conference and Exposition*, 2018.

[8] C. W. Hirt and B. D. Nichols. Volume of fluid (vof) method for the dynamics of free boundaries. *Journal of Computational Physics*, 39(1), 1981.

[9] Marc C. Keller, Samuel Braun, Lars Wieth, Geoffroy Chaussonnet, Thilo Dauch, Rainer Koch, Corina Höfler, and Hans-Jörg Bauer. Numerical modeling of oil-jet lubrication for spur gears using smoothed particle hydrodynamics. *11th international SPHERIC workshop*, 2016.

[10] D. Massini, T. Fondelli, A. Andreini, B. Facchini, L. Tarchi, and F. Leonardi. Cfd simulations of a meshing gear pair. *Proceedings of ASME Turbo Expo 2017: Turbomachinery Technical Conference and Exposition*, 2017.

[11] Daniele Massini, Tommaso Fondelli, Antonio Andreini, Bruno Facchini, Lorenzo Tarchi, and Federico Leonardi. Experimental and numerical investigation on windage power losses in high speed gears. *Journal of Engineering for Gas Turbines and Power*, 2018.

[12] Daniele Massini, Tommaso Fondelli, Bruno Facchini, Lorenzo Tarchi, and Federico Leonardi. High speed visualizations of oil jet lubrication for aero-engine gearboxes. *71st Conference of the Italian Thermal Machines Engineering Association, ATI2016, 14-16 September 2016, Turin, Italy*, 2016.

[13] Daniele Massini, Tommaso Fondelli, Bruno Facchini, Lorenzo Tarchi, and Federico Leonardi. Experimental investigation on power losses due to oil jet lubrication in high speed gearing systems. *Proceedings of ASME Turbo Expo 2017: Turbomachinery Technical Conference and Exposition*, 2017.

[14] J. Mazallo, Z. Dai, and G. M. Faeth. Primary breakup of nonturbulent round liquid jets in gas crossflows. *Automization and Sprays*, 9(3), 1999.

[15] M. Z. Mettichi, Y. Gargouri, P. H. L. Groenenboom, and F. el Khaldi. Simulating oil flow for gearbox lubrication using sph. *Proceedings of the 10th International SPHERIC Workshop*, 2015.

[16] P.-K.Wu, K. A. Kirkendall, R.P.Fulle, and A. S. Nejad. Breakup processes of liquid jets in subsonic crossflows. *Journal of Propulsion and Power*, 13(1), 1997.

[17] S. Seetharaman and A. Kahraman. Load-independent spin power losses of a spur gear pair: model formulation. *Journal of Tribology*, 131(2), 2009.

[18] P. Velex Y. Diab, F. Ville and C. Changenet. Windage losses in high speed gears-preliminary experimental and theoretical results. *Journal of Mechanical Design*, 126(5), 2004.